SPRINGER BRIEFS IN
ELECTRICAL AND COMPUTER ENGINEERING

Bannour Ahmed
Mohammad Abdul Matin

Coding for MIMO-OFDM in Future Wireless Systems

Springer

SpringerBriefs in Electrical and Computer Engineering

More information about this series at http://www.springer.com/series/10059

Bannour Ahmed · Mohammad Abdul Matin

Coding for MIMO-OFDM in Future Wireless Systems

Springer

Bannour Ahmed
L'institut Superieur D'informatique
Demahdia
Mahdia
Tunisia

Mohammad Abdul Matin
Institut Teknologi Brunei
Gadong
Brunei Darussalam

ISSN 2191-8112 ISSN 2191-8120 (electronic)
SpringerBriefs in Electrical and Computer Engineering
ISBN 978-3-319-19152-2 ISBN 978-3-319-19153-9 (eBook)
DOI 10.1007/978-3-319-19153-9

Library of Congress Control Number: 2015939996

Springer Cham Heidelberg New York Dordrecht London

Printed on acid-free paper

Springer International Publishing AG Switzerland is part of Springer Science+Business Media (www.springer.com)

Preface

MIMO-OFDM has been recognized as one of the most promising techniques for future communication systems as it supports high data rate transmission, multimedia services over fading channel that is time selective, and frequency-selective fading. This, in turn, has drawn lots of thought among researchers and students, which results in a large number of coding across space, frequency, and time for MIMO-OFDM systems to exploit three types of diversity schemes in wireless communications. Therefore, an effort has been made in this book to introduce different coding schemes to the reader and promote further research in their area of interest.

This book is concerned with the use of the Algebraic Space Time Coding (ASTC) technique combined with Orthogonal Frequency Division Multiplexing (OFDM) to overcome the frequency selectivity channel problems. The first part analyzed the performance of the ASTC codes under a correlated Rayleigh channel. The Algebraic Space Time Codes (ASTC), based on the cyclic algebras, has shown good spectral efficiency, full diversity, and a full rate under nonselective channel conditions. However, the radio-mobile channel is a selective channel whose features vary with the time. This selectivity is owed to the multi-path phenomenon and generates interferences between symbols (IES). So, the second objective of was to develop a new technique in order to adapt the ASTC codes to the frequency selective channels. It has been shown that by their construction, the Algebraic Space Time Codes have a reasonable BER when working in a nonselective channel thanks to their properties (full rank, full rate, and nonvanishing determinant for increasing rate). We have proved that it is possible to combine MIMO-OFDM systems with an ASTC encoder under a frequency-selective channel. Computer simulations have shown the efficiency of the proposed ASTC encoder either in terms of BER performance, capacity, or in terms of PAPR reduction. The third part aimed to minimize the sensibility of the ASTC codes to frequency synchronization in selective channels. A new algebraic Carrier Frequency Offset (CFO) estimation technique, for MIMO-OFDM systems with ASTC under quasi-static correlated Rayleigh frequency-selective fading channels, has been developed. The technique uses a preamble and is especially suitable for burst mode communication.

The preamble consists of orthogonal training sequences simultaneously transmitted from the various transmit antennas. The proposed system exploits all the subcarriers in frequency domain, which provides a remarkable performance improvement compared to other well-known methods and reaches the Cramèr-Rao Lower Bound (CRLB).

This book also addresses multiuser MIMO-OFDM systems which benefit from the combined space and frequency domain freedom as well as multiuser diversity. To achieve high symbol rate for multiuser MIMO-OFDM system, two coding schemes have been presented for space–frequency (SF) codes and space–time–frequency (STF), where a systematic design of high-rate, full-diversity multi-user SF and STF codes for MIMO frequency-selective fading multiple access channel has been discussed. The book highlights the unique design issues which put the reader in good pace to be able to understand the coding theory and grasp the processes involved.

Bannour Ahmed
Mohammad Abdul Matin

Contents

List of Figures

List of Tables

Chapter 1
Overview of MIMO-OFDM

1.1 Introduction

In the first chapter, we introduce the MIMO-OFDM system, in Rayleigh frequency selective-channels. Orthogonal frequency division multiplexing (OFDM) has been adopted in the wireless local-area network (WLAN) standards IEEE 802.11a [1] and IEEE 802.11g [2] due to its high spectral efficiency and ability to deal with frequency selective fading. The combination of OFDM with spectral efficient multiple antenna techniques makes the OFDM a good candidate to overcome the frequency selective problems.

1.2 MIMO

MIMO stands for Multiple-input Multiple-output. It uses multiple antennas both in transmission and receiver equipment to exploit multipath propagation in wireless radio communication. It divides the total transmit power among multiple spatial paths over which to transmit signals, driving the capacity without consuming extra radio frequency, thus increasing the aggregate spectral efficiency. Due to multipath propagation, each receiver antenna receives a linear combination of the multiple transmitted data streams. The data streams are separated at the receiver using algorithms that depend on estimates of all channels between each transmitter and each receiver.

B. Ahmed and M. Abdul Matin, *Coding for MIMO-OFDM in Future Wireless Systems*, SpringerBriefs in Electrical and Computer Engineering,
DOI 10.1007/978-3-319-19153-9_1

1.3 OFDM Modulation

1.3.1 Principal

In OFDM modulation data is transmitted simultaneously on n_s subcarriers modulated at a rate R_s/n_s, where R_s is the rate of one single carrier. In overall the total rate still the same as in a single carrier systems, further each subcarrier is less sensitive to the delay spread of the channel, it could be considered as non selective flat fading subcarrier. Figure 1.1 describe the baseband OFDM transmitter. When bits are generated, modulated and coded, we obtain OFDM codewords and symbols. The codewords fellows tow processes. First a time domain transformation is done using the IFFT. Second the obtained signal is added by a guard interval or Cycle Prefix (CP). The length of the added time domain signal should be larger than the delay spread of the channel. The OFDM complex symbols $S_1, S_2, \ldots, S_i, \ldots$ are then regrouped into blocks of length N_s (serial to parallel conversion), its transmission time is equal to $N_s.T_s$. An OFDM signal during the time $[iT_s, (i+1)T_s]$ can be expressed as

$$x_l(t) = \sum_{k=\frac{N_s}{2}}^{\frac{N_s}{2}-l} S_{l,k}\, g(t - ((i+1)T_s)) \exp(j2\pi f_k t) \tag{1.1}$$

The above equation represents the lth-OFDM symbol. The received signal could be expressed as

$$r(t) = \sum_{l=1}^{\infty} \sum_{k=\frac{N_s}{2}}^{\frac{N_s}{2}-l} S_{l,k}\, g(t - ((i+1)T_s)) \exp(j2\pi f_k t) + n_k(t) \tag{1.2}$$

where $n_k(t)$ is white Gaussian noise at the kth subcarrier.

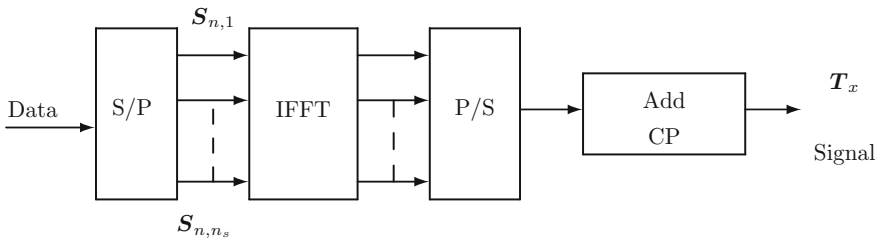

Fig. 1.1 Block diagram of an OFDM transmitter

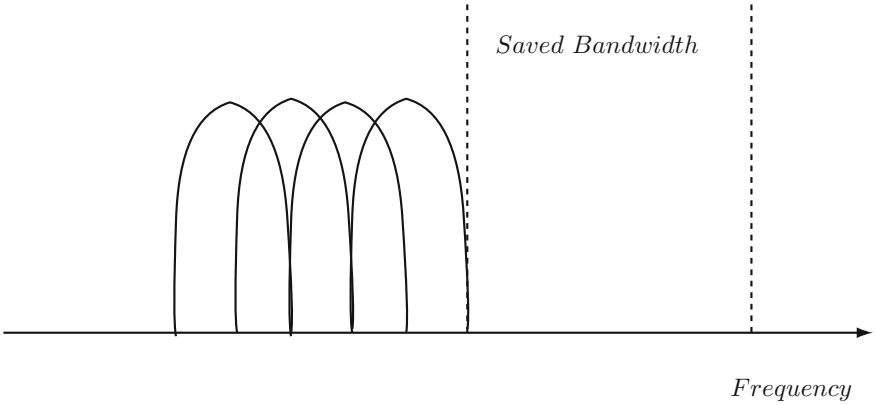

Fig. 1.2 Orthogonal multicarrier modulation technique

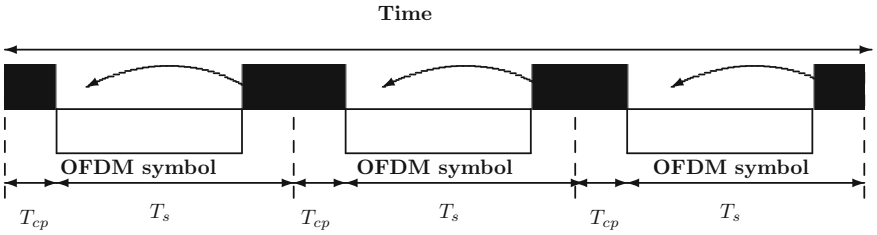

Fig. 1.3 Cyclic prefix

1.3.2 Orthogonality

To be free (ICI-free), the orthogonality is an essential condition for OFDM signal. In fact the spacing between two subcarriers is important in order to have a bandwidth efficient system. The spacing between the subcarriers should be large enough, this can cause a higher bandwidth then the the spectral efficiency will be lost. One solution is to set OFDM symbols where the center of one subcarrier is positioned such that it lands into the null of the neighboring subcarrier as shown in Fig. 1.2.

1.3.3 Cycle Prefix

The (CP) is used mainly in terrestrial systems between two consecutive OFDM symbol, to reduce the effect of the delay spread of the multipath channels as illustrated in Fig. 1.3. The CP-length is variable and should be adjusted as much as the system bandwidth is efficient.

1.3.4 Synchronization and PAPR Issue for OFDM

The message data are carried on orthogonal subcarriers for parallel transmission to prevent the distortion and the inter-symbol-interference caused by the frequency selective channel in the multi-path fading. Synchronization issues can destroy this orthogonality and then OFDM loses its powerful modulation technique. There are essentially three types of synchronization problems:

- Symbol synchronization
- Carrier synchronization

In Symbol synchronization a timing offset gives rise to a phase rotation of the subcarriers. This phase rotation is largest on the edges of the frequency band. If a timing error is small enough to keep the channel impulse response within the cyclic prefix, the orthogonality is maintained.

However in carrier synchronization, Frequency offsets are created by differences in oscillators in transmitter and receiver, Doppler shifts, or phase noise introduced by nonlinear channels. There are two destructive effects caused by a carrier frequency offset in OFDM systems. One is the reduction of signal amplitude (the sinc functions are shifted and no longer sampled at the peak) and the other is the introduction of ICI from other carriers. The latter is caused by the loss of orthogonality between the subchannels. Chapter five will focus on a new Carrier Synchronization Offset (CFO) estimation, which is a key point to hold both the powerful coding technique of ASTC and the powerful modulation technique of OFDM.

However, one major difficulty is its large peak to average power ratio (PAPR). These are caused by the coherent summation of the OFDM subcarriers. When N signals are added with the same phase, they produce a peak power that is N times the average power. These large peaks cause saturation in the power amplifiers, leading to intermodulation products among the subcarriers and disturbing out of band energy. Hence, it becomes worth to reduce PAPR.

1.3.5 Advantages of OFDM

OFDM fits with wideband wireless systems compared to Single carrier transmission due to its lower complexity equalizer to overcome the ISI problem of the multipath frequency selective channels. A significant bandwidth gain is also obtained when using the overlapping parallel subcarriers. The ISI problem is declined using the cyclic prefix to prevent the system from multipath fading.

One also can modulate each subcarrier using different modulation techniques M-PSK or M-QAM according to the requirement of the system.

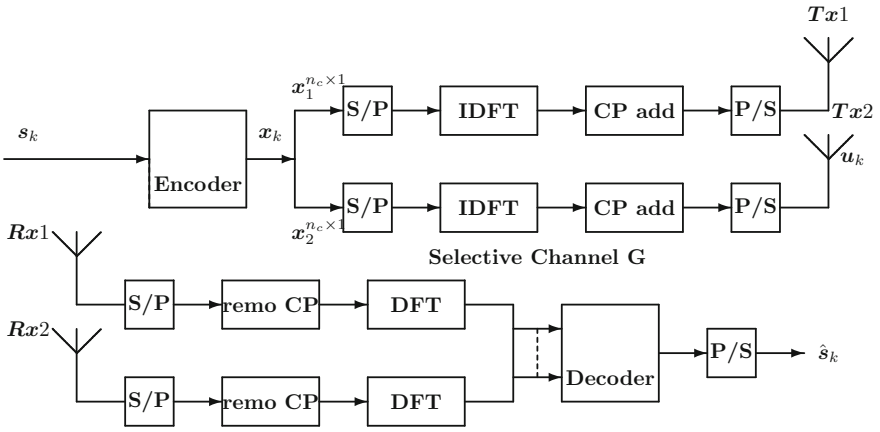

Fig. 1.4 ASTC-MIMO-OFDM transceiver

1.4 Transmitter Model

Let us consider the baseband-equivalent ASTC-MIMO-OFDM system, with $n_t = 2$ transmit antennas and $n_r = 2$ receive antennas, depicted in Fig. 1.4 [3]. The transmitted binary source sequence s_k, with bit energy E_b, is QPSK modulated. The QPSK symbols are then ASTC encoded.

We note $\boldsymbol{v}_k = [s_{4k-3}, s_{4k-2}, s_{4k-1}, s_{4k}]^T$ the QPSK symbols encoder input. The code word output is converted to a serial stream and then fed to n_t OFDM modulators with n_c subcarriers and a cycle prefix (CP) of length n_g.

In order to simplify the discussion, we denote the code word $\boldsymbol{x}_k \in \mathcal{C}^{n_c n_t \times 1}$ the kth MIMO vector to be OFDM modulated given by

$$\boldsymbol{x}_k = \begin{pmatrix} x_{1,k} \\ \vdots \\ x_{n_c n_t,k} \end{pmatrix} = \boldsymbol{\Phi} \odot (\boldsymbol{s}_k) \tag{1.3}$$

where $\odot$ refers to scaler product vector, $x_{n,k}$ is the MIMO code word to be transmitted on the nth subcarrier at time k and by the qth ($q = 1, 2$) antenna. $\boldsymbol{s}_k = [\boldsymbol{v}_{k_0} \boldsymbol{v}_{k_1} \ldots \boldsymbol{v}_{k_{\frac{(n_c n_t)}{4}}}]^T$ is in $\mathcal{C}^{n_c n_t \times 1}$ input symbols vector, and $\boldsymbol{\Phi} = [\phi_{k_0} \phi_{k_1} \ldots \phi_{k_{\frac{(n_c n_t)}{4}}}]^T$ denotes the $\mathcal{C}^{\frac{(n_c n_t)}{4} \times 1}$ vector of the block matrix ϕ_{k_p}, where ϕ_{k_p} is the coder matrix at time k_p.

After a serial to parallel conversion, the OFDM modulator uses an IDFT module and a is added. The overall vector of length $n_c + n_g$ is transmitted over a frequency and time selective MIMO channel. The CP length n_g is assumed to be longer than the largest multi-path delay spread in order to avoid OFDM inter-symbol interference.

The kth MIMO-OFDM symbol $\boldsymbol{u}_k \in \mathcal{C}^{n_t(n_c+n_g)\times 1}$ is then given by

$$\boldsymbol{u}_k = \boldsymbol{\xi}_1 \sqrt{n_c}(\boldsymbol{F}^{-1} \otimes \boldsymbol{I}_{n_t})\boldsymbol{x}_k$$

where $\boldsymbol{F}^{-1}$ is the $\mathcal{C}^{n_c n_c \times 1}$ Fourier matrix, of which the (n,k)th element is $\exp(-j2\pi nk/n_c)$, $\otimes$ denotes the Kronecker product, $\boldsymbol{I}_{n_t}$ represents the n_t identity matrix, and $\boldsymbol{\xi}_1 \in \mathcal{C}^{n_t(n_c+n_g)\times n_c n_t}$ is the CP adding matrix given by

$$\boldsymbol{\xi}_1 = \left[\begin{pmatrix} 0 \\ \boldsymbol{I}_{n_c} \end{pmatrix} \otimes \boldsymbol{I}_{n_t} \right] \tag{1.4}$$

The $n_t(n_c + n_g)$ length MIMO-OFDM symbol is transmitted over a time and frequency selective channel.

1.5 The Channel Model

As mentioned above, we assume that the MIMO-OFDM symbols are transmitted over a time and frequency selective Rayleigh channel and that the channel taps remain constant during a packet transmission. Consequently, the (CIR) between qth transmitting antenna and pth receiving antenna is modeled by a tapped delay line as

$$\boldsymbol{h}_k^{p,q} = \sum_{l=0}^{L-1} h_k^{p,q}(l)\delta(k-l) \tag{1.5}$$

where $h_k^{p,q}(l)$ is the lth path from the qth transmitting antenna to pth receiving antenna at time k and L is the largest order among all impulse responses. The channel taps sequence $\{h_k^{p,q}(l)\}$ is a correlated complex with zero mean, the same variance σ_h^2 and the

$$E\{h_k^{p,q}(l)[h_{k-k'}^{m,n}(l')]^*\} = \rho_{Rx}^{(m,p)}\rho_{Tx}^{(n,q)} J_0(2\pi f_m k')\delta(l-l') \tag{1.6}$$

where J_0 is the with zero order, f_m is the normalized Doppler shift, $\rho_{Rx}^{(m,p)}$, $\rho_{Tx}^{(n,q)}$ refers respectively to the correlation coefficient between the received antennas (m, p) and the transmitted antennas (n, q).

The received signal at the pth receiving antenna during the kth MIMO-OFDM symbol is

$$\boldsymbol{y}_k^p = \sum_{q=1}^{n_T}\sum_{l=0}^{L-1} h_k^{p,q}(l)\boldsymbol{u}_k^q(k-l) + \boldsymbol{w}_k^p \tag{1.7}$$

where $\boldsymbol{u}_k^q$ is the symbol vector transmitted by the qth antenna and $\boldsymbol{w}_k^p$ is a zero mean white Gaussian complex noise of variance $\frac{N_0}{2}$. Let us introduce the $\mathcal{C}^{n_t(n_c+n_g)\times n_t(n_c+n_g)}$ matrices $\boldsymbol{G}_k$ defined as the equivalent

$$\boldsymbol{G}_k = \begin{pmatrix} \boldsymbol{h}_k(0) & 0 & \dots & \dots & \dots & 0 \\ \boldsymbol{h}_k(1) & \ddots & & & & \vdots \\ \vdots & & \ddots & & & \\ \vdots & & & & & \\ \boldsymbol{h}_k(L-1) & \dots & \dots & \boldsymbol{h}_k(0) & & \\ 0 & \ddots & & & & \\ \vdots & & \ddots & & \ddots & \vdots \\ 0 & \dots & \dots & \boldsymbol{h}_k(L-1) & \dots & \boldsymbol{h}_k(0) \end{pmatrix} \tag{1.8}$$

where $\boldsymbol{h}_k(l) = \boldsymbol{h}_k^{p,q}(l)$.
We can thus express the MIMO-OFDM received signal in a matrix notation as

$$\boldsymbol{y}_k = \boldsymbol{G}_k \boldsymbol{u}_k + \boldsymbol{w}_k \tag{1.9}$$

where $\boldsymbol{y}_k \in \mathcal{C}^{n_r(n_c+n_g)\times 1}$ and $\boldsymbol{w}_k \in \mathcal{C}^{n_r(n_c+n_g)\times 1}$ represents the time k.

1.6 Coherent MIMO-OFDM Detector

At the receiver, after removing the CP, the signal is transformed back to the frequency domain by the mean of a DFT process. The signal at the DFT output is then given by

$$\boldsymbol{z}_k = \frac{1}{\sqrt{n_c}} \left[(\boldsymbol{F} \otimes \boldsymbol{I}_{n_t n_r}) \boldsymbol{\xi}_2 \right] \boldsymbol{y}_k \tag{1.10}$$

where the CP removing matrix $\boldsymbol{\xi}_2 \in \mathcal{C}^{n_c n_r \times (n_c n_g + 1) n_r}$, which discards the $n_g n_r$ first elements of $\boldsymbol{y}_k$, is defined as $\boldsymbol{\xi}_2 = [\boldsymbol{0}_{n_c n_g} \boldsymbol{I}_{n_g}] \otimes \boldsymbol{I}_{n_g}$.

By combining Eqs. 1.9 and 1.10, we can re-express the output as

$$\begin{aligned} \boldsymbol{z}_k &= \left[(\boldsymbol{F} \otimes \boldsymbol{I}_{n_t n_r}) \boldsymbol{\xi}_3 (\boldsymbol{F}^{-1} \otimes \boldsymbol{I}_{n_t n_r}) \right] \boldsymbol{x}_k + \boldsymbol{w}_k \\ &= \boldsymbol{H}_k \boldsymbol{x}_k + \boldsymbol{w}_k \end{aligned} \tag{1.11}$$

where the block circulant matrix $\boldsymbol{\xi}_3 \in \mathcal{C}^{n_t n_c \times n_r n_c}$ is defined as $\boldsymbol{\xi}_3 = \boldsymbol{\xi}_2 \boldsymbol{G}_k \boldsymbol{\xi}_1$ and $\boldsymbol{w}_k$ is the with zero mean and σ_w^2 and $\boldsymbol{H}_k$ is $\mathcal{C}^{n_t n_c \times n_c n_t}$ frequency domain matrix defined as

$$\boldsymbol{H}_k = \left[(\boldsymbol{F} \otimes \boldsymbol{I}_{n_t n_r}) \boldsymbol{\xi}_3 (\boldsymbol{F}^{-1} \otimes \boldsymbol{I}_{n_t n_r}) \right] \tag{1.12}$$

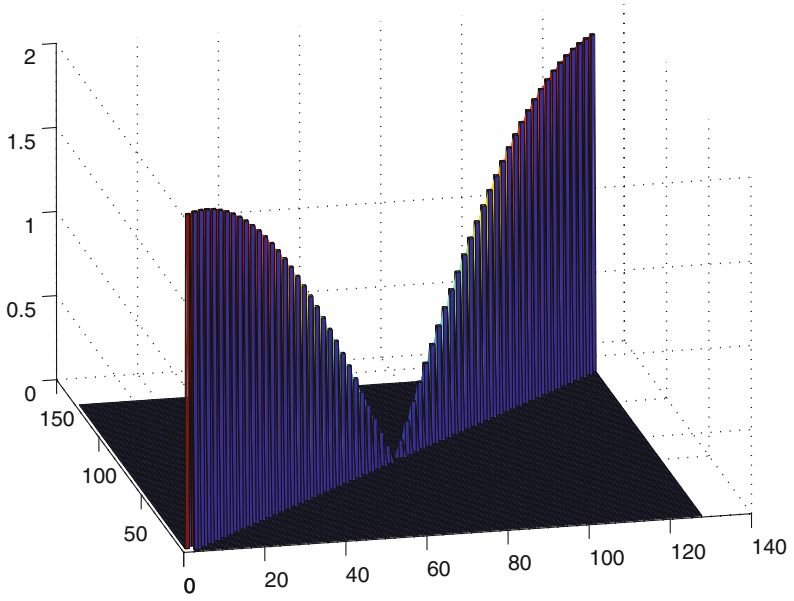

Fig. 1.5 Frequency-domain channel matrix $\boldsymbol{H}_k$ for $n_c = 32$

Under the assumption that the subcarriers are perfectly orthogonal and that the CP length is larger than the expected delay spread, it can be shown that the transmitted symbols are affected by and phase rotation. The channel gain matrix $\boldsymbol{H}_k$ (Fig. 1.5) is then a block diagonal matrix given by

$$\boldsymbol{H}_k = \begin{pmatrix} \boldsymbol{H}_k(0) & & 0 \\ & \ddots & \\ 0 & & \boldsymbol{H}_k(n_c n_t) \end{pmatrix} \tag{1.13}$$

where nth block $\boldsymbol{H}_k(n)$ represents the MIMO-OFDM channel gain at the nth subcarrier and can be written as

$$\boldsymbol{H}_k(n) = \sum_{l=0}^{L-1} \boldsymbol{h}_k(l) \exp\left(-j2\pi \frac{nk}{n_c}\right) \tag{1.14}$$

The received frequency-domain signal $z_{n,k}$ at the DFT output can be expressed as

$$z_{n,k} = \boldsymbol{H}(n) x_{n,k} + w_{n,k} \tag{1.15}$$

Therefore, we can describe the MIMO-OFDM transmission system as a set of parallel flat with correlated attenuation $\boldsymbol{H}(n)$. The channel effect (attenuation) in Eq. (1.11) is then compensated as

$$\hat{\boldsymbol{x}}_k = \boldsymbol{H}_k^{\dagger} \boldsymbol{z}_k \tag{1.16}$$

where $(.)^{\dagger}$ denotes the pseudo-inverse operator.

Once the channel effect is compensated, the decision variable $\hat{\boldsymbol{x}}_k$ is passed for decoding. A serial to parallel module, at each DFT output, is used to reshape the signal $\hat{\boldsymbol{x}}_k$ and to provide the output signal $\hat{\boldsymbol{s}}_k$.

1.7 Empirical Bit Error Rate Calculation

In order to see in closer window the design criteria of the system design we would like to analyze in this section the (PEP), we denote by $\boldsymbol{x}_1$ and $\boldsymbol{x}_2$ tow MIMO-OFDM complex Gaussian symbols such as:

$$\boldsymbol{x}_1 = [\boldsymbol{x}_1(0), \boldsymbol{x}_1(1), \boldsymbol{x}_1(2), \ldots, \boldsymbol{x}_1(N_t(N_c + N_g))]^T \tag{1.17}$$

$$\boldsymbol{x}_2 = [\boldsymbol{x}_2(0), \boldsymbol{x}_2(1), \boldsymbol{x}_2(2), \ldots, \boldsymbol{x}_2(N_t(N_c + N_g))]^T \tag{1.18}$$

The pair wise error probability, when $\boldsymbol{x}_1$ is transmitted, over an ASTC-MIMO-OFDM system, and when the received point is closer to $\boldsymbol{x}_2$ than to $\boldsymbol{x}_1$. A coherent channel $\boldsymbol{H}$, The development given in Appendix.A derived the following results

$$Pe \leq \left(1 + \frac{\sigma_s^2}{4\sigma_n^2} N_t + \sum_{i=1}^{N_i} \lambda_i + \left(\frac{\sigma_s^2}{4\sigma_n^2} \right)^{N_i N_t} \left(\prod_{i=1}^{N_i} \lambda_i \right)^{N_t} \right)^{-1} \tag{1.19}$$

where λ_i is the ith eigenvalues of $\boldsymbol{Q}_Y$ matrix.

We can see from Eq. (1.19) for small the term consisting of the summation of the eigenvalues will dominate the bounds. For asymptotically high SNR, however, the term containing the products of the eigenvalues will be dominant, resulting in the diversity and coding gain criteria.

1.8 Conclusion

It has been shown that MIMO is possible to combine with OFDM under a frequency-selective channel. PAPR reduction and frequency synchronization should taken seriously when working with OFDM. Channel selectivity problem is no more an issue when is applied, Hence after diagonalization, channel equalization is better performed.

References

1. IEEE 802.11a standard, ISO/IEC 8802-11:1999/Amd 1:2000(E)
2. IEEE 802.11g standard, Further Higher-Speed Physical Layer Extension in the 2.4 GHz Band
3. Bannour A, Ammari ML, Sun Y, Bouallegue R (2013) The capacity performance of ASTC-MIMO-OFDM system in a correlated rayleigh frequency-selective channel. Personal Wireless Communications 68(4):1365–1376

Chapter 2
Wireless Channels

2.1 Introduction

The wireless channel environment governs the performance of wireless communication systems, since the environment is unpredictable and dynamic. This will make the analysis of the wireless communication system difficult. To that end we classify the wireless channel model as illustrated in Fig. 2.1. The channel is one of the essential elements of the transmission chain. Generally, it acts as a disruptive factor that can alter the issued signal. This chapter will focus on wireless channel classification then, the channel will be introduced in information theory.

2.2 Wireless Channel Models

2.2.1 Fading Channels

In wireless communications, obstacles, such as houses, buildings, trees and mountains cause reflection, diffraction, scattering and shadowing of the transmitted signals and multipath propagation. Due to the mutipath the transmitted signals arrive in different phase angles, amplitude and time interval. The fading is the amplitude fluctuation of the received signal caused by the frequency selective or time variant of the multipath channel.

The fading process can follow Rayleigh probability distribution or Rician probability distribution, this will depend on the strength of scattering components during transmission. As illustrated in Fig. 2.2, the Rician probability distribution will be considered for strength of scattering (LOS) and the Rayleigh probability distribution will be considered for the strength less scattering (NLOS).

B. Ahmed and M. Abdul Matin, *Coding for MIMO-OFDM in Future Wireless Systems*, SpringerBriefs in Electrical and Computer Engineering,
DOI 10.1007/978-3-319-19153-9_2

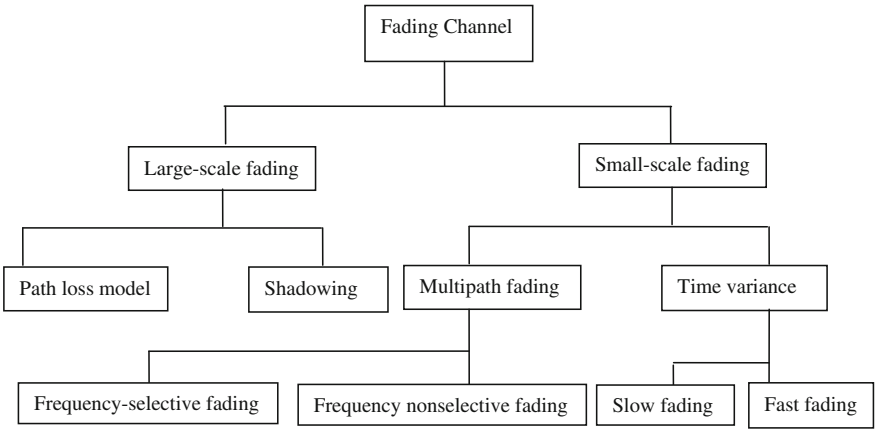

Fig. 2.1 Wireless channel model

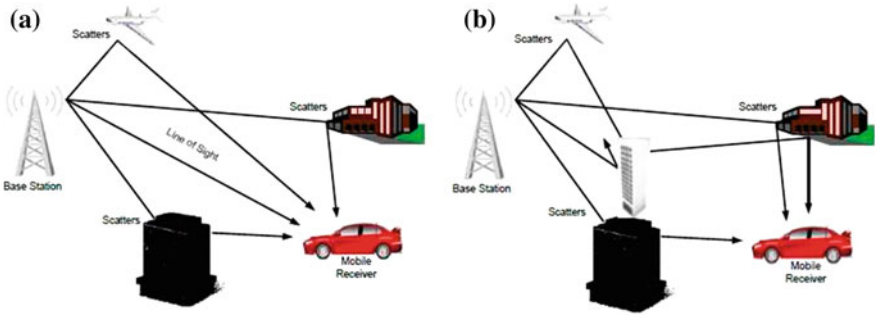

Fig. 2.2 Radio propagation environment

2.2.2 Frequency Non Selective Channel

The Multipath time delay spread or phenomenon can affect the transmitted wireless signal.

Frequency non selective channel or frequency selective channel are two categories of Multipath channels with time delay spread. When the channel bandwidth is much larger than the bandwidth of the transmitted signal, the received signals are called frequency non selective known as flat fading.

Figure 2.3 illustrates the flat fading characteristics, it can be seen that symbol period T_s is greater than the delay spread of channel τ. In this case the inter-symbol interference (ISI), is not caused. In conclusion a signal is affected by a flat fading channel if:

$$B_s \ll B_c \tag{2.1}$$

$$T_s \gg \sigma_\tau \tag{2.2}$$

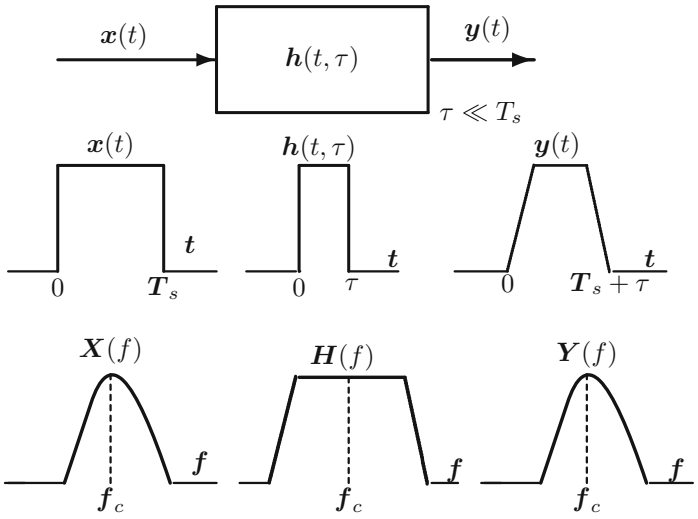

Fig. 2.3 Frequency-non-selective fading channel

where B_s and T_s represent respectively the bandwidth and symbol period of the transmitted signal, and B_c and σ_τ represent the coherence bandwidth and root mean square (rms) delay spread of the channel respectively.

2.2.3 Frequency Selective Channel

Frequency selectivity . occurs when the constant amplitude and linear phase response of the wireless channel is narrower than the signal bandwidth. In such condition the symbol period of the transmitted signal is smaller than the channel impulse response

The transmitted symbols have a short duration, compared to the multipath delay spread, this can cause a multiple attenuated and time delayed versions of the transmitted signal, which results in inter-symbol interference. As opposed to the frequency-flat nature of the frequency non-selective fading channel, the amplitude of the frequency response of the transmitted signal varies with frequency. Figure 2.4 shows the characteristics of a frequency selective fading channel. In this figure both the time and the frequency domain are illustrated to show how wide is the frequency channel window compared to the original transmitted signal up converted to frequency domain.

Frequency selective fading channels are called a wideband channels as the channel τ is much greater than the symbol period T_s of the transmitted signal.

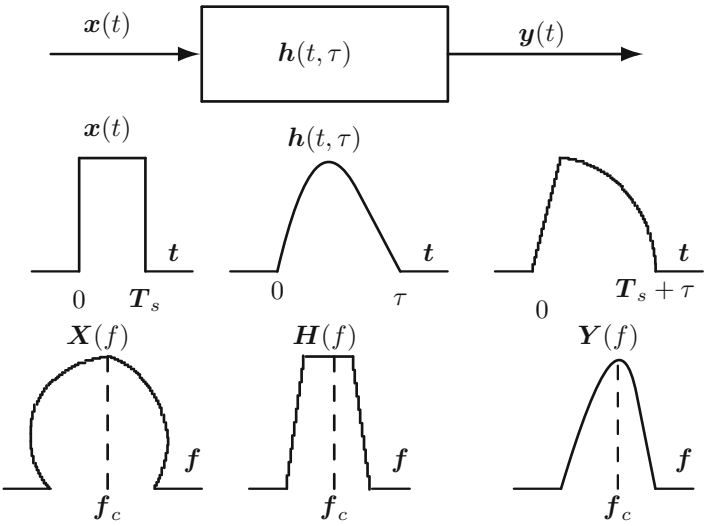

Fig. 2.4 Frequency-selective fading channel

In conclusion a signal is affected by a frequency selective channel if:

$$B_s \geq B_c \tag{2.3}$$

$$T_s \leq \sigma_\tau \tag{2.4}$$

We can consider a channel is frequency selective when $\sigma_\tau = 0.1T_s$

2.2.4 Doppler Shift

The propagation in the frequency domain due to a variation in the time domain, is caused by the movement of the transmitter or receiver. This variation in time domain is called Doppler Shift. Let f_d denote the Doppler shift of the received signal, where θ is the angle of arrival of the transmitted signal with respect to the direction of the vehicle. Given that f_c is the carrier frequency of the transmitted signal, the of the received signal is defined as:

$$f_d = \frac{\boldsymbol{v} f_c}{\boldsymbol{c}} \cos\theta \tag{2.5}$$

where $\boldsymbol{v}$ is the vehicle speed and $\boldsymbol{c}$ is the speed of light.

2.2.5 Rayleigh Channel Model

In 1968, Clarke [1] developed a model for writing the mobile radio channel by a random process. He assumes that the received signal is the sum of L plane waves. Due to the Doppler effect, the signal frequency is shifted (Fig. 2.5), the shift which depends on the speed of the mobile. The shift will follow the Eq. (2.5).

The electric field can then be expressed in terms of its components in phase and quadrature as follows:

$$E_y(t) = E^I(t)\cos(2\pi f_c t) - E^Q(t)\sin(2\pi f_c t) \tag{2.6}$$

where

$$E^I(t) = E_0 \sum_{n=0}^{L} \cos(2\pi f_n + \phi_n) \tag{2.7}$$

$$E^Q(t) = E_0 \sum_{n=0}^{L} \sin(2\pi f_n + \phi_n) \tag{2.8}$$

where E_0 is the amplitude of the transmitted field supposed constant. f_c is the carrier frequency and f_n, ϕ_n are the shifted frequency and the phase of the wave number n

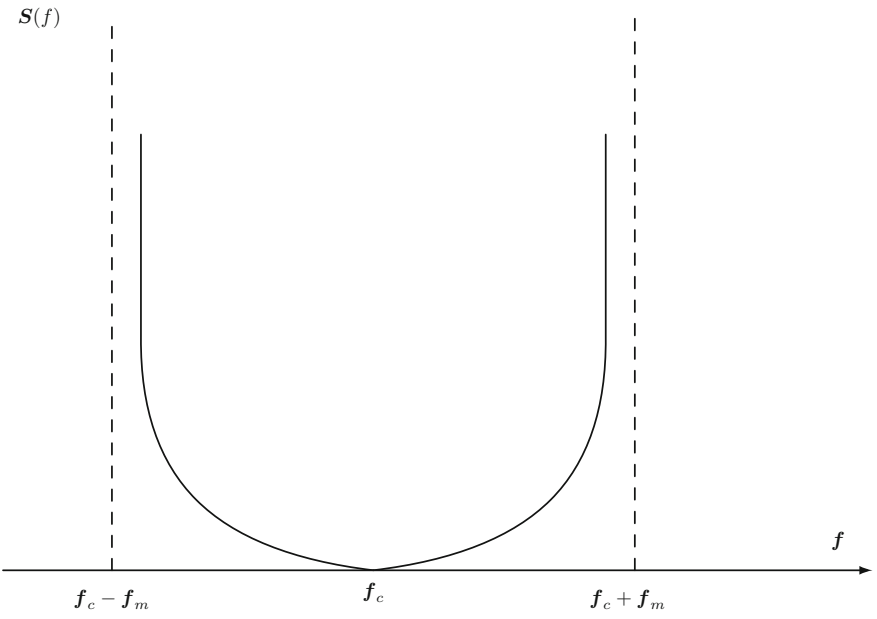

Fig. 2.5 Doppler spectrum

respectively. If the number of path L is large, ($L > 6$), according to the limit central theorem, $E^I(t)$ and $E^Q(t)$ are two random, Gaussian, and independent variable [2].

Thus, the channel coefficient $h_{n,k}$ could be considered as complex random Gaussian process. In an urban environment where the direct path is stopped by obstacles, the average of $h_{n,k}$ is null, and its variance is equal to $\sigma_h^2 = \frac{E_0^2}{2}$.

Let $h_{n,k}^I$ and $h_{n,k}^Q$ are the phase and the quadrature of $h_{n,k}$, The function of probability distribution of $h_{n,k}$ is:

$$f_H(h_{n,k}) = f_{H^I}(h_{n,k}^I) f_{H^Q}(h_{n,k}^Q) \tag{2.9}$$

$$= \frac{1}{2\pi\sigma_h^2} \exp\left[-\frac{(h_{n,k}^I)^2 + (h_{n,k}^Q)^2}{2\sigma_h^2}\right] \tag{2.10}$$

Then, the amplitude will follow the Rayleigh law. Assuming that all the reflectors have uniform distribution, Clarke showcases that the spectral density function will have the following shape: The autocorrelation function of $h_{n,k}$ is

$$\rho = E\left\{\boldsymbol{h}_k \left[\boldsymbol{h}_{k-l}\right]^*\right\} \tag{2.11}$$

$$= \sigma_h^2 \exp(j2\pi f_c l) J_0(2\pi f_m l T_s) \tag{2.12}$$

where J_0 is the Bessel function of 0 order.

2.2.6 Correlated Rayleigh Channel Generation

The most used method to generate the Rayleigh channel is that proposed by Clarke [1] in 1968. It consists in generating two identical, independent Gaussian process distribution and then filter them by identical two low pass filters with Frequency response $\boldsymbol{H}(f) = \sqrt{(\boldsymbol{S}(f))}$. This allows to filter correlated signals. The output of each filter is then injected in the inverse fast Fourier transform (IFFT) modules. The channel impulse response is then obtained as the sum of the two signals issued from the IFFT modules.

2.3 Transmission Channel in Information Theory

Messages, symbols, code words, signals, and electric waves Electromagnetic or optical used often in telecommunications, those are but a carriers to handle more fundamental and invariant entity called *information*. The information theory, introduced by Shannon in 1948, offers a basic mathematical tool to quantify this entity. The information produced by a source remains invariant with respect to messages and forms which serve as support transmission. Then it is obvious that the choice of

adequate message to present the good information is a critical element. The channel coding's role is to seek this adequate message to preserve the information quantity produced by a source. We present in this section, some notions and definitions of information theory and the famous fundamental theorem of Shannon.

2.3.1 Information Quantity, Entropy and Mutual Information

The idea of quantifying information, states that it is useless to send message if known by the receiver. This idea, however trivial, has totally defined the information quantity of a message, as a measure of its uncertainty. Thus, we can conclude that to be sure, the information quantity should be null, and uncertain event is more informative than a certain event.

Let $\boldsymbol{x}$ is the realization of an event with probability $\boldsymbol{Pr}(\boldsymbol{x})$. The intrinsic information quantity $\boldsymbol{h}(\boldsymbol{x})$ of this event will then, an increasing function of its improbability $1/\boldsymbol{Pr}(\boldsymbol{x})$, namely:

$$\boldsymbol{h}(x) = f[1/\boldsymbol{Pr}(\boldsymbol{x})] \tag{2.13}$$

where $f(.)$ is a croissant function which satisfy the following condition:

$$\lim_{Pr(\boldsymbol{x})\to 1} \boldsymbol{f}[1/\boldsymbol{Pr}(\boldsymbol{x})] = 0 \tag{2.14}$$

In addition, we hope that the joint observation of two independent events lead to an information equals to the sum of information obtained by observing individual of these two events as:

$$f(\boldsymbol{x}, \boldsymbol{y}) = f(\boldsymbol{x}) + f(\boldsymbol{y}) \tag{2.15}$$

where $\boldsymbol{x}$ and $\boldsymbol{y}$ are two events. The logarithm function well verify the conditions mentioned above. So, the Shannon defined the intrinsic information quantity of an event $\boldsymbol{x}$ by:

$$\boldsymbol{h}(\boldsymbol{x}) = \log_2[1/\boldsymbol{Pr}(\boldsymbol{x})] \tag{2.16}$$

$$= -\log_2[\boldsymbol{Pr}(\boldsymbol{x})] \tag{2.17}$$

This quantity is always positive (it is zero only if $\boldsymbol{x}$ is true). it tends to infinity if $\boldsymbol{Pr}(\boldsymbol{x})$ tends to zero. We note in Eq. (2.16), the base of the logarithmic function is 2, so we can use any base for the logarithm. However, the choice suggested by Shannon was the base 2 and the unit of the information quantity is the Shannon (Sh).

The intrinsic information by pairs of two event $\boldsymbol{x}$ and $\boldsymbol{y}$ of joint probability $Pr(\boldsymbol{x}, \boldsymbol{y})$ is given by:

$$h(\boldsymbol{x}, \boldsymbol{y}) = -\log_2[\boldsymbol{Pr}(\boldsymbol{x}, \boldsymbol{y})] \tag{2.18}$$

By the same way, the conditional information of $\boldsymbol{x}$ given $\boldsymbol{y}$, which accounts for the information quantity, remaining $\boldsymbol{x}$ subsequent to the observation $\boldsymbol{y}$, is defined by:

$$h(\boldsymbol{x}|\boldsymbol{y}) = -\log_2[\boldsymbol{Pr}(\boldsymbol{x}|\boldsymbol{y})] \tag{2.19}$$

We define the mutual information of two events $\boldsymbol{x}$ and $\boldsymbol{y}$ by:

$$i(\boldsymbol{x}, \boldsymbol{y}) = \log_2\left[\frac{\boldsymbol{Pr}(\boldsymbol{x}|\boldsymbol{y})}{\boldsymbol{Pr}(\boldsymbol{y})}\right] \tag{2.20}$$

This function accounts the average information quantity, how big the knowledge of an event $\boldsymbol{y}$ can apport to an event $\boldsymbol{x}$. This quantity is also symmetric since it measures the information that knowledge the event $\boldsymbol{x}$ how can yield on the information contained in $\boldsymbol{y}$.

Let S be a source, emitting symbols from the alphabet $s_1, s_2, \ldots, s_n$, having each a probability $\boldsymbol{Pr}(s_i)$. When the source is stationary, we can define the mean produced by this source, also called *entropy*. The entropy is then given by:

$$\boldsymbol{H}(S) = E\{h(s_i)\} \tag{2.21}$$

$$= -\sum_{i=1}^{n} \boldsymbol{Pr}(s_i)\log_2[\boldsymbol{Pr}(s_i)] \tag{2.22}$$

2.3.2 Shannon Paradigm

In order to study a system of communication in information theory Shannon adopts the simplified chain, as in Fig. 2.6. This figure presents the Shannon paradigm [3]. The source transmit unknown messages through a disturbed channel. The receiver, who has only the disturbed message at the output of the channel, He try to take a decision

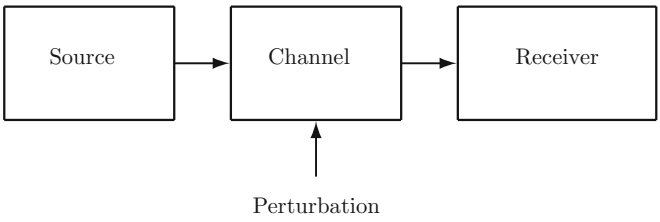

Fig. 2.6 Shannon paradigm

of the issued signal. He then makes "*Assumptions*" about the message issued and chooses the most likelihood. Let denote by $\boldsymbol{X}$ and $\boldsymbol{Y}$ random variables taking values in $\{x_1, x_2, \ldots, x_n\}$ and $\{y_1, y_2, \ldots, y_m\}$ which represent respectively the message transmitted by the source and the message received. An important quantity associated to this pair of random variables is the average mutual information defined by:

$$I(\boldsymbol{X}, \boldsymbol{Y}) = \boldsymbol{E}\{i(\boldsymbol{x}_k, \boldsymbol{y}_l)\} \tag{2.23}$$

$$= -\sum_{k=1}^{n} \sum_{m}^{l=1} \boldsymbol{Pr}(\boldsymbol{x}_k, \boldsymbol{y}_m) \log_2 \frac{\boldsymbol{Pr}(\boldsymbol{x}_k, \boldsymbol{y}_m)}{\boldsymbol{Pr}(\boldsymbol{x}_k)\boldsymbol{Pr}(\boldsymbol{y}_l)} \tag{2.24}$$

The average can also be written as

$$I(\boldsymbol{X}, \boldsymbol{Y}) = H(\boldsymbol{X}) - H(\boldsymbol{X}|\boldsymbol{Y}) \tag{2.25}$$

$$= H(\boldsymbol{Y}) - H(\boldsymbol{Y}|\boldsymbol{X}) \tag{2.26}$$

$$= H(\boldsymbol{X}) + H(\boldsymbol{Y}) - H(\boldsymbol{X}, \boldsymbol{Y}) \tag{2.27}$$

We could interpret the above equation as: The average is equal to the transmitted "information", reduced by the remaining indetermination between the transmitted and issued symbol.

2.3.3 Channel Capacity

The is a tool to measure the ability of a channel to transmit information. The capacity $\boldsymbol{C}$ of a channel is defined as the maximum of the average mutual information $\boldsymbol{I}(X, Y)$ associated with its input and its output, namely:

$$\boldsymbol{C} = \max_{\boldsymbol{Pr}(\boldsymbol{x})} I(\boldsymbol{X}, \boldsymbol{Y}) \tag{2.28}$$

The channel capacity represents the maximum information that can be transferred through a channel. According to the Eq. (2.28), this maximum is defined with respect to the distribution probability of the transmitted messages.A "good" choice of this

distribution and messages carrying the information will be an important factor in achieving or approaching this capability. Thus, it was proposed to interpose a "module" between the source and the channel to define the best forms of messages conveying information. This module is said encoder of the emitted information and the mechanism is called channel coding.

2.4 Conclusion

The Channel is an important element of the transmission chain. It often acts as a disturbing element which changes the transmitted signal. In digital communication, we are interested in studying and "fixing" the channel effects on the statistics and the shape of the issued signal. This requires channel modeling of its variations in time and frequency. Several studies have proposed mathematical models and statistics to characterize and simulate mobile radio channels. The first section of this chapter has been devoted to the description of mobile radio channel in digital communication.

In information theory, the notion of the channel takes on another meaning. In fact, this theory concerned with the amount of information carried by the issued message. Thus, the transmission channel is seen as a factor that degrades the amount of transmitted information. The quantification of information was introduced by in [3]. We saw, in this chapter, a channel is characterized in information theory by its capacity, which represents the maximum information that can be transmitted via this channel. To be in edge of the theoretical limit, the channel coding is often required. This will be the focus of the next chapter by introducing the channel coding in MIMO-OFDM systems.

References

1. Clarke R (1968) A statistical theory of mobile radio reception. Bell Syst Tech J 47:957–1000
2. Jakes WC (1974) Microwave mobile communications. Wiley, New York
3. Battail G (1997) Theorie de l'information: application aux techniques de communication. Masson, Paris

Chapter 3
Code Design for MIMO-OFDM System

3.1 Introduction

Future broadband wireless systems will provide extreme high data rate and better performance over time-selective and frequency-selective channel. To support this high speed data transmission and high performance, two powerful technologies, namely, multiple-input multiple-output (MIMO) antennas and orthogonal frequency division multiplexing (OFDM) modulation are combined together. The first one which is MIMO technology provides transmission of different information simultaneously over wireless channel through multiple antennas, thereby boosting the system throughput. The second one that is OFDM system divides the transmitted information bits into many different sub-blocks and sends them over a large number of closely spaced different sub-channels. Therefore, MIMO-OFDM has the potential to achieve more reliable performance at higher data rate since MIMO can boost the capacity and the diversity and OFDM can mitigate the detrimental effects due to multipath fading. In this chapter, an overview of space-time (ST), space frequency (SF), and space-time-frequency (STF) as well as a systematic design of high rate full diversity SF and STF coding for multiuser MIMO-OFDM is reported full diversity of SF code design criteria is derived.

MIMO-OFDM systems offer huge freedoms in space, time, and frequency. Therefore, ST, SF, and STF can be applied to exploit the maximum diversity from MIMO channels. Space-time (ST) coding is a potent scheme that can improve the reliability of data transmission in MIMO systems. It encodes a data stream across different transmit antennas and time slots, so that multiple redundant copies of the data stream can be transmitted through independent fading channels. It combines coding with transmit diversity to achieve high diversity performance in wireless systems. Such a

B. Ahmed and M. Abdul Matin, *Coding for MIMO-OFDM in Future Wireless Systems*, SpringerBriefs in Electrical and Computer Engineering,
DOI 10.1007/978-3-319-19153-9_3

coding scheme in general can be classified into two major classes: ST trellis codes and ST block codes. This coding scheme is effective in flat-fading channels only. However, the MIMO channels experience frequency-selective fading, which complicates the design of ST codes because of ISI.

The full diversity SF code design criteria were derived in [1]. To exploit the full diversity in MIMO multipath fading channels, an SF code design approach was proposed by multiplying the input information stream with a part of the DFT matrix. Though the resulting SF codes can achieve full diversity, a large bandwidth efficiency loss has occurred. The symbol rate is not more than $1/(A_t, L)$. In [2] a systematic design of full diversity SF block codes (SFBC) was proposed. By repeating each row of the ST codes matrix on L different subchannels of the same OFDM block, the SF codes provide higher data rates than the approach described in [1]. However, the main drawback is that they cannot achieve a rate larger than *1/L*.

The design of full diversity SFBC with rate-1 was recently proposed in MIMO-OFDM systems for any number of transmit antennas and arbitrary power delay profiles [3]. Recently, a systematic design of high rate SFBC was proposed to achieve the rate-A_t and the full diversity in MIMO-OFDM systems for any number of transmit antennas [4]. However, because a zero-padding matrix has to be used when $N$is not an integer multiple of $A_t L$, the symbol transmission rate A_t cannot always be guaranteed. To address this issue, a universal design of SFBC, as a special case of STF coding, was then proposed in [5] that can always achieve the rate-A_t and the full diversity for any number of transmit antennas and any arbitrary channel power delay profiles. It is constructed by applying the layering concept, which was used in the design of threaded algebraic space-time (TAST) code [6], with algebraic component codes, where each component code is assigned to a "thread" and interleaved over space and frequency.

STF codes have been proposed for exploiting multipath diversity in MIMO-OFDM systems over quasi-static channels [1, 7–9]. The performance of STF codes in MIMO-OFDM systems was also recently studied for a variety of system configurations and channel conditions in [7]. It was shown that the maximum diversity is the product of time diversity, frequency diversity, and space diversity [9]. Recently, a systematic design of high-rate STF codes was proposed for MIMO frequency-selective block-fading channels in [5]. By spreading the algebraic coded symbols across different OFDM subchannels, transmit antennas, and fading blocks, the proposed STF codes can achieve a rate-A_t and a full diversity of $A_t A_r A_u L$, where is the number of independent fading blocks in the codewords.

The performance comparison among aforementioned ST coding, SF coding and STF coding approaches for MIMO-OFDM systems is presented in Table 3.1.

Table 3.1 Performance comparison among ST/SF/STF-Coded OFDM

Coding approach	Code rate	Diversity gain
ST-OFDM [10]	1	$A_t A_r$
ST-OFDM [11]	$1 : L$	$A_t A_r L$
SF-OFDM [2]	$1 : L$	$A_t A_r L$
SF-OFDM [12]	1	$A_t A_r L$
SF-OFDM [5]	A_t	$A_t A_r L$
STF-OFDM [13]	1	$A_t A_r A_u L$
STF-OFDM [10]	A_t	$A_t A_r A_u L$
SF-OFDM [14]	A_t	$A_t A_r L$ for each user
SF-OFDM [15] for multiuser MIMO-OFDM	1	$A_t A_r L$ for each user
STF-OFDM [16] for multiuser MIMO-OFDM	A_t	$A_t A_r A_u L$ for each user

3.2 Symbols and Notations

Throughout this chapter, the following notations are being used. Z, Q and C stands for the integer ring, the rational number field, and complex number field respectively. $Q(J)$ represents the field generated by j and rational where $j = \sqrt{-1}$. $Z[j]$ denotes the field generated by the j and integer ring. $[x]$ represents the smallest integer larger than x. $[x]$ represents the largest integer smaller then x. The subscripts T and H denotes the transpose and Hermitian of a complex matrix respectively. $\otimes$ and $\circ$ denotes the kronecker and Hadamard product respectively.

3.3 System Model

Consider in a single-cell network the MIMO-OFDM system has Z users of which each user is equipped with A_t transmit antennas while base station (BS) has A_r receive antennas and N-tone OFDM (Fig. 3.1). The channels experiences wideband multi-path fading induced by L independent paths between each transmit-receive antennas. The multiuser MIMO channels are subject to the following assumptions:

- All channels are subject to block-fading; that means the channel gains between each pair of transmit and receive antennas are constant over one fading block, but varies independently in another fading block. Each OFDM symbol is transmitted during the fading block d, where $d = 1, \ldots, A_u$.
- All path gains between any pair of transmit and receive antennas during any fading block follow the same power profile, $E[|h_{m,n}(a)|^2] = \delta_a^2 > 0$.

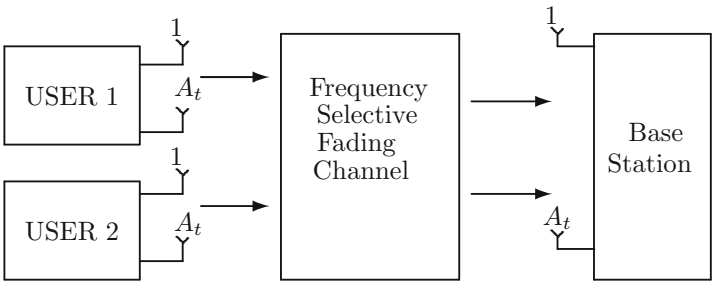

Fig. 3.1 Multiuser MIMO-OFDM System

- The fading channel for any pair of transmit and receive antenna is assumed to be given by, n

$$h_{m,n}(t) = \sum_{a=0}^{L-1} h_{m,n}(a)\delta(t-\tau_a) \text{ for, m} = 1, \ldots, \text{A}_r; \text{ n} = 1, \ldots, \text{A}_t \text{ and z} = 1, \ldots, \text{Z}; \tag{3.1}$$

where n is the transmit antenna of user z and m is the receive antenna of BS during the fading block d. τ_a is the ath path delay and each $h_{m,n}(a)$ denotes the channel coefficient of ath the path from the transmit antenna n to the receive antenna m. $\delta(t-\tau_a)$ represents the unit impulse function that determines the specific multi-path bins that have components at time t and excess delay τ_a.

- MIMO channels are to be spatially uncorrelated. The statistics of the channel $h^d_{m,n}(t)$ are given by δ^2_a and τ_a, for, $a = 0, 1, 2 \ldots, L-1$ and is assumed that the average path delay is known at the transmitter. The system has been developed for the coherent scenario where the channel state information (CSI) $h_{m,n}(a)$ is perfectly known at the receiver.
- All path gains between any pair of transmit and receive antennas during any fading block follow the same power profile $E[|h_{m,n}(a)|^2] = \delta^2_a > 0$.
- Moreover, it is assumed that

Let,

$$h_{m,n}(t) = [h^z_{m,n}(0), \ldots, h^z_{m,n}(L-1)] \tag{3.2}$$

for, $m = 1, A_r$; and $n = 1, Z$; denote the complex channel between the n-th transmit antenna of user z and m-th receive antenna of BS. $H^{(z)}_{m,n}$ denotes the frequency response of the channel from the n-th transmit antenna of user z to the m-th receive antenna of BS during fading block d. It can be given by the DFT of the channel impulse response as follows,

$$H^{(z)}_{m,n} = F[h^z_{m,n}] \tag{3.3}$$

where, the partial DFT matrix can be given by

$$F = [f^{\tau_0}, \ldots, f^{\tau_{L-1}}] \tag{3.4}$$

And

$$H_{m,n}^{(z)} = \left[H_{m,n}^{(0)}, \ldots, H_{m,n}^{(N-1)}\right]^T \tag{3.5}$$

The column vector f is given by, $f = [1, \zeta, \ldots, \zeta^{N-1}]$ and $\zeta = \exp(\frac{-j2\pi}{T_s})$. Where T_s denotes the duration of one OFDM symbol.

The source generates a block of N_s information symbols S which are QAM from the discrete alphabet τ. The information symbol vector $S \in \mathcal{T}^{\mathcal{N}_f}$ is encoded into $N \times A_t$ code matrix $C^{(z)} \in \mathcal{T}^{N \times A_t}$. The symbol rate of the code matrix is given by $\mathcal{R} = \frac{N_s}{N}$.

The system is developed for the coherent scenario where the channel state information (CSI) $h_{m,n}(a), a = 0, 1, \ldots, L-1$ is perfectly known at the receiver which is stated earlier. The statistic of the channel is given by δ_a^2 and τ_a where $a = 0, 1, \ldots, L-1$ and is known at the transmitter (i.e. τ_a). Assuming for user z, the OFDM symbol $X_n^{(z)}$ transmitted from the nth transmit antenna and assuming each user has N-tone OFDM the codeword $C^{(z)}$ can be written as $C^{(z)} = \left[X_1^{(z)} \ldots X_{A_t}^{(z)}\right]$.

Assume that each user uses N-pt OFDM and transmits the OFDM symbol $X_n^{(z)}$ through the nth transmit antenna of user z. At the BS, the received signal in the frequency domain can be given by Two codeword, $C^{(z)}$ and $C^{(z')}$ of two different users z and z' are assumed to be independent. Assume that the perfect synchronization is available at the receiver. Then the received signal at the base station can be given by

$$Y_m = \sum_{n=1}^{A_t} \sum_{z=1}^{Z} diag\left(X_n^{(z)}\right) H_{m,n}^{(z)} + n_m \tag{3.6}$$

where,

- $Y_m = \left[Y_m^{(z)}(0)\, Y_m^{(z)}(1) \ldots Y_m^{(z)}(N-1)\right]^T$, $n_m \mathcal{T}^N$ is Additive White Gaussian Noise (AWGN) with zero mean and covariance $N_0 \mathrm{I_N}$
- $Y_m \in \mathcal{T}^N$ is the received signal at the mth antenna of base station.

Using (3.3) and (3.6) we get,

$$Y_m = \sum_{n=1}^{A_t} \sum_{z=1}^{Z} diag\left(X_n^{(z)}\right) F h_{m,n}^{(z)} + n_m \tag{3.7}$$

$$= \sum_{n=1}^{A_t} \sum_{z=1}^{Z} diag\left(X_n^{(z)}\right) \sum_{a=0}^{L-1} f^{\tau_l} h_{m,n}^{(z)}(a) + n_m \tag{3.8}$$

Let

$$E_a = diag(f^{\tau_a}) \tag{3.9}$$

$$E_a X_n^{(z)} = diag\left(X_n^{(z)}\right) f^{\tau_a} \tag{3.10}$$

Substituting (3.9) in (3.7), we get

$$Y_m = \sum_{n=1}^{A_t} \sum_{z=1}^{Z} \sum_{a=0}^{L-1} E_a X_n^{(z)} h_{m,n}^{(z)}(a) + n_m \tag{3.11}$$

Let, $h_m^{(z)}(a) = \left[h_{m,1}^{(z)}(a) \ldots h_{m,A_t}^{(z)}(a)\right]^T$; again as $C^{(z)} = \left[X_1^{(z)} \ldots X_{A_t}^{(z)}\right]$ from (3.11) we get

$$Y_m = \sum_{z=1}^{Z} \sum_{a=0}^{L-1} E_a C^{(z)} h_m^{(z)}(a) + n_m \tag{3.12}$$

Let,

$$P^{(z)} = \left[E_0 C^{(z)} \ldots E_{L-1} C^{(z)}\right] \tag{3.13}$$

And, $h_m^{(z)} = \left[h_m^{(z)}(0) \ldots h_m^{(z)}(L-1)\right]^T$. Then, $Y_m = \sum_{z=1}^{Z} p^{(z)} h_m^{(z)} + n_m$ Let,

$$P = \left[p^{(1)} \ldots p^{(Z)}\right] \tag{3.14}$$

and

$$h_m = \left[h_m^{(1)} \ldots h_m^{(Z)}\right]^T \tag{3.15}$$

We have,

$$Y_m = P h_m + n_m \tag{3.16}$$

Moreover, using the following notations: $Y = \left[Y_1^T \ldots Y_{A_r}^T\right]^T$, $h = \left[h_1^T \ldots h_{A_r}^T\right]^T$, $n = \left[n_1^T \ldots n_{A_r}^T\right]^T$ and $X = \mathrm{I}_{\mathrm{A_r}} \otimes P$

$$Y = \sqrt{\frac{\rho}{A_t}} X h + n \tag{3.17}$$

$\sqrt{\frac{\rho}{A_t}}$ ensures that the SNR at each receive antenna ρ, independently of the transmitter A_t. A systematic design of multiuser SF codes for MIMO frequency-selective fading MAC is presented based on the code design criteria.

3.4 Code Design Criteria

The criterion for space-time/ frequency is based on the error event analysis which was first discussed in [17]. Following this, a ST code design criteria for multiple access channel has been established in [18], but it was only for two users. Addressing this issue, a systematic design of full diversity SF codes for any number of users has been considered in [15]. Depending on the desired transmission rate tuple for two users, dominant error event regions for the two users MAC was discussed [17]. It was shown that for the rate region with user-1 or user-2 is in error, and then the well known single user ST/SF codes are sufficient. But, for the rate region where both users are in error, a joint code design is necessary for optimization, i.e.:- to get full-diversity for any error event. Moreover, the code design criteria were based on high-SNR and low-SNR region. As, the effect is less pronounced for low SNR, the code design criteria for SF code MAC is based on the high-SNR region.

is given as,

$$P\left(C^{(z)} \to \hat{C}^{(z)} | H\left(e^{j\frac{2\pi}{N}i}\right)\right) = Q\sqrt{\frac{E_s}{2\sigma_n^2} d^2\left(C^{(z)}, \hat{C}^{(z)} | H\left(e^{j\frac{2\pi}{N}i}\right)\right)} \tag{3.18}$$

where, the squared Euclidian distance between the codeword $C^{(z)}$ and $(\breve{C})^{(z)}$ noted by

$$d^2\left(C^{(z)}, \hat{C}^{(z)} | \bar{H}\right) = \left\| \left(I_{A_r} \otimes \breve{C}^{(z)}\right) \bar{H} \right\|^2 \tag{3.19}$$

where $\bar{H} = H\left(e^{j\frac{2\pi}{N}i}\right)$, using $Q(x) \leq e^{\frac{-x^2}{2}}$ we get:

$$P\left(C^{(z)} \to \hat{C}^{(z)} | \bar{H}\right) \leq e^{\frac{-E_s}{4\sigma_n^2} d^2\left(C^{(z)}, \hat{C}^{(z)} | \bar{H}\right)} \tag{3.20}$$

Denoting, $\rho = \frac{E_s}{\sigma_n^2}$ as SNR, the (3.20) can be written as,

$$P\left(C^{(z)} \to \hat{C}^{(z)} | \bar{\mathrm{H}}\right) \leq e^{\frac{-\rho}{4}\left\| \left(I_{A_r} \otimes \breve{C}^{(z)}\right) \bar{H} \right\|^2} \tag{3.21}$$

As every Eigen value of the $A_t \times A_t$ matrix $\left(C^{(z)} - \hat{C}^{(z)}\right)\left(C^{(z)} - \hat{C}^{(z)}\right)^T$ is an Eigen value of $A_t A_r \times A_t A_r$ matrix, $\left[\left(C^{(z)} - \hat{C}^{(z)}\right)\left(C^{(z)} - \hat{C}^{(z)}\right)^T\right] \times I_{A_r}$ (with multiplicity A_r).

Let, $R^{(z)} = I_{A_r} \otimes \left(\breve{C}^{(z)^H} \breve{C}^{(z)} \right)$ and then using singular value decomposition, we get $R^{(z)} = U^H \Lambda U$, where, $\Lambda = \text{diag}\left(\lambda_1, \ldots, \lambda_{\mathrm{W_L W_t A_r}}\right)$ with, $\lambda_{\mathrm{f}} \geq 0$ for $\mathrm{f} = 1, 2, \ldots, \mathrm{w_L w_t A_r}$ where,

$$\mathrm{w_L} = 2^{\lceil \log_2 \mathrm{L} \rceil} \mathrm{W_t} = 2^{\lceil \log_2 \mathrm{A_t} \rceil}$$

Therefore, $\left\| \left(I_{A_r} \otimes \breve{C}^{(z)} \right) \bar{H} \right\|^2 = \bar{H}^H U^H \Lambda \mathrm{U} \bar{H}$ Let, $\bar{\gamma} = \mathrm{U}\bar{H}$ and $\bar{\gamma}_{\mathrm{f}}$ denotes the fth element of the vector $\bar{\gamma}$ then

$$\left\| \left(I_{A_r} \otimes \breve{C}^{(z)} \right) \bar{H} \right\|^2 = \sum_{f=1}^{W_L W_t A_r} \lambda_f |\gamma_f|^2 \tag{3.22}$$

Substituting (3.22) into (3.21) we get,

$$P\left(C^{(z)} \to \hat{C}^{(z)} | \bar{H}\right) \leq e^{-\left(\frac{\rho}{4} \sum_{f=1}^{W_L W_t A_r} \lambda_f |\gamma_f|^2\right)} \tag{3.23}$$

Taking the expectation of (3.23), we get,

$$P\left(C^{(z)} \to \hat{C}^{(z)}\right) \leq \prod_{f=1}^{r} \left(\frac{1}{1 + \rho \frac{\lambda_f}{4}} \right) \tag{3.24}$$

where r is the rank of the matrix $R^{(z)}$. As our SF code design criteria is based on high-SNR thus for high-SNR, $\rho \ggg 1$ thus (3.25) reduced to,

$$P\left(C^{(z)} \to \hat{C}^{(z)}\right) \leq \left(\frac{\rho}{4}\right)^{-r_z} \prod_{f=1}^{r_z} \frac{1}{\lambda_f} \tag{3.25}$$

Simplifying the equation, we get,

$$P\left(C^{(z)} \to \hat{C}^{(z)}\right) \leq \rho^{-r_z} \prod_{f=1}^{r_z} \frac{1}{\lambda_f} \tag{3.26}$$

For 2-user system, let, 2-users transmitted codeword denoted by, $C = \left[C^{(1)} C^{(2)}\right]$. Let, $\hat{C}$ denotes the detected codeword. Three types of error event such as type-1, type-2, type-3 are assumed, where type-1 and type-2 represents the error events when user-1 or user-2 is in error, and type-3 represents the error events when more

than one user are in error [19]. Thus for given $\bar{H}$, the total average pair wise error probability is given by

$$P_e = P_{e1} + P_{e2} + P_{e3} \tag{3.27}$$

where $P_{eq} = E\left[P_{eq}|\bar{H}\right]$ and $\left[P_{eq}|\bar{H}|\right]$, for q = 1, 2, 3. The three terms in (3.27) depicts all error events when the pair wise error $C \neq \hat{C}$ occurs. The first and second term denotes the probability of the error event that only the first or second users are in error. The last term represent the probability of the error events that both users are in error. Now,

$$P_{e1} \leq \left(\rho^{-d_1}\right)\left(\prod_{f=1}^{d_1}\frac{1}{\lambda_f}\right)(1-\beta_1)\,\beta_2 \tag{3.28}$$

Similarly,

$$P_{e2} \leq \left(\rho^{-d_2}\right)\left(\prod_{f=1}^{d_2}\frac{1}{\lambda_f}\right)(1-\beta_2)\,\beta_1 \tag{3.29}$$

And,

$$P_{e3} \leq \left(\rho^{-d_3}\right)\left(\prod_{f=1}^{d_3}\frac{1}{\lambda_f}\right)(1-\beta_1)\,(1-\beta_2) \tag{3.30}$$

where the inequality is obtained from the PEP of a single user codeword given in (3.26) with $[d_q]$ being the diversity gain, and $\prod_{f=1}^{d_q}\frac{1}{\lambda_f}$ being the coding gain specifically,

$d_q = A_r.\min_{\forall C^{(z)} \neq \hat{C}^{(z)}} rank\left(\breve{C}^{(z)}\right)$, for q = 1, 2, 3, and, for z = 1, 2

Zang and Letaief showed that single user SF codes are not optimal for multi-user system because the optimal code should achieve full diversity for all of the cases given in (3.28), (3.29) and (3.30) [15]. Thus for MAC, joint code design is necessary. For a general case of Z users, let, the code word $C = \left[C^{(1)}C^{(2)}\ldots C^{(z)}\right]$ and $\hat{C}$ denotes the detected code word. Assume $\breve{C} = C - \hat{C}$ and $\breve{C}^{(z)} = C^{(z)} - \breve{C}^{(z)}$. Then, the probability of symbol error can be upper bounded as [15],

$$P_e \leq \sum_{|D|=1}\left(\rho^{-r_1}\right)\left(\prod_{f=1}^{r_1}\frac{1}{\lambda_f}\right)(P(|D|=1)) + \cdots + \sum_{|D|=Z}\left(\rho^{-r_Z}\right)\left(\prod_{f=1}^{r_Z}\frac{1}{\lambda_f}\right)(P(|D|=Z)) \tag{3.31}$$

where, $\mathrm{D} = \left\{ z | \, C^{(z)} \neq \hat{C}^{(z)} \right\}$ *and for* $C \neq \hat{C}, |D| \geq 1 . r_w \, (w = 1, \ldots, Z)$ is the rank of the matrix

$$R = I_{A_r} \otimes \left(\breve{C}^{H} \breve{C} \right)$$

where only w out of Z user have $\breve{C}^{(z)} \neq 0$ and the probability that only w out of Z users have $C^{(z)} \neq \hat{C}^{(z)}$ is denoted by $P \, (|D| = w)$. Now, P_{eq} is dominated by the codeword difference matrices with minimum rank [20]. As r_w denotes the diversity order of the error event when w out of Z users are in error, the full-diversity for every error event should be guaranteed by the code design. Thus in this coherent scenario, the code design criteria of full diversity SF codes for MAC over MIMO frequency-selective block-fading channels as follows:

3.4.1 Rank Criterion

Maximize the transmit diversity gain,

$$r_w = A_r . rank \left(C - \widehat{C} \right) \tag{3.32}$$

over all pairs of distinct codeword C and $\hat{C}$ when only w out of Z users have for $\mathrm{w} = 1 \ldots \mathrm{Z}$.

3.4.2 Block Fading Product Criterion

Maximize the coding gain;

$$C_w = \prod_{f=1}^{r_w} \lambda_f \tag{3.33}$$

over all pairs of distinct codeword C and $\hat{C}$ when only w out of Z users have for $\mathrm{w} = 1 \ldots \mathrm{Z}$.

3.5 Multiuser Space-Frequency Code Design

Gartner and Bolcskei in [?] show that joint code designs are necessary whenever multiple users transmit concurrently at high rates. Otherwise, employing the traditional single-user ST/SF codes for each of the users is optimal. But their work is limited to a 2-user case only and no explicit systematic code design was given. Based on this concept, Zhang and Letaief propose a systematic design of SF codes to achieve the full diversity when multiple user error dominates. The achievable gain can be

up to $A_r A_t L$ for every user, where A_t and A_R denote the number of transmit and receive antennas, respectively, and L denotes the number of independent channel taps. However, the transmit rate of each user is limited to 1. Therefore, in [14], an idea of high-rate SF codes is presented and increase the transmit rate to A_t per user. In this section, a systematic design of full diversity $A_r A_t L$ and high code rate (i.e. rate-A_t) has been proposed. Few examples of the proposed multi-user SF codes have also been given. The SF code has been constructed by applying threaded layering concept which was first used in the design of threaded algebraic space-time (TAST code). Utilizing the duality space-frequency coding in frequency-selective channel is constructed from space-time coding in time-selective channel. The design of full diversity $A_r A_t L$ and high rate A_t SF codes has been shown in Fig. 3.2. It is assumed the system has N-OFDM tones. Let

$$Q = W_Z W_L W_t$$

where, $W_L = 2^{\lceil \log_2 L \rceil}$, $W_t = 2^{\lceil \log_2 A_t \rceil}$, $W_Z = 2^{\lceil \log_2 Z \rceil}$, A block of NA_t information symbols $S^{(z)} = [{S_1}^{(z)} {S_2}^{(z)} \ldots {S_{BQ}}^{(z)}]^T$. Where, $S^{(z)} \in \mathcal{T}^{NA_t}$, and S is a constellation are normalized into the unit power and are evenly splitting into $B = \frac{N}{Q}$ subblocks,

$$S^{(z)} = \left[\left({S_1}^{(z)} \right)^T \left({S_2}^{(z)} \right)^T \ldots \left({S_B}^{(z)} \right)^T \right]^T \tag{3.34}$$

Each sub block ${S_b}^{(z)} \in \mathcal{T}^{W_Z A_t W_L W_t}$, where $b = 1, 2, \ldots, B$, is composed of the signal vectors ${S_w}^{(z)} \in \mathcal{T}^{\tilde{w}}$, $w = 1, 2, 3, \ldots$, and $\tilde{w} = W_Z W_L A_t$. The signal vector is composed of QAM symbols. Thus,

$$ {S_b}^{(z)} = \left[\left({S_1}^{(z)} \right)^T \left({S_2}^{(z)} \right)^T \ldots \left({S_{w_t}}^{(z)} \right)^T \right]^T \tag{3.35}$$

Each one of the component vector is than encoded independently using constituent encoder, where, is the output alphabet and given by

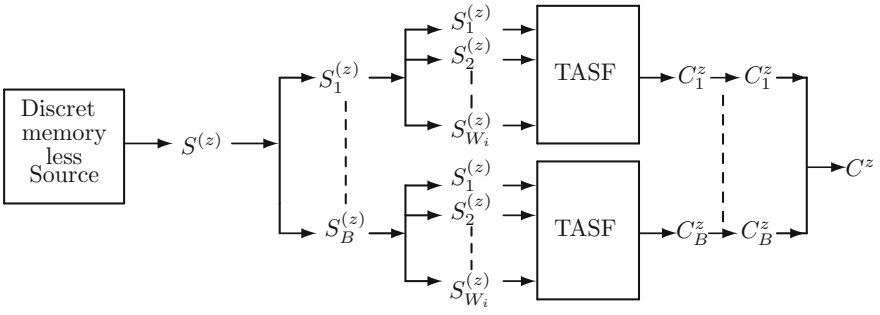

Fig. 3.2 SF coding structure in MIMO-OFDM system

$$\bar{X}_w^{(z)}\left(S_w{}^{(z)}\right) = \phi_{1,w}\Theta S_w{}^{(z)} \tag{3.36}$$

$$= \phi_{1,w}\bar{X}_w^{(z)} \tag{3.37}$$

where Θ, is an $\tilde{w} \times \tilde{w}$ unitary matrix () and it is constructed by the first principal matrix of the following matrix:

$$\psi = F_{\tilde{y}}^H diag\left(1, \varphi, \ldots, \varphi^{\tilde{y}}\right) \tag{3.38}$$

where, $\tilde{y} = 2^{\lceil \log_2 \tilde{w} \rceil}$, $F_{\tilde{y}}$ is the $\tilde{y} \times \tilde{y}$ discrete Fourier transform (DFT) matrix and $\varphi = e^{\left(\frac{j2\pi}{4\tilde{y}}\right)}$. $\phi_{1,w}$ is the Diophantine number, and are chosen to ensure full diversity and maximize the for the joint code. Here, $\phi_1 = \theta^{\frac{1}{W_t}}$, where θ is an algebraic clement with degree at least $W_L W_t$ over $\mathcal{A}$. $\mathcal{A}$ is the extension of $\mathbb{Q}$ which contains the signal alphabet $\mathcal{T} \subset \mathbb{Z}[]$, all the entries of Θ and $e^{\frac{-j2\pi\tau_l}{T_s}}$ $(l = 0, 1, \ldots, \mathrm{L}-1)$.

Each $\phi_{1,w}$ is chosen from the wth diagonal layer of the $W_t \times A_t$ matrix.

$$\Phi_1 = \begin{pmatrix} 1 & \phi_1{}^{(w_t-1)} & \ldots & \phi_1{}^{(w_t-A_t)+1} \\ \phi_1 & 1 \ldots & & \phi_1{}^{(w_t-A_t)+2} \\ \phi_1{}^2 & \phi_1 \ldots & & \vdots \\ \vdots & \vdots \ddots & & \vdots \\ \phi_1{}^{(w_t-1)} & \phi_1{}^{(w_t-2)} & \ldots & \phi_1{}^{\left(1-\frac{A_t}{W_t}\right)W_t} \end{pmatrix}$$

From (3.36) after multiplying with $S_w{}^{(z)}$ the rotational matrix Θ we get $\bar{X}_w^{(z)} = \left[X_w{}^{(z)}(1)\, X_w{}^{(z)}(2) \ldots X_w{}^{(z)}(\tilde{w})\right]$

$$= \left[\bar{x}_{w,1}^{(z)} \ldots \bar{x}_{w,w_L}^{(z)}\right]^T \tag{3.39}$$

$$= \Theta S_w{}^{(z)}. \tag{3.40}$$

It is worth noting that, multiplying information symbol vector $S_w{}^{(z)}$ by the rotational matrix Θ maximize the associated minimum product distance.

$$d_{\tilde{w}} \stackrel{\Delta}{=} \min_{\bar{X}^{(z)}=\Theta\left(S^{(z)}-S'^{(z)}\right), S^{(z)} \neq S'^{(z)}} \prod_{w=1}^{\tilde{w}} \left|\bar{X}_w^{(z)}\right|, \text{ where } \bar{X}^{(z)} = \left[\bar{X}_1^{(z)} \bar{X}_2^{(z)} \ldots \bar{X} w_t{}^{(z)}\right]^T$$

As coding gains are proportional to the minimum product distances associated with the rotational matrix used, the maximization of the coding gain in the code design criteria is achieved. In (3.39), the terms $\bar{\chi}_{w,i}^{(z)}$ is given by,

$$\bar{\chi}_{w,i}^{(z)} = \left[X_w{}^{(z)}\left(P_i{}^l + 1\right) \ldots X_w{}^{(z)}\left(P_i{}^l + A_t\right)\right] \tag{3.41}$$

For $i = 1, 2W_L$, where the index, ${P_i}^l = (i-1)\,A_t + (l-1)W_L A_t$ and $l = 1, 2, \ldots, W_Z$. Next, a space-frequency formatter $f_W\left(\bar{X}_w^{(z)}\left({S_w}^{(z)}\right)\right)$ assigns the wth code symbols ${X_w}^{(z)}\left({P_i}^l + n\right), n = 1, 2, \ldots, A_t$ of the row vector $\bar{x}_{w,i}^{(z)}$ on the wth layer of the $W_t \times A_t$ matrix, $\bar{X}_{i,l}^{(z)} = {\chi_i}^{(z)} \circ \Phi_1$ where $W_t \times A_t$ denotes the Hadamard product, and the matrix ${\chi_i}^{(z)}$ is given by,

$$
{\chi_i}^{(z)} = \begin{pmatrix}
{X_1}^{(z)}\left({P_i}^l + 1\right) & {X_{W_t}}^{(z)}\left({P_i}^l + 1\right) & \ldots\ldots & {X_{(W_t - A_t)+2}}^{(z)}\left({P_i}^l + 1\right) \\
{X_2}^{(z)}\left({P_i}^l + \left\lfloor \frac{\mathrm{A_t}}{\mathrm{w_t}} + 1 \right\rfloor\right) & {X_1}^{(z)}\left({P_i}^l + 2\right) & \ldots\ldots & {X_{(W_t - A_t)+3}}^{(z)}\left({P_i}^l + 2\right) \\
{X_3}^{(z)}\left({P_i}^l + 2\right) & {X_2}^{(z)}\left({P_i}^l + \left\lfloor \frac{\mathrm{A_t}}{\mathrm{w_t}} + 2 \right\rfloor\right) & \ddots & {X_{(W_t - A_t)+4}}^{(z)}\left({P_i}^l + 3\right) \\
\vdots & \vdots & \vdots & \vdots \\
{X_{W_t}}^{(z)}\left({P_i}^l + \mathrm{A_t}\right) & {X_{W_t - 1}}^{(z)}\left({P_i}^l + \mathrm{A_t}\right) & \ldots\ldots & {X_{\left(1 - \frac{A_t}{W_t}\right)W_t + 1}}^{(z)}\left({P_i}^l + \mathrm{A_t}\right)
\end{pmatrix}
$$

The diagonal layer index of $\bar{X}_{i,l}^{(z)}$ is shown in Fig. 3.3, $A_t = 5$ and $W_t = 8$

$$
\begin{pmatrix}
1 & 8 & 7 & 6 & 5 \\
2 & 1 & 8 & 7 & 6 \\
3 & 2 & 1 & 8 & 7 \\
4 & 3 & 2 & 1 & 8 \\
5 & 4 & 3 & 2 & 1 \\
6 & 5 & 4 & 3 & 2 \\
7 & 6 & 5 & 4 & 3 \\
8 & 7 & 6 & 5 & 4
\end{pmatrix}
$$

Figure 3.3 example of symbols placement in the diagonal layers of $\bar{X}_{i,l}^{(z)}$ matrix for $A_t = 5$ and $W_t = 8$. Thus each sub-block, ${S_b}^{(z)} \mathcal{T}^{W_Z A_t W_L W_t}$ $b = 1, 2, 3, ., B$ is encoded into an SF code matrix C_b of size $Q \times A_t$ matrix, where,

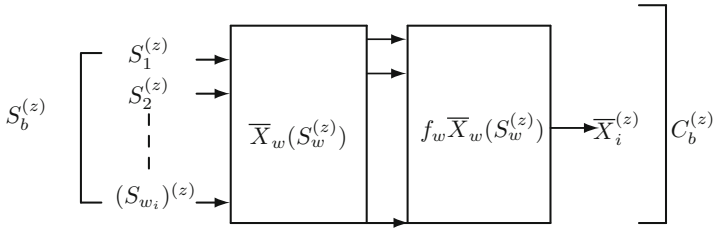

Fig. 3.3 Threaded algebraic SF code design

$$c_b{}^{(z)} = \begin{pmatrix} \bar{X}_{1,1}^{(z)} \\ \vdots \\ \bar{X}_{1,W_Z}^{(z)} \\ \vdots \\ \bar{X}_{W_L,1}^{(z)} \\ \vdots \\ \bar{X}_{W_L,W_Z}^{(z)} \end{pmatrix} \tag{3.42}$$

Next for multi-user MIMO-OFDM MAC, the encoded codeword $\bar{C}_b^{(z)}$ is given by,

$$\bar{C}_b^{(z)} = C_b{}^{(z)} \circ \left(\Phi_{2,z} \otimes 1_{1\times A_t}\right) \tag{3.43}$$

where, $\Phi_{2,z}$ is the zth column of the matrix $Q \times W_Z$, Φ_2 which is given by

$$\Phi_2 = \begin{pmatrix} 1 & \phi_2{}^{(Q-1)} & \dots & \phi_2{}^{(Q-Z)+1} \\ \phi_2 & 1 & \dots & \phi_2{}^{(Q-Z)+2} \\ \vdots & \vdots & \dots & \vdots \\ \vdots & \vdots & \ddots & \vdots \\ \phi_2{}^{(Q-1)} & \phi_2{}^{(Q-2)} & \dots & \phi_2{}^{\left(1-\frac{Z}{Q}\right)Q} \end{pmatrix} \tag{3.44}$$

where ϕ_2 is given by $\phi_2 = \phi^{\frac{1}{Q}}$ where ϕ is an algebraic number with degree of at least QW_L over $\mathcal{A}$ where $\mathcal{A}$ is the field extension of $\mathbb{Q}$ which contains all the entries of the Θ signal alphabet, $\mathcal{T} \subset \mathbb{Z}[j]$ and $e^{\frac{-j2\pi\tau_l}{T_s}}$, $(l = 0, 1, \dots, L-1)$. Note that, the co-operation between the users is not necessary because the difference of the proposed SF codes between any two users is determined by the design of $\Phi_{2,z}$ in (3.44) which is the column matrix of Φ_2 and different columns Φ_2 are selected for different users. It is worth noting that, according to the Theorem 1 and Theorem 2 given in [15], the coding gain expresses the simultaneous Diophantine approximation of the numbers $\{\phi_1^0, \phi_1^1 = \theta^{\frac{1}{w_t}}, \dots, \phi_1^{w_t-1} = \theta^{\frac{w_t-1}{w_t}}\}$ and $\{\phi_2^0 = 1, \phi_2^1 = \phi^{\frac{1}{\rho}}, \dots, \phi_2^{Q-1} = \phi^{\frac{Q-1}{\rho}}\}$ by other algebraic numbers, depending on the constellation used. This observation implies that optimizing the coding gain is equivalent to choosing these Diophantine numbers to be "badly approximated" by other algebraic number. The presented SF coding applies the same coding strategy to every encoded sub block $\overline{C}_b^z$, $b = 1, 2, \dots, B$. So, for convenience, we have just showed the SF coding of one sub block $\overline{C}_b^z$ as illustrated in Fig. 3.3. Thus, the code rate-A_t SF codes $C^{(z)} \in \mathcal{T}^{N\times M_t}$ for the zth user is of the form:

$$C^{(z)} = \left[\left(\bar{C}_1^{(z)}\right)^T \left(\bar{C}_2^{(z)}\right)^T \ldots \left(\bar{C}_B^{(z)}\right)^T\right]^T \tag{3.45}$$

Note that as code confirms that N is the integer multiple of Q, no zero-padding matrix is required in the code structure. Thus the rate-A_t can be always guaranteed.

3.5.1 Code Design Example

For convenience because the same coding strategies can be applied to every sub-block $\bar{C}_b^{(z)}$, $b = 1, \ldots, B$.

3.5.2 Example 1

Let, $A_t = 2$, $L = 2$, $Z = 2$ for z = 1,

$$\bar{C}_1^{(1)} = \begin{pmatrix} {X_1}^{(1)}(1) & \phi_1 {X_2}^{(1)}(1) \\ \phi_2\phi_1 {X_2}^{(1)}(2) & \phi_2 {X_1}^{(1)}(2) \\ {\phi_2}^2 {X_1}^{(1)}(5) & {\phi_2}^2\phi_1 {X_2}^{(1)}(5) \\ {\phi_2}^3\phi_1 {X_2}^{(1)}(6) & {\phi_2}^3 {X_1}^{(1)}(6) \\ {\phi_2}^4 {X_1}^{(1)}(3) & {\phi_2}^4\phi_1 {X_2}^{(1)}(3) \\ {\phi_2}^5\phi_1 {X_2}^{(1)}(4) & {\phi_2}^5 {X_1}^{(1)}(4) \\ {\phi_2}^6 {X_1}^{(1)}(7) & {\phi_2}^6\phi_1 {X_2}^{(1)}(7) \\ {\phi_2}^7\phi_1 {X_2}^{(1)}(8) & {\phi_2}^7 {X_1}^{(1)}(8) \end{pmatrix} \tag{3.46}$$

For z = 2

$$\bar{C}_1^{(2)} = \begin{pmatrix} {\phi_2}^7 {X_1}^{(2)}(1) & \phi_2^7\phi_1 {X_2}^{(2)}(1) \\ \phi_1 {X_2}^{(2)}(2) & {X_1}^{(2)}(2) \\ {\phi_2}^1 {X_1}^{(2)}(5) & {\phi_2}^1\phi_1 {X_2}^{(2)}(5) \\ {\phi_2}^2\phi_1 {X_2}^{(2)}(6) & {\phi_2}^2 {X_1}^{(2)}(6) \\ {\phi_2}^3 {X_1}^{(2)}(3) & {\phi_2}^3\phi_1 {X_2}^{(2)}(3) \\ {\phi_2}^4\phi_1 {X_2}^{(2)}(4) & {\phi_2}^4 {X_1}^{(2)}(4) \\ {\phi_2}^5 {X_1}^{(2)}(7) & {\phi_2}^5\phi_1 {X_2}^{(2)}(7) \\ {\phi_2}^6\phi_1 {X_2}^{(2)}(8) & {\phi_2}^6 {X_1}^{(2)}(8) \end{pmatrix} \tag{3.47}$$

where, $[X_w\,(1) \ldots\ldots\ldots\ldots X_W(8)]^T = \Theta\left[S_{8(W-1)+1} \ldots\ldots S_{8W}\right]^T$, $W = 1, 2$.

3.5.3 Example 2

For, $A_t = 3$, $L = 2$, $Z = 2$, for z = 1,

$$\bar{C}_1^{(1)} = \begin{pmatrix} X_1{}^{(1)}(1) & \phi_1{}^3 X_4{}^{(1)}(1) & \phi_1{}^2 X_3{}^{(1)}(1) \\ \phi_2\phi_1 X_2{}^{(1)}(1) & \phi_2 X_1{}^{(1)}(2) & \phi_2\phi_1{}^3 X_4{}^{(1)}(2) \\ \phi_2{}^2\phi_1{}^2 X_3{}^{(1)}(2) & \phi_2{}^2\phi_1 X_2{}^{(1)}(2) & \phi_2{}^2 X_1{}^{(1)}(3) \\ \phi_2{}^3\phi_1{}^3 X_4{}^{(1)}(3) & \phi_2{}^3\phi_1{}^2 X_3{}^{(1)}(3) & \phi_2{}^3\phi_1 X_2{}^{(1)}(3) \\ \phi_2{}^4 X_1{}^{(1)}(7) & \phi_2{}^4\phi_1{}^3 X_4{}^{(1)}(7) & \phi_2{}^4\phi_1{}^2 X_3{}^{(1)}(7) \\ \phi_2{}^5\phi_1 X_2{}^{(1)}(7) & \phi_2{}^5 X_1{}^{(1)}(8) & \phi_2{}^5\phi_1{}^3 X_4{}^{(1)}(8) \\ \phi_2{}^6\phi_1{}^2 X_3{}^{(1)}(8) & \phi_2{}^6\phi_1 X_2{}^{(1)}(8) & \phi_2{}^6 X_1{}^{(1)}(9) \\ \phi_2{}^7\phi_1{}^3 X_4{}^{(1)}(9) & \phi_2{}^7\phi_1{}^2 X_3{}^{(1)}(9) & \phi_2{}^7\phi_1 X_2{}^{(1)}(9) \\ \phi_2{}^8 X_1{}^{(1)}(4) & \phi_2{}^8\phi_1{}^3 X_4{}^{(1)}(4) & \phi_2{}^8\phi_1{}^2 X_3{}^{(1)}(4) \\ \phi_2{}^9\phi_1 X_2{}^{(1)}(4) & \phi_2{}^9 X_1{}^{(1)}(5) & \phi_2{}^9\phi_1{}^3 X_4{}^{(1)}(5) \\ \phi_2{}^{10}\phi_1{}^2 X_3{}^{(1)}(5) & \phi_2{}^{10}\phi_1 X_2{}^{(1)}(5) & \phi_2{}^{10} X_1{}^{(1)}(6) \\ \phi_2{}^{11}\phi_1{}^3 X_4{}^{(1)}(6) & \phi_2{}^{11}\phi_1{}^2 X_3{}^{(1)}(6) & \phi_2{}^{11}\phi_1 X_2{}^{(1)}(6) \\ \phi_2{}^{12} X_1{}^{(1)}(10) & \phi_2{}^{12}\phi_1{}^3 X_4{}^{(1)}(10) & \phi_2{}^{12}\phi_1{}^2 X_3{}^{(1)}(10) \\ \phi_2{}^{13}\phi_1 X_2{}^{(1)}(10) & \phi_2{}^{13} X_1{}^{(1)}(11) & \phi_2{}^{13}\phi_1{}^3 X_4{}^{(1)}(11) \\ \phi_2{}^{14}\phi_1{}^2 X_3{}^{(1)}(11) & \phi_2{}^{14}\phi_1 X_2{}^{(1)}(11) & \phi_2{}^{14} X_1{}^{(1)}(12) \\ \phi_2{}^{15}\phi_1{}^3 X_4{}^{(1)}(12) & \phi_2{}^{15}\phi_1{}^2 X_3{}^{(1)}(12) & \phi_2{}^{15}\phi_1 X_1{}^{(1)}(12) \end{pmatrix} \tag{3.48}$$

For z = 2,

$$\bar{C}_1^{(2)} = \begin{pmatrix} \phi_2{}^{15} X_1{}^{(2)}(1) & \phi_2{}^{15}\phi_1{}^3 X_4{}^{(2)}(1) & \phi_2{}^{15}\phi_1{}^2 X_3{}^{(2)}(1) \\ \phi_1 X_2{}^{(2)}(1) & X_1{}^{(2)}(2) & \phi_1{}^3 X_4{}^{(2)}(2) \\ \phi_2{}^1\phi_1{}^2 X_3{}^{(2)}(2) & \phi_2{}^1\phi_1 X_2{}^{(2)}(2) & \phi_2{}^1 X_1{}^{(2)}(3) \\ \phi_2{}^2\phi_1{}^3 X_4{}^{(2)}(3) & \phi_2{}^2\phi_1{}^2 X_3{}^{(2)}(3) & \phi_2{}^2\phi_1 X_2{}^{(2)}(3) \\ \phi_2{}^3 X_1{}^{(2)}(7) & \phi_2{}^3\phi_1{}^3 X_4{}^{(2)}(7) & \phi_2{}^3\phi_1{}^2 X_3{}^{(2)}(7) \\ \phi_2{}^4\phi_1 X_2{}^{(2)}(7) & \phi_2{}^4 X_1{}^{(2)}(8) & \phi_2{}^4\phi_1{}^3 X_4{}^{(2)}(8) \\ \phi_2{}^5\phi_1{}^2 X_3{}^{(2)}(8) & \phi_2{}^5\phi_1 X_2{}^{(2)}(8) & \phi_2{}^5 X_1{}^{(2)}(9) \\ \phi_2{}^6\phi_1{}^3 X_4{}^{(2)}(9) & \phi_2{}^6\phi_1{}^2 X_3{}^{(2)}(9) & \phi_2{}^6\phi_1 X_2{}^{(2)}(9) \\ \phi_2{}^7 X_1{}^{(2)}(4) & \phi_2{}^7\phi_1{}^3 X_4{}^{(2)}(4) & \phi_2{}^7\phi_1{}^2 X_3{}^{(2)}(4) \\ \phi_2{}^8\phi_1 X_2{}^{(2)}(4) & \phi_2{}^8 X_1{}^{(2)}(5) & \phi_2{}^8\phi_1{}^3 X_4{}^{(2)}(5) \\ \phi_2{}^9\phi_1{}^2 X_3{}^{(2)}(5) & \phi_2{}^9\phi_1 X_2{}^{(2)}(5) & \phi_2{}^9 X_1{}^{(2)}(6) \\ \phi_2{}^{10}\phi_1{}^3 X_4{}^{(2)}(6) & \phi_2{}^{10}\phi_1{}^2 X_3{}^{(2)}(6) & \phi_2{}^{10}\phi_1 X_2{}^{(2)}(6) \\ \phi_2{}^{11} X_1{}^{(2)}(10) & \phi_2{}^{11}\phi_1{}^3 X_4{}^{(2)}(10) & \phi_2{}^{11}\phi_1{}^2 X_3{}^{(2)}(10) \\ \phi_2{}^{12}\phi_1 X_2{}^{(2)}(10) & \phi_2{}^{12} X_1{}^{(2)}(11) & \phi_2{}^{12}\phi_1{}^3 X_4{}^{(2)}(11) \\ \phi_2{}^{13}\phi_1{}^2 X_3{}^{(2)}(11) & \phi_2{}^{13}\phi_1 X_2{}^{(2)}(11) & \phi_2{}^{13} X_1{}^{(2)}(12) \\ \phi_2{}^{14}\phi_1{}^3 X_4{}^{(2)}(12) & \phi_2{}^{14}\phi_1{}^2 X_3{}^{(2)}(12) & \phi_2{}^{14}\phi_1 X_1{}^{(2)}(12) \end{pmatrix} \tag{3.49}$$

where, $[X_w(1) \ldots\ldots\ldots\ldots X_W(12)]^T = \Theta\left[S_{12(W-1)+1} \ldots\ldots S_{12W}\right]^T$, $W = 1, 2, 3, 4$.

3.6 Conclusion

This chapter presents a general MIMO-OFDM system model. The analysis is carried out for the coherent scenario where the channel state information is perfectly known at the receiver. Later on, the basic issues such as code design criteria for MIMO-OFDM links with frequency-selective fading are investigated. The chapter also demonstrates the maximum achievable diversity order and coding gain of SF code. Two examples of code constructions are presented that can achieve full space-frequency diversity.

References

1. Li QC, Li KH,Teh KC (2008) Noncoherent space-frequency codes for broadband MIMO systems over frequency-selective fading channels. In: Proceedings of the 67th IEEE vehicular technology conference, VTC Spring 2008, 11–14 May 2008, Singapore, pp 554–558
2. Su W, Safar Z, Olfat M, Liu KJR (2003) Obtaining full-diversity space-frequency codes from space-time codes via mapping. IEEE Trans Signal Process 51(11):2905–2916
3. Liu Z, Xin Y, Giannakis GB (2002) Space-time-frequency coded OFDM over frequency-selective fading channels. IEEE Trans Signal Process 50(10):2465–2476
4. Amin MR, Trapasiya SD (2012) Space time coding scheme for MIMO system-literature survey. Procedia Eng 38:3509–3517
5. Zhang W, Xia X, Ching P (2007) High-rate full-diversity space-time-frequency codes for broadband MIMO block-fading channels. IEEE Trans Commun 55(1):25–34
6. El Gamal H, Damen M (2003) Universal space-time coding. IEEE Trans Inf Theory 49(5):1097
7. Fozunbal M, McLaughlin SW, Schafer RW (2005) On space-time-frequency coding over MIMO-OFDM systems. IEEE Trans Wirel Commun 4(1):320–331
8. Molisch AF, Win MZ, Winters JH (2002) Space-time-frequency (STF) coding for MIMO-OFDM systems. IEEE Commun Lett 6(9):370–372
9. Su W, Safar Z, Olfat M, Liu K (2005) Towards maximum achievable diversity in space, time, and frequency: performance analysis and code design. IEEE Trans Wirel Commun 4:1847–1857
10. A space-time coded transmitter diversity technique for frequency selective fading channels
11. Liu Y, Zhang W, Ching PC (2013) Full-diversity distributed space-time codes with an efficient ML decoder for asynchronous cooperative communications. In: IEEE international conference on acoustics, speech and signal processing, ICASSP 2013, Vancouver, BC, Canada, 26–31 May 2013, pp 5011–5015
12. Su W, Safar Z, Liu KJR (2005) Full-rate full-diversity space-frequency codes with optimum coding advantage. IEEE Trans Inf Theory 51(1):229–249
13. Kundu S, Pados DA, Su W, Grover R (2013) Toward a preferred 4×4 space-time block code: a performance-versus-complexity sweet spot with linear-filter decoding. IEEE Trans Commun 61(5):1847–1855
14. Shelim R, Matin MA, Alam AU (2013) A systematic design of high-rate full-diversity space-frequency codes for multiuser MIMO-OFDM system. WSEAS Trans Commun 12:154–163
15. Zhang W, Ben Letaief K (2010) A systematic design of full diversity multiuser. IEEE Trans Signal Process 58(3):1732–1740

16. Shelim R, Matin MA, Alam AU (2011) High-rate full-diversity space-time-frequency code for multiuser MIMO-OFDM systems over frequency selective multiple access channels. J Converg Inf Technol 6:8–22
17. Gallager R (1985) A perspective on multiaccess channels. IEEE Trans Inf Theory 31:124–142
18. Multiuser space-time/frequency code design
19. Gärtner ME, Bölcskei H (2006) Multiuser space-time/frequency code design. In: Proceedings of IEEE ISIT, Seattle, WA, 9–14 July, pp 2819–2823
20. Badr M, Belfiore J (2008) Distributed space-time block codes for the MIMO multiple access channel. In: 2008 IEEE international symposium on information theory, ISIT 2008, Toronto, ON, Canada, 6–11 July 2008, pp 2553–2557

Chapter 4
Algebraic Space-Time (ST) Codes: An Overview

4.1 Introduction

This chapter introduces (ASTC). Alamouti works in MIMO systems, makes the MIMO under high consideration with the invention of Space Time Block Code (STBC) in [1] for two transmitter and one receiver antenna. The idea was to improve the channel capacity by exploiting the spatial diversity which can mitigate the detrimental effects due to multipath fading. The most performed algebraic space-time codes for 2×2 MIMO systems are then described and tested under a **non selective Rayleigh correlated channel** condition.

4.2 ST-MIMO Channel

The transmission scheme that we consider in this chapter is a multiple antenna system Multi Input Multi Output (MIMO) using a Space-Time coding (ST), (Fig. 4.1), with n_t transmitting antennas and n_r receiving antennas. The outer code is a standard binary code (block code, convoluted code, turbo-code,…). The inner code is a space-time code. Its role is to disperse bits or symbols modulated on the different degrees of freedom of the channel, Space-Time codes brings a dependence between the temporal and spatial field in order to increase both the spectral efficiency and the diversity order. The coefficient h_{ij} represents the fading of the path between the transmitting antenna i and receiving antenna j. At the output of the modulation, the information symbols are encoded by the ST code, and subsequently transmitted through a transmission channel. At the reception, the ST-decoder allows the recovery of information symbols, which after demodulation generate information bits. The codeword $\boldsymbol{X}$ is a matrix of dimension $n_t \times T$, where T is the temporal length code. Each component of the codeword $\boldsymbol{X}$ is a linear combination of information symbols.

B. Ahmed and M. Abdul Matin, *Coding for MIMO-OFDM in Future Wireless Systems*, SpringerBriefs in Electrical and Computer Engineering,
DOI 10.1007/978-3-319-19153-9_4

Fig. 4.1 ST-MIMO system

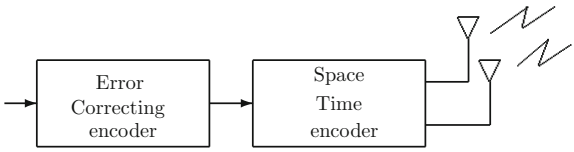

Table 4.1 ST codes by channel use

Coherent	Differential	Non-coherent case
$\min(n_r, n_t)$	$\frac{1}{2}\min(n_r, n_t)$	$M^*\left(1-\frac{M^*}{T}\right)$

$M^* = \min\left(n_r, n_t, \frac{T}{2}\right)$

The signal received by each antenna is the superposition of signals transmitted by all transmitting antennas through the noisy transmission channel. The received code word is then written as

$$\boldsymbol{Y}_{n_r \times T} = \boldsymbol{H}_{n_r \times n_t}.\boldsymbol{X}_{n_t \times T} + \boldsymbol{W}_{n_r \times T} \tag{4.1}$$

where $\boldsymbol{H}$ is the matrix of the transmission channel, $\boldsymbol{W}$ is the Additive White Gaussian Noise (AWGN). There are two classes of transmission system depending on knowledge of the transmission channel at the receiver as presented in Table 4.1. We speak about a **coherent system**, if the channel coefficients are assumed to be perfectly known at the receiver. If the channel coefficients are unknown by the receiver, two cases are possible: the first corresponds to the system that uses non-coherent techniques for estimating the coefficients of the transmission channel, such as sending training sequences. The second is the differential system which decodes the ST code without knowledge of the channel. The optimum number diversity degrees by channel is function of n_t, n_r and T as in Table 4.1.

In this chapter, we consider the transmission channel, as a quasi-static Rayleigh channel, assumed unknown at the receiver (non-coherent case). In the following we will look at the space-time coding for the coherent case.

4.2.1 Construction Criterion for ST Codes

The idea is to find a criterion of "pseudo-distance" from the expression of asymptotic errors probability to minimize the probability of error, such as:

- The Hamming distance for the symmetrical binary channel.
- The product distance for Rayleigh channel.

Thus, to establish criteria for building space time codes (Fig. 4.2), we should evaluate the expression of the pairwise error probability.

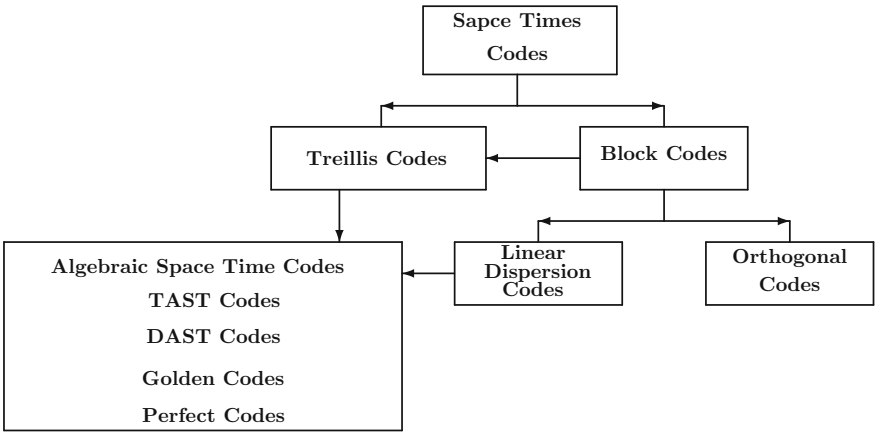

Fig. 4.2 Family tree of space time codes

Let $\boldsymbol{X}$ and $\boldsymbol{T}$ are two distinct codeword. The asymptotic pairwise error probability for a Rayleigh quasi-static channel is bounded by:

$$Prob(X \rightarrow T) \leq \left(\frac{1}{\prod_{i=1}^{r} \left(1 + \frac{E_s \lambda_i}{8N_0}\right)} \right)^{n_r} \tag{4.2}$$

where $i = 1 \ldots n$ are the singular values of the matrix $(\boldsymbol{X} - \boldsymbol{T})^H (\boldsymbol{X} - \boldsymbol{T})$ and r is its rank. At high SNR, the pairwise error probability is bounded by:

$$Prob(X \rightarrow T) \leq \left(\left(\prod_{i=1}^{r} \lambda_i \right)^{-n_r} \left(\frac{1}{\frac{E_s}{8N_0}} \right)^{r.n_r} \right) \tag{4.3}$$

The diversity order of the system is the exponent of the inverse of the Signal to Noise Ratio: $r \times n_r$. One can immediately notice that the space diversity in reception is acquired, it remains to recover the space diversity in transmission. The criteria for construction of space-time codes base on the last remarks are:

- **The rank criterion**: In order to achieve maximum diversity $n_t n_r$, the matrix $(\boldsymbol{X} - \boldsymbol{T})^H (\boldsymbol{X} - \boldsymbol{T})$ must be full rank.
- **The determinant criterion**: To maximize the coding gain, the determining minimum of the matrix $(\boldsymbol{X} - \boldsymbol{T})^H (\boldsymbol{X} - \boldsymbol{T})$ must be maximized.

4.3 Algebraic Space Time Codes

We have seen in the last section, space-time codes were constructed to minimize error probability per code word. For that they must achieve a high diversity (rank test) and to be closer to the maximum diversity order for MIMO channel and this is corresponding to the number of transmit antennas multiplied by the number of reception antennas $n_t \times n_r$. So, for a fixed rate R, the error probability decreases with the signal to noise ratio.

The study of the ergodic of MIMO channel highlighted the existence of spatial multiplexing gain K which increases the capacity of the channel. This gain in Multiplexing is the number of degrees of freedom of the channel: $K = \min(n_t, n_r)$.

A MIMO transmission system associated with an ST code can benefit both the multiplexing gain and the diversity gain. However, both are difficult to reconcile: In fact a MIMO system may have simultaneously the diversity gain and multiplexing gain space, but the maximization of one does not necessarily result in maximizing the other.

Algebraic Space Time Codes are then constructed to achieve the rank and the determinant criterion and to reconcile between the multiplexing gain and the diversity gain. This is done based on unique algebraic methodology as explained in the next sub-section.

4.3.1 Construction Criterion for ASTC

The construction of ASTC codes is based on the following approach as described in [2]:

1. Choice of the base
2. Choice of the extension
3. Definition of the cyclic algebra
4. Definition of ST code

The base is the body on which the extension base is defined and to which the information symbols belong. We consider the base $L = Q(i)$ or $L = Q(j)$.

The expansion base is the body on which the division is cyclic algebra where is constructed. In the case of ASTC, we must then choose an extension cyclic base K of L of degree $n_t \times L$. Then we could define σ the Galois group generator of base K, $Gal(K/L)$.

Let $\gamma \in A = Gal(K/L, \sigma, \gamma)$ a cyclic algebra of n_t degree. The algebra A is a division algebra, which requires that $\gamma, \gamma^2, \ldots, \gamma^{n_t-1}$ are not norm in K^*. Also, γ must be in $\boldsymbol{Z}[i]$ or $\boldsymbol{Z}[j]$ to ensure a minimum determinant of ST code does not faint.

4.3.2 Definition of AST Codes

The code is a 2×2 diagonal space time algebraic code obtained using the turned constellations of integer algebra, with rate 1 $Symbole/uc$, and full diversity. The construction of DAST is valid codes only for multiple of 4, $n_t \in 1, 2, 4, 2^n$. The code word is described as follows [3]:

$$\boldsymbol{X}_{\mathbf{Dast}} = \boldsymbol{H}_{n_t}.diag(\boldsymbol{M}\boldsymbol{v}_{n_t}) \tag{4.4}$$

where

$$\boldsymbol{M} = \frac{1}{\sqrt{2}}\begin{pmatrix} 1 & \theta \\ 1 & -\theta \end{pmatrix} \qquad \theta = \exp(i\pi/4) \tag{4.5}$$

where $\boldsymbol{H}_{n_t}$ is the Hadamard matrix of n_t degree.

As shown in [3, 4], the code is a 2×2 space time algebraic code obtained using the integer algebra, with rate $R = N_t = 2$ Symbole/uc (used code word), and diversity $D = n_t \times n_r = 4$. Each space time layer is associated with its proper algebraic space φ in order to alleviate the problem of ISI (Inter-Symbol-Interferences). The TAST codes return full yield, maximum diversity but the coding gain vanishes when the size of the constellation increases. For $n_t = n_r = T = 2$ the code word is expressed as:

$$\boldsymbol{X}_{\mathbf{Tast}} = \frac{1}{\sqrt{2}}\begin{pmatrix} (\boldsymbol{v}(1) + \theta\,\boldsymbol{v}(2)) & \varphi\,(\boldsymbol{v}(3) + \theta\,\boldsymbol{v}(4)) \\ \varphi\,(\boldsymbol{v}(3) - \theta\,\boldsymbol{v}(4)) & (\boldsymbol{v}(1) - \theta\,\boldsymbol{v}(2)) \end{pmatrix} \tag{4.6}$$

where

$$\theta = \exp(i\lambda) \qquad \lambda \in \Re \qquad \varphi = \theta^2$$

A linear dispersion code, constructed from cyclic algebras division center $Q(i)$ is a perfect code if it satisfies:

- A full rate
- (NVD) when the spectral efficiency increases

The perfect codes are valid only for $n_t \in 2, 3, 4, 6$. The following perfect codes are defined for $n_t = n_r = 4$:

$$\boldsymbol{C}_{k,4\times4} = \sum_{n=0}^{n_t-1} \operatorname{diag}\left(\frac{1}{\sqrt{15}}\boldsymbol{M}\boldsymbol{d}_k[n]\right)\boldsymbol{E}^n \tag{4.7}$$

where

$$\boldsymbol{M} = \begin{bmatrix} 0.2582 - 0.3122i & 0.3455 - 0.4178i & -0.4178 + 0.5051i & -0.2136 + 0.2582i \\ 0.2582 + 0.0873i & 0.4718 + 0.1596i & 0.1596 + 0.054i & 0.7633 + 0.2582i \\ 0.2582 + 0.2136i & -0.5051 - 0.4178i & -0.4178 - 0.3455i & 0.3122 + 0.2582i \\ 0.2582 - 0.7633i & -0.054 + 0.1596i & 0.1596 - 0.4718i & -0.0873 + 0.2582i \end{bmatrix}$$

and

$$\boldsymbol{E} = \begin{bmatrix} 0\ 1\ 0\ 0 \\ 0\ 0\ 1\ 0 \\ 0\ 0\ 0\ 1 \\ i\ 0\ 0\ 0 \end{bmatrix}$$

The following perfect codes are defined for $n_t = n_r = 2$, these codes are the optimal perfect code, called the "Golden Code" because it achieves the rank and the determinant criterion and reconciles between the multiplexing gain and the diversity gain, for that reason this code will be tested and analyzed in a sever channel conditions.

$$\boldsymbol{C}_{k,2\times 2} = \frac{1}{\sqrt{5}} \begin{bmatrix} \alpha(\boldsymbol{v}_k[1] + \theta \boldsymbol{v}_k[2]) & \alpha(\boldsymbol{v}_k[3] + \theta \boldsymbol{v}_k[4]) \\ \overline{\alpha}(\boldsymbol{v}_k[3] + \overline{\theta} \boldsymbol{v}_k[4]) & \overline{\alpha}(\boldsymbol{v}_k[1] + \overline{\theta} \boldsymbol{v}_k[2]) \end{bmatrix} \tag{4.8}$$

where

$$\theta = \frac{1+\sqrt{5}}{2}; \overline{\theta} = \frac{1-\sqrt{5}}{2}; \alpha = 1 + i - i\theta; \overline{\alpha} = 1 + i - i\overline{\theta}$$

4.4 Golden Codes Performances in Fading Channels

In this section, we analyze the performance of the most performed Algebraic Space Time Codes (ASTC), known as Golden codes, in correlated Rayleigh channel. We consider a coherent demodulator and we analyze the channel estimation error impact.

4.4.1 System Encoder

We consider a coherent system over a non selective MIMO channel 2×2, with imperfect channel estimation. The baseband system model used in this paper is shown in Fig. 4.3. The binary source sequence b_i of length L is modulated using the QAM-4 modulator, then encoded using the Golden code mapper. Each information sequence is encoded by the ASTC encoder into two stream constellations as follows

$$\boldsymbol{v}_{n_i, n_i+1} = [s_{(2n_{i+1})-3}, s_{(2n_{i+1})-2}, s_{(2n_{i+1})-1}, s_{(2n_{i+1})}] \tag{4.9}$$

The output of the encoder can be written in matrix form as described in (4.8)

$$\boldsymbol{X}_{N\times N} = \frac{1}{\sqrt{p}} \begin{pmatrix} \alpha\,(\boldsymbol{v}(1) + \theta\,\boldsymbol{v}(2))\ \alpha\,(\boldsymbol{v}(3) + \theta\,\boldsymbol{v}(4)) \\ \overline{\alpha}\,(\boldsymbol{v}(3) + \overline{\theta}\,\boldsymbol{v}(4))\ \overline{\alpha}\,(\boldsymbol{v}(1) + \overline{\theta}\,\boldsymbol{v}(2)) \end{pmatrix} \tag{4.10}$$

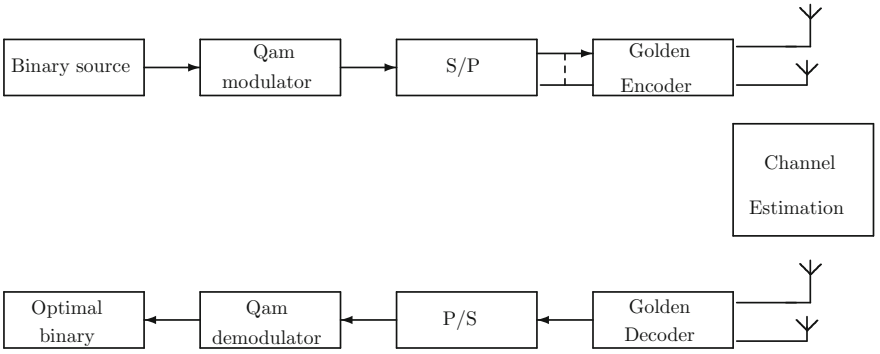

Fig. 4.3 Block diagram of MIMO-ASTC system

where

$$\theta = \frac{1+\sqrt{5}}{2} \qquad \overline{\theta} = \frac{1-\sqrt{5}}{2} \alpha = 1 + i - i\theta \qquad \overline{\alpha} = 1 + i - i\overline{\theta}$$

We note here that the encoder can transmit 4 symbols on each antenna at the same time, whereas the Alamouti [1] encoder can only code 2 symbols at a time. The best ASTC "Golden codes" is for p = $\sqrt{5}$ the received matrix is:

$$\boldsymbol{Y}_{n_t \times n_r} = \boldsymbol{H}_{n_t \times n_r} . \boldsymbol{X}_{n_r \times n_t} + \boldsymbol{W}_{n_t \times n_r} \tag{4.11}$$

where $\boldsymbol{X}$ is the transmitted codeword of duration T, $\boldsymbol{H}$ is the channel matrix and $\mathbf{W}$ is the i. i. d. Gaussian noise matrix. Subscripts indicate the dimensions of the matrices. In this work, we consider square ($n_t = T = 2$) linear dispersion to have full-rate square codes using QAM. We can re-express the total code word $\boldsymbol{X}$ of length L at time (n_i, n_{i+1}) as the follows:

$$\boldsymbol{X}_{n_i} = \frac{1}{\sqrt{5}} \begin{pmatrix} (\alpha\,(s_{(2n_{i+1})-3} + \theta\, s_{(2n_{i+1})-2}))_{(n_i,1)} \\ (\overline{\alpha}\,(s_{(2n_{i+1})-1} + \overline{\theta}\, s_{(2n_{i+1})}))_{(n_{i+1},1)} \\ (\alpha\,(s_{(2n_{i+1})-1} + \theta\, s_{(2n_{i+1})}))_{(n_i,2)} \\ (\overline{\alpha}\,(s_{(2n_{i+1})-3} + \overline{\theta}\, s_{(2n_{i+1})-2}))_{(n_{i+1},2)} \end{pmatrix} \tag{4.12}$$

To obtain the lattice representation of the system above we should re-express the total transmitted system over a non selective channel $\boldsymbol{H}_{n_i}$ with time variation:

$$\boldsymbol{H}_{n_i} = \frac{1}{\sqrt{5}} \begin{pmatrix} h_{n_i}^{11} & h_{n_{i+1}}^{21} & 0 & 0 \\ h_{n_i}^{12} & h_{n_{i+1}}^{22} & 0 & 0 \\ 0 & 0 & h_{n_i}^{11} & h_{n_{i+1}}^{21} \\ 0 & 0 & h_{n_i}^{12} & h_{n_{i+1}}^{22} \end{pmatrix} \tag{4.13}$$

where h_{n_i} is the channel coefficient at time n_i. To decode the received signal we use the MMSE decoder. The solution of the linear MMSE is given by [5]:

$$\hat{\boldsymbol{x}}_{MMSE} = \left(\frac{1}{SNR}\boldsymbol{I} + \hat{\boldsymbol{H}}^H.\hat{\boldsymbol{H}}\right)^{-1} \hat{\boldsymbol{H}}^H.\boldsymbol{y} \tag{4.14}$$

where $\boldsymbol{H}$ is a $L \times 4$ matrix, $\boldsymbol{y}$ is a $L \times 1$ vector and $\boldsymbol{I}$ is the identity $L \times L$ matrix. The decision vector for each 4 transmitted symbol is then:

$$\hat{\boldsymbol{s}}_{MMSE} = \Phi^{-1} \times \hat{\boldsymbol{x}}_{MMSE} \tag{4.15}$$

where

$$\Phi = \begin{pmatrix} \alpha & \alpha\theta & 0 & 0 \\ 0 & 0 & i\overline{\alpha} & i\overline{\alpha\theta} \\ 0 & 0 & \alpha & \alpha\theta \\ \overline{\alpha} & 0 & 0 & 0 \end{pmatrix} \tag{4.16}$$

4.4.2 Correlated Rayleigh Fading Channel

We suppose that the encoded signal is transmitted over a non selective Rayleigh fading channel. We adopt here the Clarke channel model. The received signal is the sum of q waves, we take into account the Doppler shifts effect. To obtain a correlated Rayleigh fading channel, the autocorrelation function of $\left\{h_k^j\right\}$ process is given by:

$$\begin{aligned} r_h &= E[h_k^j h_{k-q}^j] \\ &= \sigma_h^2 exp(j2\pi f_c q) J_0(2\pi f_m q T_s) \end{aligned} \tag{4.17}$$

where J_0 is the Bessel function with zero order, f_m is the maximum Doppler shift and j is the antenna's number.

4.4.3 Channel Estimation

The basic assumption was that the receiver has perfect channel knowledge. However, this does not apply to real situations. In such cases, it becomes necessary to estimate the channel parameters. In this section, we present a channel estimation method for systems using pilot symbols. We use, at pilot location the LS (Least Squares) estimation method [6–8]. The pilot insertion scheme is shown in Fig. 4.4. The estimate channel can be obtained by minimizing the error matrix $\boldsymbol{E}_k^2$ per symbol where $\boldsymbol{E}_k^2$ is given by [7]

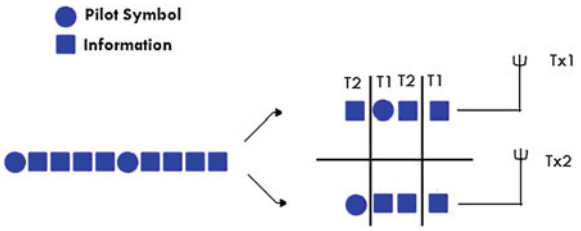

Fig. 4.4 Space time repartition of pilot symbol

$$\boldsymbol{E}_k^2 = \left(\boldsymbol{y}_k^p - \boldsymbol{x}_k^p \boldsymbol{h}_k^p\right)^H \left(\boldsymbol{y}_k^p - \boldsymbol{x}_k^p \boldsymbol{h}_k^p\right) \tag{4.18}$$

where $\boldsymbol{y}_k^p$ is the received vector with the kth pilot symbol, $\boldsymbol{x}_k^p$ is the kth transmitted pilot sample, and $\boldsymbol{h}_k^p$ is the channel coefficient for the kth symbol. The least squares solution for the estimate channel is obtained by:

$$\boldsymbol{h}^{LS} = \left[(\boldsymbol{x}_k^p)^H \boldsymbol{x}_k^p\right]^{-1} (\boldsymbol{x}_k^p)^H \boldsymbol{y}_k^p \tag{4.19}$$

where $(.)^H$ denotes the Hermitian operator, p indicates pilot symbols. Thus the estimate channel coefficients at 4 consecutive symbol pilot positions are denoted by:

$$\boldsymbol{h}^{LS} = \begin{pmatrix} \boldsymbol{x}_k(1)^p & \boldsymbol{x}_k(2)^p & 0 & 0 \\ 0 & 0 & \boldsymbol{x}_k(1)^p & \boldsymbol{x}_k(2)^p \\ \boldsymbol{x}_k(3)^p & \boldsymbol{x}_k(4)^p & 0 & 0 \\ 0 & 0 & \boldsymbol{x}_k(3)^p & \boldsymbol{x}_k(4)^p \end{pmatrix}^{\dagger} \boldsymbol{y}_{n_i}^{LS} \tag{4.20}$$

where † is the pseudo-inverse operator. We use the (Linear Minimum Mean Squares Estimation) method in order to optimize the estimation, by minimizing the following mean-square error [6]

$$\hat{\boldsymbol{h}}_{ij,LMMSE}(p) = \left[\boldsymbol{x}_i(p)^H \boldsymbol{x}_i(p) + {\sigma_w}^2\right]^{-1} \boldsymbol{x}_i(p)^H \boldsymbol{y}_j(p) \tag{4.21}$$

At non pilot position we assume that the maximum Doppler shift f_m is small enough to suppose that the channel is slow fading over the duration of one MIMO symbol. We can estimate the channel response at a data symbol location using a decision feedback equalizer [8]. In this case, the channel transfer function is estimated using past estimated values. First, channel values at already estimated locations are used to make an initial decision on the transmitted code word.

$$\widetilde{\boldsymbol{x}}_{n_i} = (\boldsymbol{h}_{n_i}^{LMMSE})^{\dagger} \boldsymbol{y}_{n_i}^{LMMSE} \tag{4.22}$$

After that, the channel estimation is updated by:

$$\widetilde{\boldsymbol{h}}_{n_i}^{LMMSE} = \left[(\widetilde{\boldsymbol{x}}_{n_i})^H \widetilde{\boldsymbol{x}}_{ni} \right]^{-1} (\widetilde{\boldsymbol{x}}_{n_i})^H \boldsymbol{y}_{n_i} \tag{4.23}$$

4.4.4 Simulation Results

To investigate the performance of the proposed space time code, a series of Monte Carlo simulations were carried out. Transmitted symbols belong to 4-QAM. For all simulations the BER curves were averaged over 100,000 trials.

This subsection compares the BER performances of the Golden code and the classical Alamouti code.

Figure 4.5 shows, that for a high SNR, the Golden code have a good performance in terms of BER. However, for a SNR near to 10dB, the BER remains close to BER, despite, we are coding 4 symbols at the same time. However we code only 2 symbols with Alamouti, then the gain still significant in terms of rate (full rate). These results lead us to deal with real channel conditions mainly if we use a correlated Rayleigh channel with a severe decoder like MMSE and with an unknown channel coefficients.

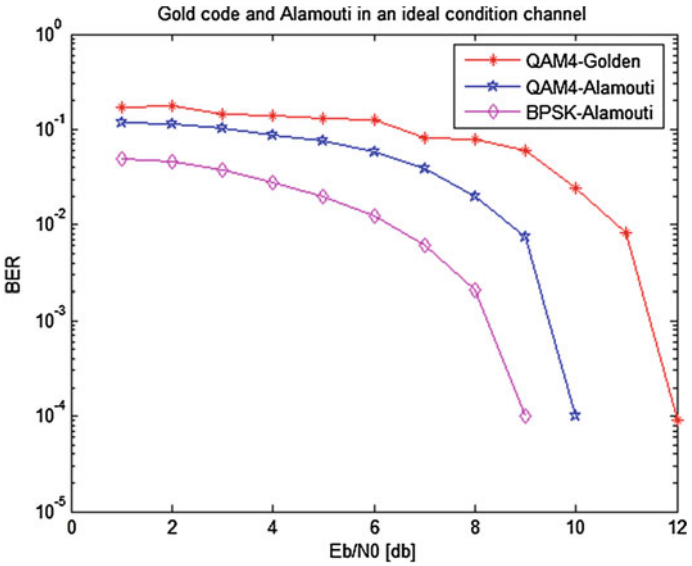

Fig. 4.5 Golden code versus Alamouti in an ideal channel condition

Figure 4.6 shows the effect of Doppler shift, to better understand the behavior of ASTC in time varying channel. It is shown when $fd = 0.001$, and $fd = 0.005$, the gain obtained is about 0.8 dB at a BER equals to 10^{-3}. This gain is less significant when the normalized Doppler frequency increases.

Figure 4.7 presents the performance of ASTC when the channel is unknown to the receiver. For LS estimator, the BER is close to 10^{-4} at SNR equals to 23 dB, however, in case of the method at SNR equals to 22 dB, the BER is about 10^{-4}, then the gain is around 2 dB for the LMMSE estimator. The LS estimator suffers from a high mean-square error and does not take into account the channel correlation property. These drawbacks can be addressed by the channel estimation technique, which helps reducing the estimation error. The ASTC tested under thoses server channel condition maintain its properties.

Figure 4.8 shows the LMMSE estimation error for a set of SNR. We note that at 40 dB, the error is the lowest.

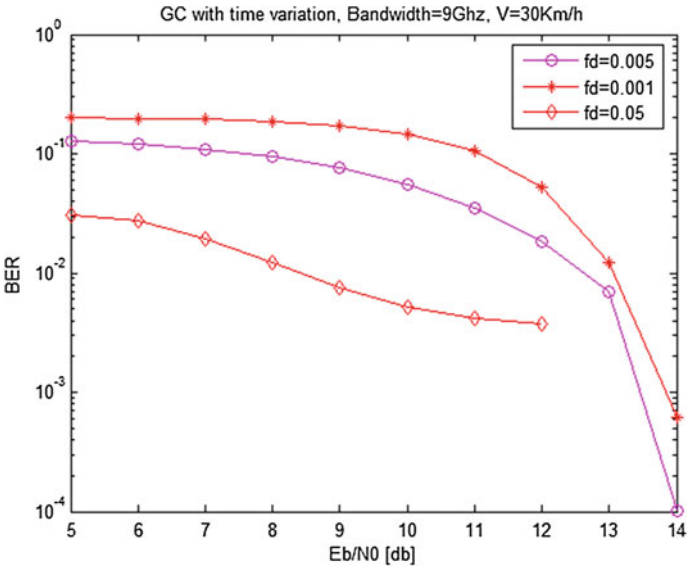

Fig. 4.6 BER performance for Golden Code, with MMSE decoder, 4-QAM modulation, band width = 9 GHz

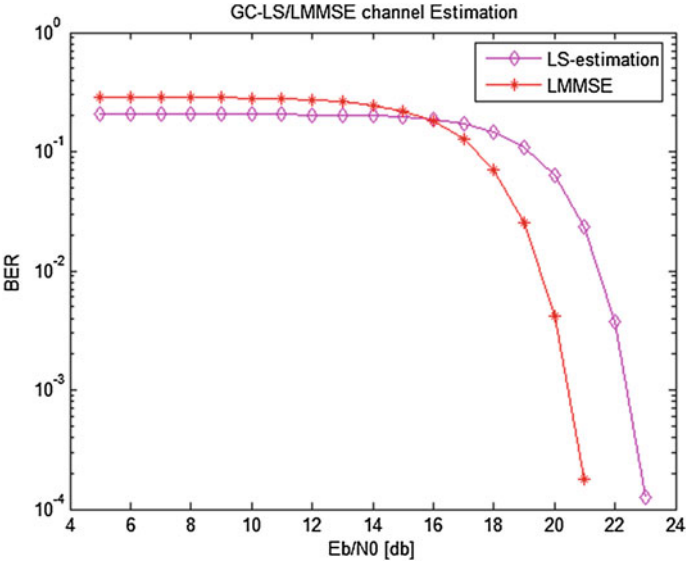

Fig. 4.7 Golden Code with channel estimation and MMSE decoder, $f_d = 0.005$, Band width = 9 GHz, V = 30 km/h

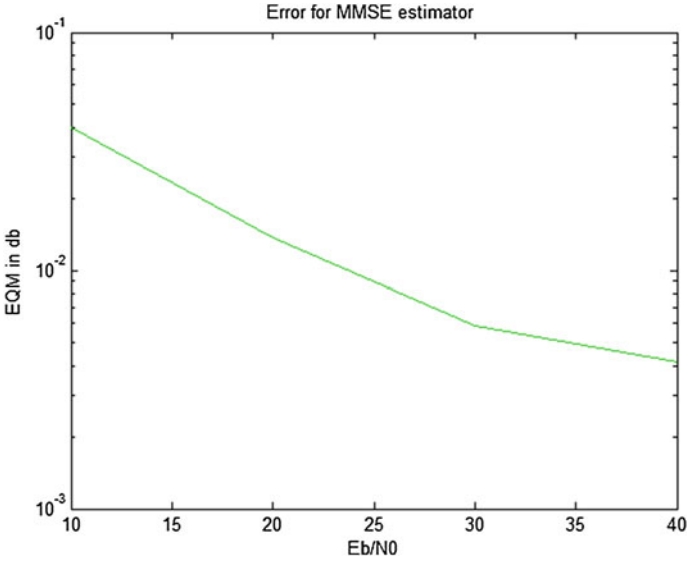

Fig. 4.8 BER performance for the LMMSE Error estimation

4.5 Conclusion

This chapter presents an overview of ASTC. ASTC code has reasonable BER obtained from numerical results when working in a realistic environment. In fact, ASTC provides full rank, full rate, and non-vanishing determinant for an increasing rate. Based on the theoretical analysis and simulation results, this chapter concludes that it is interesting to implement the Golden code in the future generation of cellular networks. The difficulties to deal with realistic conditions push us to think how we can use those codes, when working on a selective channel without losing any of its spectral performance [7, 8].

References

1. Alamouti SM (1998) A simple transmit diversity technique for wireless communications. IEEE J Sel Areas Commun 16(8):1451–1458
2. Belfiore J, Rekaya G, Viterbo E (2005) The golden code: a 2×2 full-rate space-time code with nonvanishing determinants. IEEE Trans Inf Theory 51(4):1432–1436
3. ben Othman GR (2004) Nouvelles constructions algbriques de codes spatio-temporels atteignant le compromis "multiplexage-diversit", Ph.D. dissertation, ENST
4. Belfiore JC, Rekaya G, Viterbo E (2004) "The golden code: a 2×2 full-rate space-time code with non-vanishing determinants,". In: International symposium on information theory, p 310
5. Mody AN, Stuber GL (2001) "Parameter estimation for OFDM with transmit receive diversity,". IEEE Veh Technol Conf 2:820–824
6. Edfors O, Sandell M, van de Beek J, Wilson SK, Börjesson PO (1998) OFDM channel estimation by singular value decomposition. IEEE Trans Commun 46(7):931–939
7. Morelli M, Mengali U (2001) A comparison of pilot-aided channel estimation methods for OFDM systems. IEEE Trans Signal Process 49(12):3065–3073
8. Ammari ML (1988) Iterative channel estimation and decoding of turbo-coded OFDM symbols in selective Rayleigh channel. IEEE Can J Electr Comput Eng 32(1):9–18

Chapter 5
ASTC-MIMO to ASTC-MIMO-OFDM System

5.1 Introduction

In the first part of this chapter, we propose to analyze the capacity of a MIMO-OFDM system using the ASTC codes in Rayleigh frequency selective-channels. The ASTC-MIMO-OFDM transmitter model is as described in Chap. 1. We develop analytically the capacity expression of an ASTC-MIMO-OFDM system, and we present simulation results for different scenarios.

The second part presents a new algebraic Carrier Frequency Offset (CFO) estimation technique for multi-input multi-output (MIMO) orthogonal frequency division multiplexing (OFDM) system, to overcome the sensitivity of Algebraic Space Time Codes (ASTC) to frequency synchronization. In fact OFDM and ASTC are very sensitive to the transmitter and receiver synchronization imperfections [1, 2]. Thus, the synchronization is crucial for ASTC-MIMO-OFDM-based systems. Frequency synchronization errors destroy the orthogonality among the subcarriers, which results in inter-carrier interference (ICI) [3–6]. Therefore an accurate CFO estimation is essential for OFDM receiver design. Various carrier synchronization schemes have been proposed for SISO OFDM systems. Some schemes rely on pilot or preamble data [7–16] and some use the inherent structure of the OFDM symbol in either frequency [17] or time domain [18]. For multiple antenna OFDM, data-aided schemes are proposed for receiver diversity and MIMO in [19, 20], respectively. A blind method for receiver diversity combined with OFDM is proposed in [21].

5.1.1 Contributions

The proposed estimator uses an algebraic method to extract the frequency domain matrix perturbation from the MIMO-OFDM signal. The main contributions of this work are:

B. Ahmed and M. Abdul Matin, *Coding for MIMO-OFDM in Future Wireless Systems*, SpringerBriefs in Electrical and Computer Engineering,
DOI 10.1007/978-3-319-19153-9_5

- The proposed CFO estimation technique is applied for MIMO-OFDM systems employing algebraic space time coding schemes with random CFO among all transmit and receive antenna pairs [22].
- We use the same training symbol for the CFO and channel estimation, simplifying the process and reducing bandwidth utilization for the estimation.
- We studied the correlation effect on the CFO estimator.
- The proposed estimator out-performs the CP-based [23], Moose [7] and Classen [24] methods and reaches the CRLB at high signal to noise ratio.

5.2 ASTC-MIMO-OFDM System Model

Let us consider the baseband-equivalent system, with n_t transmit antennas and n_r receive antennas, depicted in Fig. 5.1. The transmitted binary source sequence s_k is QPSK modulated. The QPSK symbols are then ASTC encoded.

We note $\boldsymbol{v}_k = [s_{4k-3}, s_{4k-2}, s_{4k-1}, s_{4k}]^T$ and $\boldsymbol{d}_k = [\boldsymbol{v}_{4k-3}, \boldsymbol{v}_{4k-2}, \boldsymbol{v}_{4k-1}, \boldsymbol{v}_{4k}]^T$ as the ASTC encoder input. $\boldsymbol{C}_{k,2\times 2}$ and $\boldsymbol{C}_{k,4\times 4}$ are the ASTC encoder output at time k, respectively for the perfect codes ($n_t = 2 \times n_r = 2$) and the perfect codes ($n_t = 4 \times n_r = 4$), given by [25]

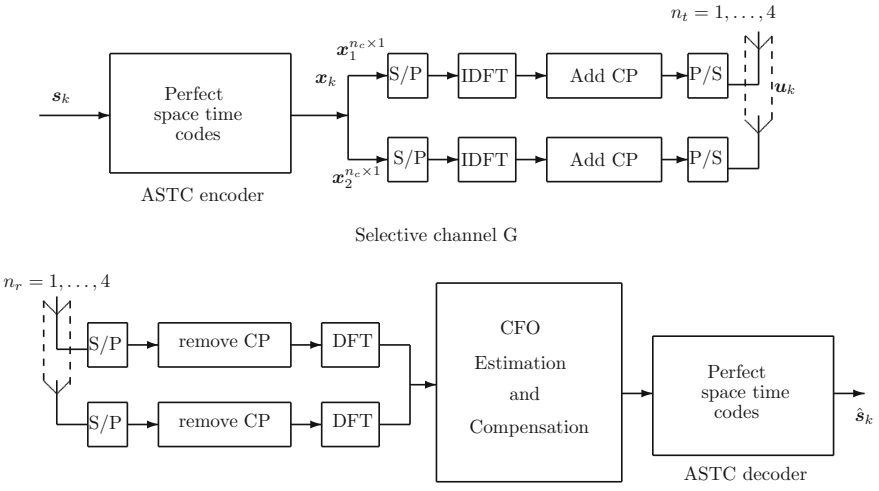

Fig. 5.1 MIMO-OFDM system employing perfect codes ASTC

5.3 Capacity Analysis of ASTC-MIMO-OFDM System in Frequency Selective Channels

To obtain the analytic expression of the information capacity of ASTC-MIMO-OFDM system for a given channel matrix $\boldsymbol{H}$, the mutual information between transmitted code word $\boldsymbol{x}_k$ and received vector $\boldsymbol{z}_k$ should be determined. The mutual information is given as defined in Chap. 2 and Eq. (2.25) by

$$I(\boldsymbol{x}_k, \boldsymbol{z}_k) = H(\boldsymbol{z}_k) - H(\boldsymbol{z}_k|\boldsymbol{x}_k) = H(\boldsymbol{z}_k) - H(\boldsymbol{w}_k) \tag{5.1}$$

where $H(y)$ denotes the entropies of multivariate distribution y. The capacity equals the maximum mutual information. Maximizing $I(\boldsymbol{x}_k, \boldsymbol{z}_k)$ is equivalent to maximizing $H(\boldsymbol{z}_k)$. Thus we can derive the capacity as

$$C = \max(H(\boldsymbol{z}_k)) - H(\boldsymbol{w}_k) \tag{5.2}$$

We have to derive the exact expression of $H(\boldsymbol{z}_k))$ to obtain the capacity expression. The entropies of $\boldsymbol{z}_k$ is given by [26]

$$\begin{aligned} H(\boldsymbol{z}_k) &= -\int p(\boldsymbol{z}_k) \log_2 [p(\boldsymbol{z}_k)] \, d\boldsymbol{z}_k \\ &= \log_2 \det(\pi \boldsymbol{Q}_z e) \end{aligned} \tag{5.3}$$

where $\boldsymbol{Q}_z$ is the of $\boldsymbol{z}_k$.
From Eq. (1.11), we can derive the covariance relationship between the received signal $\boldsymbol{z}_k$ and the transmitted codeword $\boldsymbol{x}_k$ as

$$\begin{aligned} \boldsymbol{Q}_{z_k} &= \boldsymbol{Q}_{w_k} + \boldsymbol{H} \boldsymbol{Q}_{x_k} \boldsymbol{H}^H \\ \text{where } \boldsymbol{Q}_{w_k} &= \sigma_{w_k}^2 \boldsymbol{I}_{n_c n_t} \end{aligned} \tag{5.4}$$

The above analysis leads to the following capacity expression

$$\begin{aligned} C &= \max(H(\boldsymbol{z}_k)) - H(\boldsymbol{w}_k) \\ &= \log_2 \det(\pi \boldsymbol{Q}_{z_k} e) - \log_2 \det(\pi \boldsymbol{Q}_{w_k} e) \\ &= \log_2 \det\left(\pi e(\boldsymbol{Q}_{w_k} + \boldsymbol{H} \boldsymbol{Q}_{x_k} \boldsymbol{H}^H)\right) + \log_2 \det(\pi \boldsymbol{Q}_{w_k} e)^{-1} \\ &= \log_2 \det\left(\boldsymbol{I}_{n_c n_t} + \frac{1}{\sigma_{w_k}^2} \boldsymbol{H} \boldsymbol{Q}_{x_k} \boldsymbol{H}^H\right) \\ &= \log_2 \det\left(\boldsymbol{I}_{n_c n_t} + \frac{1}{\sigma_{w_k}^2} \boldsymbol{Q}_{x_k} \boldsymbol{H}^H \boldsymbol{H}\right) bits/s/Hz \end{aligned} \tag{5.5}$$

We can derive the expression of the covariance matrix $\boldsymbol{Q}_{x_k}$ for the two transmitted codewords as

$$\begin{aligned}\boldsymbol{Q}_{x_k} &= E\left(\boldsymbol{x}_k {\boldsymbol{x}_k}^H\right) \\ &= E\left(\boldsymbol{\Phi} \odot \boldsymbol{s}_k (\boldsymbol{\Phi} \odot \boldsymbol{s}_k)^H\right) \\ &= \{\boldsymbol{\Phi}\boldsymbol{\Phi}^H\}\boldsymbol{I}_{n_c n_t}\end{aligned} \tag{5.6}$$

Then the capacity expression will be

$$C = \log_2 \det\left(\boldsymbol{I}_{n_c n_t} + \frac{1}{\sigma_w^2}\boldsymbol{\Phi}\boldsymbol{\Phi}^H \boldsymbol{H}^H \boldsymbol{H}\right) \tag{5.7}$$

Since the frequency domain channel $\boldsymbol{H}_{n,k}$ is a diagonal matrix, from (1.13) we can derive the following expression

$$\begin{aligned}\|\boldsymbol{H}_k\|^2 &= \begin{pmatrix} \|\boldsymbol{H}_k(0)\|^2 & & 0 \\ & \ddots & \\ 0 & & \|\boldsymbol{H}_k(n_c n_t)\|^2 \end{pmatrix} \\ &= \boldsymbol{H}_k \boldsymbol{H}_k^H \\ &= n_c n_t \|\boldsymbol{H}(n)\|^2 \forall\ 1 \le n \le n_c n_t\end{aligned}$$

whereas

$$\|\boldsymbol{H}_k(n)\|^2 = \|\sum_{l=0}^{L-1} \boldsymbol{h}_k(l) \exp\left(-j2\pi \frac{nk}{n_c}\right)\|^2 \tag{5.8}$$

$$\le \sum_{l=0}^{L-1} \|\boldsymbol{h}_k(l) \exp\left(-j2\pi \frac{nk}{n_c}\right)\|^2 \tag{5.9}$$

$$\le \sum_{l=0}^{L-1} \|\boldsymbol{h}_k(l)\|^2 = L.P_h^2 \tag{5.10}$$

where $P_h = E\{h_k^{p,q}(l)\left[h_{k-k'}^{m,n}(l')\right]^*\}$ denotes the mean power to each channel coefficient in time domain. If we derive the exact expression of $\boldsymbol{\Phi}\boldsymbol{\Phi}^H$ we get $\boldsymbol{I}_{n_c n_t}$. At this step, we can bound the last capacity expression by

$$C = \log_2 \det\left(\boldsymbol{I}_{n_c n_t}\left[1 + \frac{1}{\sigma_{w_k}^2}\|\boldsymbol{H}_k\|^2\right]\right)$$

$$C = \log_2\left(\left[1 + \frac{1}{\sigma^2_{w_k}} n_c n_t L \|\boldsymbol{H}_k\|^2\right]^{n_c n_t}\right) \tag{5.11}$$

$$C \leq \log_2\left(\left[1 + \frac{1}{\sigma^2_{w_k}} n_c n_t L P_h^2\right]^{n_c n_t}\right)$$

$$C \leq n_c n_t \log_2\left(\left[1 + \frac{1}{\sigma^2_{w_k}} n_c n_t L P_h^2\right]\right)$$

If we average over the capacity of $n_c n_t$ narrowband channels we derive the following capacity

$$C \leq \log_2\left(\left[1 + \frac{1}{\sigma^2_{w_k}} n_c n_t L P_h^2\right]\right) \text{bits/s/Hz} \tag{5.12}$$

5.4 Simulation Analysis

We consider the case when $\boldsymbol{H}$ is chosen according to (1.12). We investigate 1000 independent channel realizations for a fixed number of $n_t \times n_r = 2 \times 2$ antennas. The (CCDF) is used as tool, to give the probability that the capacity $\boldsymbol{C}$ is larger than the capacity abscissa $\boldsymbol{C}_x$.

Figures 5.2 and 5.3, depict the CCDF of the capacity C developed in (5.12), respectively for GC and TC codes. In Fig. 5.2, the CCDF of the capacity is plotted for up to 10 dB. The results show that at 90 % probability, the capacity is larger than 11 bits/s/Hz when the normalized Doppler frequency $f_d = 0.01$, and becomes larger than 11.5 bits/s/Hz when $f_d = 0.0001$. It can be observed that the capacity increases almost linearly when f_d decreases.

In Fig. 5.3, the CCDF of the capacity is plotted for up to 10 dB. The results show that at 90 % probability, the capacity is larger than 11.4 bits/s/Hz when the number of subcarrier uses is $n_c = 48$, and becomes larger than 11.6 bits/s/Hz when $n_c = 64$ subcarrier. We observe also that the CCDF curves became closer to each other when the number of subcarriers increase. This means that the number of n_c subcarriers increases, the capacity will reach the saturation level, mainly when $n_c \geq 64$.

The as function of SNR per receive antenna, for both the analytic capacity expression, derived in (5.11) and the simulated expression using (5.5), is shown in Fig. 5.4. The simulated curves of the two algebraic space time codes GC and TC, remain the same, this is clearly shown by the analytic capacity expression. It can be observed also that the match between the analytic and the simulated capacity, is more perfect for high SNR, mainly when SNR $\geq$ 16 dB.

In Figs. 5.5 and 5.6 we show the effect of the correlation parameter on the theoretical capacity found in (31). As it can be seen from the figures when the correlation parameter P_h increases the capacity performance of the ASTC-MIMO-OFDM

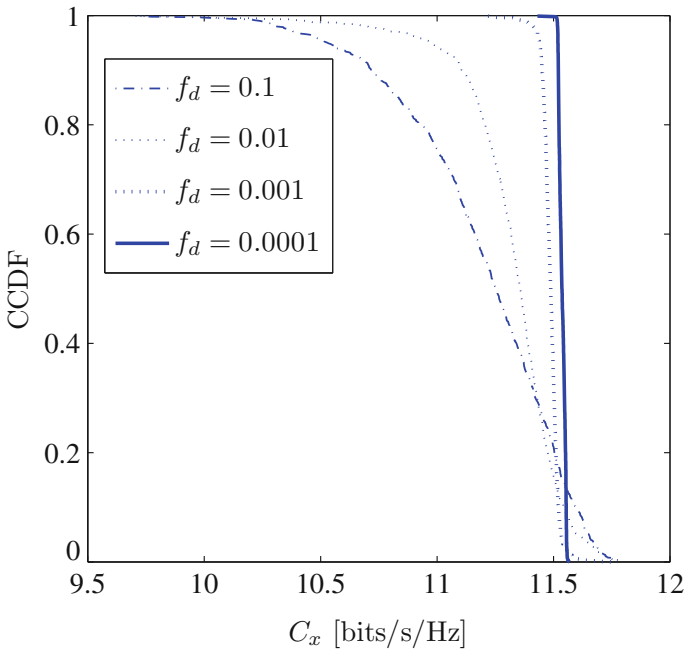

Fig. 5.2 Doppler effects on the capacity for GC-MIMO-OFDM with $\sigma_w = 10$ dB, $n_t = n_r = 2$ and $n_c = 48$ subcarriers

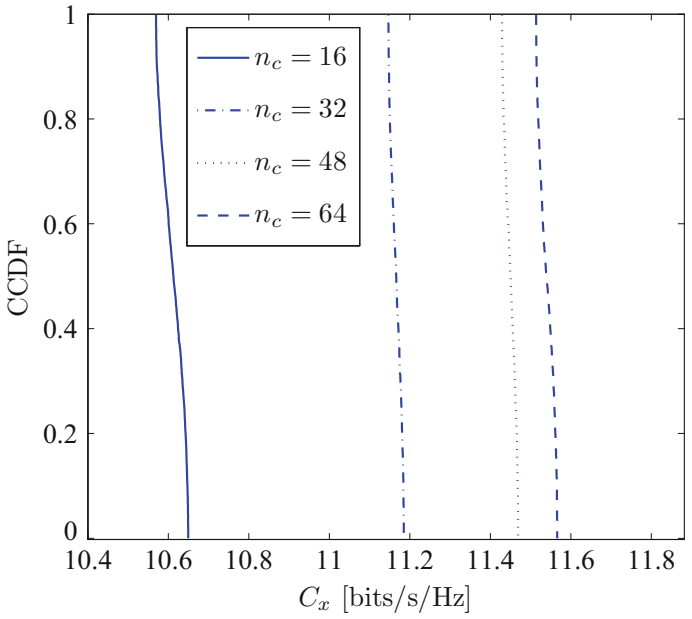

Fig. 5.3 Subcarrier effects on the capacity for TC-MIMO-OFDM with $\sigma_w = 10$ dB and n_t=n_r=2

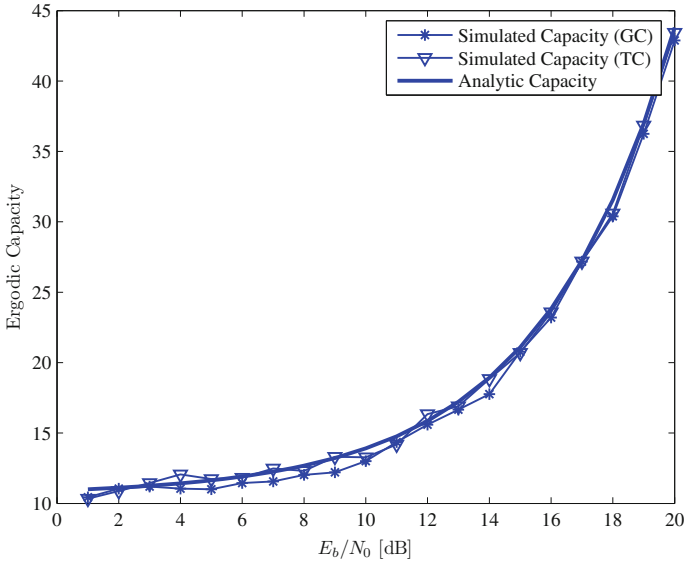

Fig. 5.4 Ergodic capacity of GC and TC codes in MIMO-OFDM with $n_t = n_r = 2$ and $n_c = 48$ subcarrier

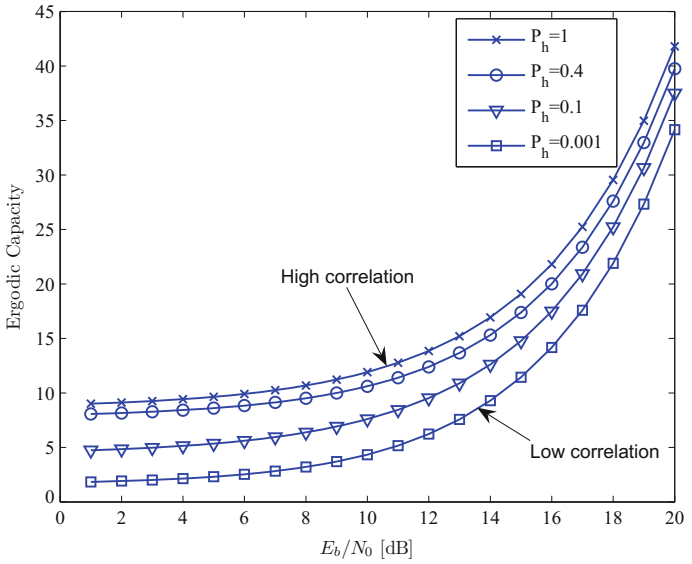

Fig. 5.5 Analytic capacity versus SNR for high and low correlation, $n_t = n_r = 2$ and $n_c = 48$ subcarrier

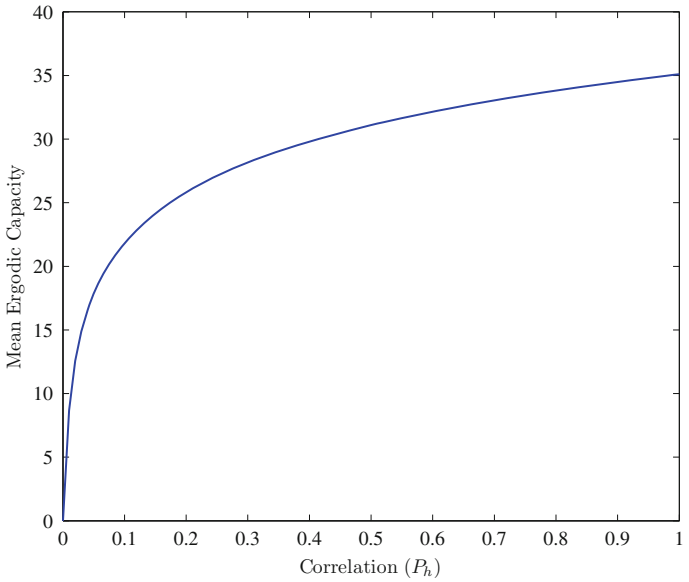

Fig. 5.6 Analytic capacity versus correlation for $\sigma_{w_k} = 30$ dB and $n_t = n_r = 2$ and $n_c = 48$ subcarrier

system become better. From Fig. 5.5, for example at the capacity equal to 15 bits/s/Hz, the gain obtained is about 1 dB at high correlation ($P_h = 1$) compared with that at low correlation ($P_h = 0.001$).

These codes maintain their properties under a multi-path channel and achieve good capacity.

5.5 New CFO Estimator

To investigate the performance of ASTC codes in OFDM systems, we have to reduce the sensitivity of the codes to CFOs. For this reason accurate synchronization is important, preferably before reception of the data. Therefore the data packet is preceded by a section of predefined data, which is called the preamble. MIMO channel estimates are also drawn from the preamble.

The preamble is used for both frequency synchronization and channel estimation. For the proposed frequency synchronization algorithm a repetition of the training symbol is not required. The preamble is formed by orthogonal codes.

The can be several times as large as the sub-channel spacing. It is usually divided into an integer part and a fractional part. The integer part causes a circular shift of the transmitted symbols, but does not cause ICI as the orthogonality of the subcarriers is maintained. The fractional part, however, causes ICI. So the fractional CFO degrades

the ASTC performance more seriously. For this reason, in this work we have focused on the fractional CFO.

At the receiver, when CFO does not occur $\Delta f = f^{T_x} - f^{R_x} = 0$. After removing the CP, the signal is transformed back to the frequency domain by means of a DFT process. The signal at the DFT output is then given by

$$z_k = \frac{1}{\sqrt{n_c}} \left[(\boldsymbol{F} \otimes \boldsymbol{I}_{n_t n_r}) \boldsymbol{\xi}_2 \right] \boldsymbol{y}_k \tag{5.13}$$

where the CP removing matrix $\boldsymbol{\xi}_2 \in \mathcal{C}^{n_c n_r \times (n_c n_g + 1) n_r}$, which discards the first $n_g n_r$ elements of $\boldsymbol{y}_k$, is defined as $\boldsymbol{\xi}_2 = [\boldsymbol{0}_{n_c n_g} \boldsymbol{I}_{n_g}] \otimes \boldsymbol{I}_{n_g}$. By combining Eqs. (1.9) and (5.13), we can re-express the DFT output as

$$\begin{aligned} z_k &= \left[(\boldsymbol{F} \otimes \boldsymbol{I}_{n_t n_r}) \boldsymbol{\xi}_3 (\boldsymbol{F}^{-1} \otimes \boldsymbol{I}_{n_t n_r}) \right] \boldsymbol{x}_k + \boldsymbol{w}_k \\ &= \boldsymbol{H}_k \boldsymbol{x}_k + \boldsymbol{w}_k \end{aligned} \tag{5.14}$$

where the block circulant matrix $\boldsymbol{\xi}_3 \in \mathcal{C}^{n_t n_c \times n_r n_c}$ is defined as $\boldsymbol{\xi}_3 = \boldsymbol{\xi}_2 \boldsymbol{G}_k \boldsymbol{\xi}_1$, $\boldsymbol{w}_k$ is the frequency domain noise with zero mean and variance σ_w^2 and $\boldsymbol{H}_k \in \mathcal{C}^{n_t n_c \times n_c n_t}$ is a frequency domain matrix defined as

$$\boldsymbol{H}_k = \left[(\boldsymbol{F} \otimes \boldsymbol{I}_{n_t n_r}) \boldsymbol{\xi}_3 (\boldsymbol{F}^{-1} \otimes \boldsymbol{I}_{n_t n_r}) \right] \tag{5.15}$$

When frequency offset occurs, $\Delta f \neq 0$. The received frequency domain signal at the DFT output will become

$$\begin{aligned} \boldsymbol{r}_k &= \left(\boldsymbol{F} \otimes \boldsymbol{I}_{n_t n_r} \right) \boldsymbol{\xi}_2 \boldsymbol{E} \boldsymbol{G}_k \boldsymbol{\xi}_1 (\boldsymbol{F}^{-1} \otimes \boldsymbol{I}_{n_t n_r}) \boldsymbol{x}_k + \boldsymbol{w}_k \\ &= (\boldsymbol{G}_{\Delta f} \otimes \boldsymbol{I}_{n_r}) \boldsymbol{H}_k \boldsymbol{x}_k + \boldsymbol{w}_k \\ &= \boldsymbol{B} \boldsymbol{H}_k \boldsymbol{x}_k + \boldsymbol{w}_k \end{aligned} \tag{5.16}$$

where $\boldsymbol{E} = \text{diag}(\text{e}_0, \text{e}_1, \ldots, \text{e}_{\text{n}_\text{c}+\text{n}_\text{g}-1}) \otimes \boldsymbol{I}_{n_r}$ denotes the phase rotation due to the CFO, with $e_m = \exp(j 2\pi \Delta f T_s (n_c + n_g) + m)$. T_s denotes the sample time. It is clear that $\xi_2 \boldsymbol{E} \boldsymbol{G}_k \boldsymbol{\xi}_1$ is no longer block circulant and can thus not be diagonalized by the DFT and IDFT operations. The $\mathcal{C}^{n_c n_r \times n_c n_r}$ matrix $\boldsymbol{B} = \boldsymbol{G}_{\Delta f} \otimes \boldsymbol{I}_{n_r}$ shows the influence of the CFO on the received frequency domain symbols. $\boldsymbol{G}_{\Delta f}$ is given by [19, 27]

$$\boldsymbol{G}_{\Delta f} = \begin{bmatrix} g_0 & g_{-1} & \cdots & g_{-(n_c-1)} \\ g_1 & g_0 & \cdots & g_{-(n_c-2)} \\ \vdots & \vdots & \ddots & \vdots \\ g_{n_c-1} & g_{n_c-2} & \cdots & g_0 \end{bmatrix} \tag{5.17}$$

where [19, 27]

$$g_q = \frac{\sin(\pi(\delta - q))}{n_c \sin(\frac{\pi}{n_c}(\delta - q))} \times \exp\left(j\frac{\pi(n_c - 1)}{n_c}(\delta - q)\right) \times \exp\left(j\frac{2\pi\delta}{n_c}(n_c + 2n_g)\right) \tag{5.18}$$

where $\delta = \Delta f n_c / f_s \ll 1$ is the frequency offset normalized to the subcarrier spacing f_s/n_c (f_s is the sampling frequency). We clearly see the following effects of frequency offset: the wanted carrier multiplied with g_0 are rotated and their amplitudes are reduced, and the other elements of $\boldsymbol{G}$, for $q \neq 0$, introduce cross terms which result in ICI. From the development of CFO approximation we have another expression of g_q under the consideration $n_g = n_c/4$, given by

$$g_q = \frac{\sin(\pi(\delta - q))\cos\left(4\pi\delta + \frac{\pi q}{n_c} - \frac{\pi\delta}{n_c}\right)}{n_c \sin\left(\frac{\pi}{n_c}(\delta - q)\right)}(1 \pm j\tan(\theta)) \tag{5.19}$$

where $\theta = \frac{\pi}{n_c}(4\pi\delta + \frac{\pi q}{n_c})$.

When n_c is large $\theta \simeq 0$ and further $\tan(\theta) \simeq \theta$. Thus, for large n_c, as θ can be approximated as $\theta \approx \frac{\pi}{n_c}(4\pi\delta)$. In the noise free case and by assuming that δ is sufficiently small, we can re-express the received signal $\boldsymbol{r}_k$ in (5.16) as

$$\boldsymbol{r}_k = \|\boldsymbol{B}\| \exp(j\theta)\boldsymbol{H}_k\boldsymbol{x}_k \tag{5.20}$$

where $\|\boldsymbol{B}\|$ and θ are the magnitude and phase of the CFO matrix. In order to estimate the magnitude of the CFO matrix, we use orthogonal training symbols which satisfy the orthogonality relation $\boldsymbol{x}_k\boldsymbol{x}_k^H = \boldsymbol{I}_{n_c n_t}$. Thus we can evaluate $\|\boldsymbol{B}\|$ as

$$\|\boldsymbol{B}\| = \left(\|\boldsymbol{r}_k \odot \boldsymbol{x}_k\| \left[\|\boldsymbol{H}_k\|\right]^{-1} \boldsymbol{I}_{n_t n_c}\right) \tag{5.21}$$

We can derive that

$$\begin{aligned}
\|\boldsymbol{H}_k\|^2 &= \boldsymbol{H}_k\boldsymbol{H}_k^H \\
&= (\boldsymbol{F} \otimes \boldsymbol{I}_{n_t n_r})\boldsymbol{\xi}_3(\boldsymbol{F}^{-1} \otimes \boldsymbol{I}_{n_t n_r}) \\
&\times \left[(\boldsymbol{F} \otimes \boldsymbol{I}_{n_t n_r})\boldsymbol{\xi}_3(\boldsymbol{F}^{-1} \otimes \boldsymbol{I}_{n_t n_r})\right]^H \\
&= (\boldsymbol{F} \otimes \boldsymbol{I}_{n_t n_r})\boldsymbol{\xi}_3(\boldsymbol{F}^{-1} \otimes \boldsymbol{I}_{n_t n_r}) \\
&\times (\boldsymbol{F}^{-1} \otimes \boldsymbol{I}_{n_t n_r})^H \boldsymbol{\xi}_3^H (\boldsymbol{F} \otimes \boldsymbol{I}_{n_t n_r})^H \\
&= \boldsymbol{\xi}_3\boldsymbol{\xi}_3^H \\
&= \xi_2\boldsymbol{G}_k\xi_1(\xi_1^H\boldsymbol{G}_k^H\xi_2^H) \\
&= \|\boldsymbol{G}_k\|^2
\end{aligned} \tag{5.22}$$

If we focus on the shape of $\boldsymbol{G}_k$ matrix and suppose that channel coefficients have roughly the same power during one MIMO-OFDM packet, we can derive $\|\boldsymbol{G}_k\|^2$ as

$$\begin{aligned}\|\boldsymbol{G}_k\|^2 &= \sum_{i,j} |\boldsymbol{h}_k(i,j)|^2 \\ &= \left(\frac{L^2}{2} + (\lambda - L)L\right) P_h \end{aligned} \tag{5.23}$$

where $\lambda = (n_c + n_g)n_t$ and P_h denotes the power to each channel coefficient in time domain. Since the channel is selective and correlated we can estimate from (1.6) the power profile of the time domain channel $\boldsymbol{G}_k$. From (5.21), (5.22) and (5.23) we evaluate $\|\boldsymbol{B}\|$ as

$$\widehat{\|\boldsymbol{B}\|} = \frac{1}{\left(\left(\frac{L^2}{2} + (\lambda - L)L\right) P_h\right)^{\frac{1}{2}}} (\|\boldsymbol{r}_k \odot \boldsymbol{x}_k\|) \tag{5.24}$$

Now we estimate the phase of the CFO matrix. In fact when δ is sufficiently small, we approximate the phase rotation $\exp(j\theta)$ by Taylor series expansion up to the second order term, $J_\theta = \exp(j\theta) \approx 1 + j\theta - \frac{1}{2}\theta^2$. From (5.20) we derive $J_{\widehat{\theta}}$ as

$$\begin{aligned}|J_{\widehat{\theta}}|^2 \boldsymbol{I}_{n_t n_c} &= \left[\widehat{\|\boldsymbol{B}\|}^2\right]^{-1} \|\boldsymbol{r}_k \odot \boldsymbol{x}_k\|^2 \left[\|\boldsymbol{H}_k\|^2\right]^{-1} \boldsymbol{I}_{n_t n_c} \\ &= \left(1 + \frac{\widehat{\theta}^4}{4}\right)^2 \boldsymbol{I}_{n_t n_c} \\ &= \widehat{\alpha} \boldsymbol{I}_{n_t n_c} \end{aligned} \tag{5.25}$$

Since $\widehat{\alpha}$ is known we estimate $\widehat{\theta}$ as

$$\widehat{\theta} = \sqrt[4]{\widehat{\alpha} - 1} \tag{5.26}$$

Then we could correct the received signal $\boldsymbol{r}_k$ to

$$\begin{aligned}\widetilde{\boldsymbol{r}_k} &= \left[\widehat{\|\boldsymbol{B}\|} \exp(j\widehat{\theta})\right]^{-1} \boldsymbol{r}_k \\ &= \widehat{\boldsymbol{H}_k} \boldsymbol{x}_k \end{aligned} \tag{5.27}$$

$\widehat{\boldsymbol{H}_k}$ is diagonalized by the IDFT and DFT operations and can be estimated using both $\widetilde{\boldsymbol{r}_k}$ and the same pilots symbols as (without any training symbol repetition)

$$\widetilde{\boldsymbol{H}_k} = \mathrm{diag}(\boldsymbol{x}_k)^\dagger \widetilde{\boldsymbol{r}_k} \tag{5.28}$$

Table 5.1 summarizes the procedure of CFO estimation and correction.

Table 5.1 The compensation steps of CFO

Steps	Operations
1	Estimate magnitude of the CFO Matrix as in (5.24)
2	Estimate the phase of the CFO Matrix as in (5.25)
3	Correct the received signal as in (5.27) $r_k \Rightarrow \widetilde{r_k}$
4	Estimate the frequency domain channel as in (5.28)

5.6 ASTC Decoder

Once the channel effect is compensated we can estimate the data signal as $\hat{\boldsymbol{x}}_k = \widetilde{\boldsymbol{H}}_k^{\dagger}\widetilde{r_k}$ which will be passed for decoding. The maximum-likelihood perfect codes decoding can be performed using the sphere decoder or the Schnorr-Euchner algorithm. In this work, we propose to use the zero forcing sub-optimum decoder which reduces the numerical complexity without significant performance loss. A serial to parallel module, at each DFT output, is used to reshape the signal $\hat{\boldsymbol{x}}_k$ and to provide the output signal $\hat{\boldsymbol{s}}_k$. If we re-express the received code word $\hat{\boldsymbol{x}}_k$ in function of $\hat{\boldsymbol{s}}_k$ we can derive the decoder matrix $\boldsymbol{\Phi}$ for both 2×2 and 4×4 perfect codes as

$$\boldsymbol{\Phi}_{2\times 2} = \frac{1}{\sqrt{5}} \begin{bmatrix} \alpha & \alpha\theta & 0 & 0 \\ 0 & 0 & i\overline{\alpha} & i\overline{\alpha\theta} \\ 0 & 0 & \alpha & \alpha\theta \\ \overline{\alpha} & \overline{\alpha\theta} & 0 & 0 \end{bmatrix} \tag{5.29}$$

$$\boldsymbol{\Phi}_{4\times 4} = \begin{bmatrix} \boldsymbol{\phi}_1 & \boldsymbol{\phi}_2 & \boldsymbol{\phi}_3 & \boldsymbol{\phi}_4 \end{bmatrix} \tag{5.30}$$

where $\boldsymbol{\phi}_i$ is the decoder block matrix for each received symbol defined as

$$\boldsymbol{\phi}_1 = \begin{bmatrix} a_1 & a_5 & a_9 & a_{13} \\ 0 & 0 & 0 & 0 \\ 0 & 0 & 0 & 0 \\ 0 & 0 & 0 & 0 \\ 0 & 0 & 0 & 0 \\ a_2 & a_6 & a_{10} & a_{14} \\ 0 & 0 & 0 & 0 \\ 0 & 0 & 0 & 0 \\ 0 & 0 & 0 & 0 \\ 0 & 0 & 0 & 0 \\ a_3 & a_7 & a_{11} & a_{15} \\ 0 & 0 & 0 & 0 \\ 0 & 0 & 0 & 0 \\ 0 & 0 & 0 & 0 \\ 0 & 0 & 0 & 0 \\ a_4 & a_8 & a_{12} & a_{16} \end{bmatrix} \quad \boldsymbol{\phi}_2 = \begin{bmatrix} 0 & 0 & 0 & 0 \\ 0 & 0 & 0 & 0 \\ 0 & 0 & 0 & 0 \\ ia_4 & ia_8 & ia_{12} & ia_{16} \\ a_1 & a_5 & a_9 & a_{13} \\ 0 & 0 & 0 & 0 \\ 0 & 0 & 0 & 0 \\ 0 & 0 & 0 & 0 \\ a_2 & a_6 & a_{10} & a_{14} \\ 0 & 0 & 0 & 0 \\ 0 & 0 & 0 & 0 \\ 0 & 0 & 0 & 0 \\ 0 & 0 & 0 & 0 \\ 0 & 0 & 0 & 0 \\ a_3 & a_7 & a_{11} & a_{15} \\ 0 & 0 & 0 & 0 \end{bmatrix} \tag{5.31}$$

$$\boldsymbol{\phi}_3 = \begin{bmatrix} 0 & 0 & 0 & 0 \\ 0 & 0 & 0 & 0 \\ ia_3 & ia_7 & ia_{11} & ia_{15} \\ 0 & 0 & 0 & 0 \\ 0 & 0 & 0 & 0 \\ 0 & 0 & 0 & 0 \\ 0 & 0 & 0 & 0 \\ ia_4 & ia_8 & ia_{12} & ia_{16} \\ a_1 & a_5 & a_9 & a_{13} \\ 0 & 0 & 0 & 0 \\ 0 & 0 & 0 & 0 \\ 0 & 0 & 0 & 0 \\ a_2 & a_6 & a_{10} & a_{14} \\ 0 & 0 & 0 & 0 \\ 0 & 0 & 0 & 0 \\ 0 & 0 & 0 & 0 \end{bmatrix} \boldsymbol{\phi}_4 = \begin{bmatrix} 0 & 0 & 0 & 0 \\ ia_2 & ia_6 & ia_{10} & ia_{14} \\ 0 & 0 & 0 & 0 \\ 0 & 0 & 0 & 0 \\ 0 & 0 & 0 & 0 \\ 0 & 0 & 0 & 0 \\ ia_3 & ia_7 & ia_{11} & ia_{15} \\ 0 & 0 & 0 & 0 \\ 0 & 0 & 0 & 0 \\ 0 & 0 & 0 & 0 \\ 0 & 0 & 0 & 0 \\ ia_4 & ia_8 & ia_{12} & ia_{16} \\ a_1 & a_5 & a_9 & a_{13} \\ 0 & 0 & 0 & 0 \\ 0 & 0 & 0 & 0 \\ 0 & 0 & 0 & 0 \end{bmatrix} \tag{5.32}$$

$\boldsymbol{M}$ defined in (4.7) is re-defined as

$$\boldsymbol{M} = \begin{bmatrix} a_1 & a_5 & a_9 & a_{13} \\ a_2 & a_6 & a_{10} & a_{14} \\ a_3 & a_7 & a_{11} & a_{15} \\ a_4 & a_8 & a_{12} & a_{16} \end{bmatrix} \tag{5.33}$$

The decision for the output signal $\hat{\boldsymbol{s}}_k$ will be

$$\hat{\boldsymbol{s}}_k = \begin{cases} \boldsymbol{\Phi}^{\dagger}_{2\times 2}\hat{\boldsymbol{x}}_k & \text{for } 2 \times 2 \text{ perfect code} \\ \boldsymbol{\Phi}^{\dagger}_{4\times 4}\hat{\boldsymbol{x}}_k & \text{for } 4 \times 4 \text{ perfect code} \end{cases} \tag{5.34}$$

5.6.1 Complexity Analysis

Now we compare the complexity of the proposed method to those of the methods published in [28–30]. From Table 5.2, we can see that the major computational complexity of the proposed method is n_c^3 times less than those of the algorithms in [28–30]. This saving is significant especially for large n_c and shows the computational advantage of our method.

Table 5.2 Complexity analysis

Methods	Complexity
[28]	$\boldsymbol{O}\left(2(n_c n_t(n_c+n_g))^3 + (n_c n_t)(n_c+n_g)^2 + n_c^4(n_t+n_g)^3\right)$
[29]	$\boldsymbol{O}\left((n_c n_t)^2(n_c+n_g)^2 + (n_c^3 n_t^2)(n_c+n_g)^2 + (n_c n_t)^3(n_c+n_g)^3\right)$
[30]	$\boldsymbol{O}\left(2(n_c n_t(n_c+n_g))^3 + (n_c n_t)(n_c+n_g)^2\right)$
This work	$\boldsymbol{O}\left(4(n_c n_t)^3 + n_c n_t\right)$

5.7 Simulation Results and Discussion

We consider an OFDM orthogonal pilot symbol with a total of $n_c = 128$ subcarriers and no virtual subcarriers. A cyclic prefix of length $n_g = n_c/4$ is inserted. The discrete-time channel has 16 taps. The channel coefficients are assumed to be correlated Rayleigh fading with known mean power delay profile $P_h = |h(i, j)|^2$. We consider 1-user 2×2 and 4×4 MIMO systems. The CFO was selected randomly from a range of $[-0.5 \ldots 0.5]$. For all results 10,000 independent realizations were simulated. The system parameters are summarized in Table 5.3. To check the optimality of the algorithm we derived the Cramer-Rao Lower Bound (CRLB) for the MIMO frequency offset as a measure of accuracy of the CFO estimator, which can be considered as the theoretical value of the variance of the estimate. We assume that the noise used is AWGN, and the signal to be estimated is unbiased. The information to be estimated in our case is the CFO values, which is provided by the imaginary part of the approximated function J_δ. The CRLB expression can be written as

$$\text{CRLB} \geq \frac{\sigma^2}{\sum_{\mathrm{p}=1}^{(\mathrm{n_r n_c}-1)} \left[\frac{\partial \Im(\mathrm{J}_\delta)}{\partial \delta}\right]^2} = \frac{\mathrm{n_c}\sigma^2}{16\pi^4 \mathrm{n_r}} \tag{5.35}$$

where σ^2 is the variance of the AWGN used. The CRLB is equal to the theoretical value of the variance.

The estimated CFO values in Figs. 5.7 and 5.8 for high signal to noise ratio fit asymptotically with the CRLB curves. The implemented algorithm for 2×2 and 4×4 MIMO configurations outperforms the estimators proposed in [7, 23] and [24] at all signal to noise ratio range. For both 2×2 and 4×4 configurations the variance follows the CRLB asymptotically.

It is clear from the results in Fig. 5.9 that the frequency synchronization method has some degradation in performance at low signal to noise ratio, which can be explained by the less accurate estimation of the frequency offset at these $\frac{E_b}{N_0}$ values. In the BER range of interest, however, the degradation compared to perfect synchronization is very small for both 2×2 and 4×4 ASTC. We note that for 2×2 perfect codes the gain is about 2 dB, which is due to the full rate, full diversity and good spectral efficiency of the 2×2 perfect codes. The use of the perfect codes with 4×4 configuration

Table 5.3 Simulation parameters

System parameter	Parameter value
Modulation	QPSK
Bandwidth	18MHz
Number of subcarriers	$n_c = 128$
Cyclic prefix length	$n_g = \frac{n_c}{4} = 32$
Channel coding	Perfect code 2×2 and 4×4

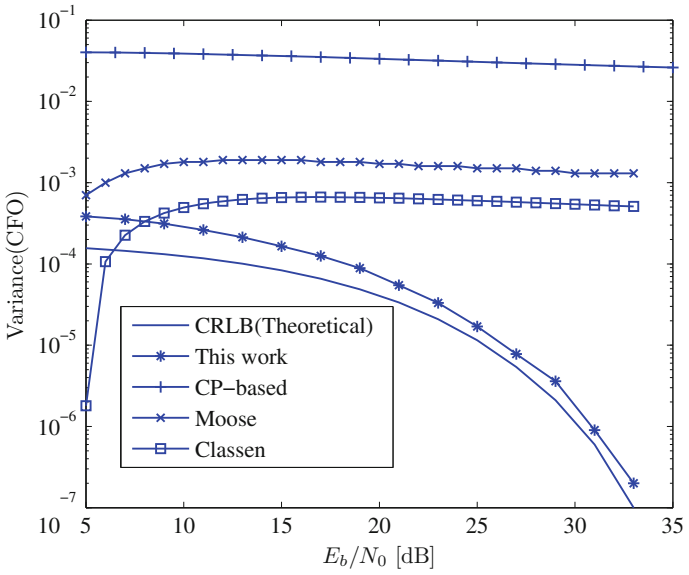

Fig. 5.7 Theoretical and simulated variance of CFO for MIMO configuration of 2×2

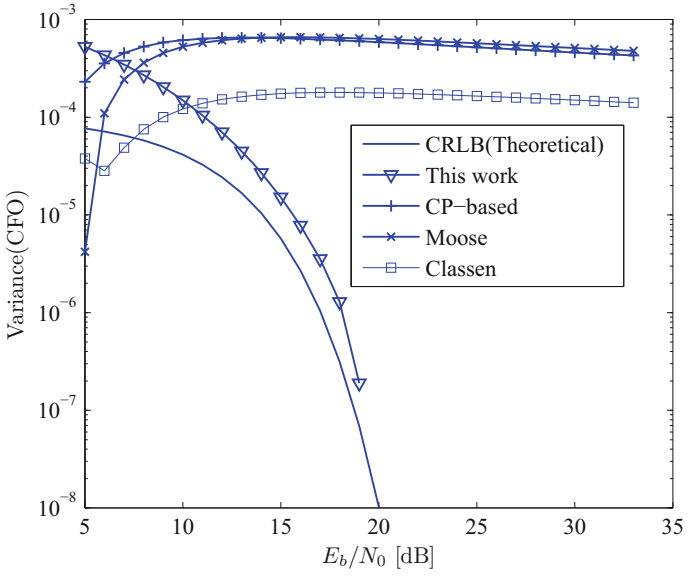

Fig. 5.8 Theoretical and simulated variance of CFO for MIMO configuration of 4×4

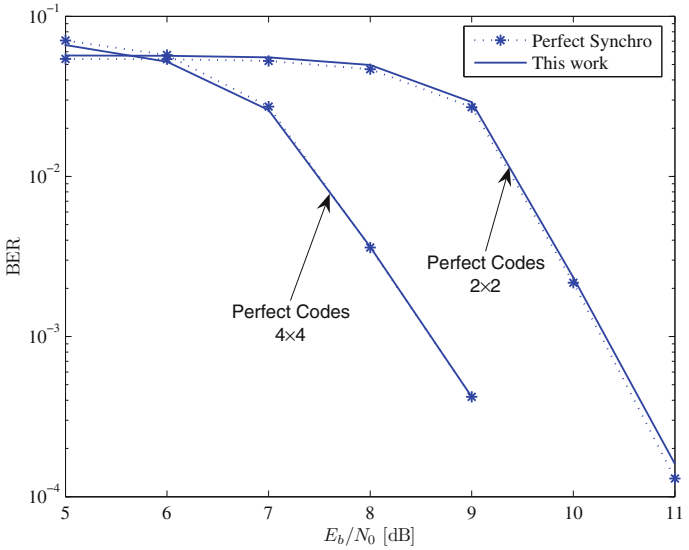

Fig. 5.9 Performance of the proposed method using perfect and implemented synchronization for 2×2 and 4×4 configurations, $n_c = 128$ subcarriers, with an ASTC scheme

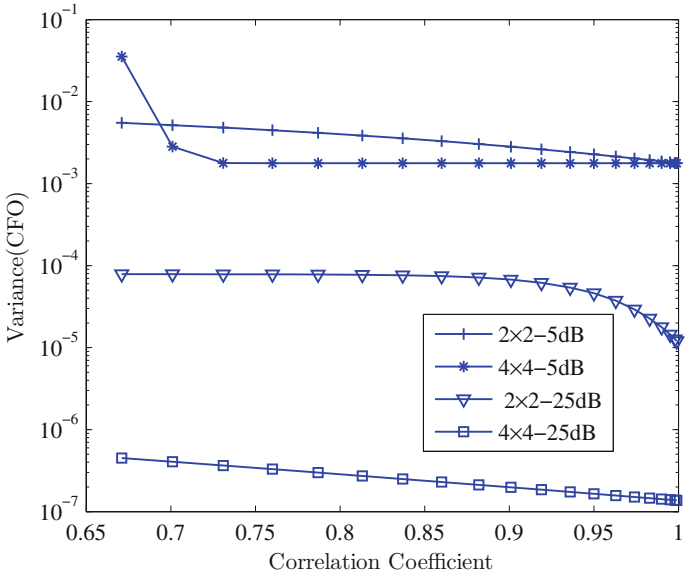

Fig. 5.10 Estimator performance with respect to correlation for 2×2 and 4×4 MIMO configurations and 5 dB and 25 dB $\frac{E_b}{N_0}$ values

increases notably the performance of the proposed MIMO-OFDM system at low signal to noise ratio and achieve the frequency synchronization more accurately.

In Fig. 5.10 we show the variance performance of the proposed estimator with respect to correlation coefficient for different $\frac{E_b}{N_0}$ values and antenna numbers. It can be noticed that as the correlation coefficient increases, the variance of CFO will decrease to the minimum. The variance will become much smaller for higher $\frac{E_b}{N_0}$ values and larger antenna numbers.

5.8 Conclusion

This chapter presents a new algebraic CFO estimation technique for MIMO OFDM systems over frequency-selective fading channels employing algebraic space time coding schemes with random CFO among all transmit and receive antenna pairs. The performance of the new CFO compensation is evaluated using Monte Carlo simulation for different correlation and MIMO scenarios, employing two ASTC codes, and compared with the empirical bound defined by the CRLB and other three known CFO estimators: CP-based, Moose and Classen techniques. The simulation results have revealed that the new method reaches the empirical bound very closely and outperforms those published estimators.

References

1. Bannour A, Ammari M, Bouallegue R (2010) Adaptation of golden codes with a correlated Rayleigh frequency-selective channel in OFDM system with imperfect channel estimation. In: 7th International symposium on wireless communication systems (ISWCS), pp 159–163
2. Bannour A, Ammari M, Y S, Bouallegue R (2011) On the capacity of ASTC-MIMO-OFDM system in a correlated Rayleigh frequency-selective channel. In: IEEE Vehicular technology conference, pp 1–5
3. Al-Dweik AH, Renfors MR (2007) Blind estimation of large carrier frequency offset in wireless OFDM systems. IEEE Trans Veh Technol 56:965–968
4. Salberg A, Swami AB (2005) Doppler and frequency-offset synchronization in wideband OFDM. IEEE Trans Wirel Commun 4:2870–2881
5. Wei L, Schlegel C (2002) Synchronization requirements for multi-user OFDM on satellite mobile and two-path Rayleigh fading channels. IEEE Trans Commun 43:887–895
6. Pollet T, Peeters M (2002) Synchronization with DMT modulation. IEEE Commun Mag 37:80–86
7. Moose PH (1994) A technique for orthogonal frequency division multiplexing frequency offset correction. IEEE Trans Commun 42:2908–2914
8. Schmidl TM, Cox DC (2007) Robust frequency and timing synchronization for OFDM. IEEE Trans Commun 45:1613–1621
9. Santella G (2002) A frequency and symbol synchronization system for OFDM signals: architecture and simulation results. IEEE Trans Veh Technol 49:254–275
10. Morelli M, Mengali U (2002) An improved frequency offset estimator for OFDM applications. IEEE Commun Lett 3:75–77

11. Hyoung-Kyu S, Young-Hwan Y, Jong-Ho P, Yong-Soo C (2000) Frequency-offset synchronization and channel estimation for OFDM-based transmission. IEEE Commun Lett 4:95–97
12. Luise M, Reggiannini R (2005) Carrier frequency acquisition and tracking for OFDM systems. IEEE Trans Commun 44:1590–1598
13. Sun Y, Xiong Z, Wang X (2005) Em-based iterative receiver design with carrier-frequency offset estimation for MIMO-OFDM systems. IEEE Trans Commun 53:581–586
14. Roman T, Enescu M, Koivunen V (2004) Joint time-domain tracking of channel and frequency offsets for MIMO-OFDM systems. Wirel Pers Commun 53:181–200
15. Minn H, Al-Dhahir N, Li Y (2006) Optimal training signals for MIMO-OFDM channel estimation in the presence of frequency offset and phase noise systems. IEEE Trans Commun 54:1754–1759
16. Mounir G, Swami A (2006) Training design for multipath channel and frequency-offset estimation in MIMO systems. IEEE Trans Commun 54:3957–3965
17. Tureli U, Liu H, Zoltowski M D(2007) A high efficiency carrier estimator for OFDM communications. In: Conference record of the thirty-first asilomar conference on signals, systems and computers, pp 505–509
18. van de Beek JJ, Sandell M, Borjesson PO (2002) ML estimation of time and frequency offset in OFDM systems. IEEE Trans Signal Process 45:1800–1805
19. Czylwik A (1999) Synchronization for systems with antenna diversity. In: 50th IEEE Vehicular technology conference, vol 2, pp 728–732
20. Mody A N, Stuber G L (2001) Synchronization for MIMO OFDM systems. In: IEEE Global telecommunications conference, pp 509–513
21. Tureli U, Kivanc D, Liu H (2001) Multicarrier synchronization with diversity. In: 54th Vehicular technology conference, pp 952–956
22. Bannour A, Sun Y, Ammari M L, Delestre F, Bouallegue R (2012) A novel algebraic carrier frequency offset estimator for ASTC-MIMO-OFDM systems over a correlated frequency selective channels. IEEE Trans Veh Technol 61:2468–2475
23. Yue X, Xia L, Shaoqian L (2007) Improved CP-based carrier frequency offset estimator for OFDM systems. In: International conference on wireless communications, networking and mobile computing, pp 209–211
24. Classen F, Meyr H (1994) Frequency synchronization algorithms for OFDM systems suitable for communication over frequency selective fading channels. In: IEEE 44th Vehicular technology conference, pp 1655–1659
25. Yang S, Belfiore J C, Rekaya G, Othman B (2006) Perfect space-time block codes for parallel MIMO channels. IEEE
26. Telatar I (1995) Capacity of multi-antenna Gaussian channels. Eur Trans Telecommun 10:585–595
27. Haring L, Czylwik A (2004) Synchronization in MIMO OFDM systems. Adv Radio Sci 2:147–153
28. Feng G, Zhang X, Wu H, Li J, Xu D (2011) Novel carrier frequency offset estimator in MIMO-OFDM system. Int J Digi Content Technol Appl 5:59–66
29. Feng B, Zhang X, Wang D, Yu J (2009) Multiple invariance ESPRIT-based blind carrier frequency offset estimation for OFDM system with array antennas. In: 1st International conference on information science and engineering, pp 604–607
30. Niu Y, Shen Y, Sun S (2008) Blind frequency synchronization in MIMO-OFDM system based on ESPRIT. In: International conference on microwave and millimeter wave technology, vol 4, pp 1972–1975

Chapter 6
Space Time Frequency (STF) for Multiuser MIMO-OFDM

6.1 Introduction

In this chapter, the design procedure of STF code [1] which is capable of achieving full diversity $A_t A_r A_u L$ and high code rate (i.e. rate-A_t) over MIMO frequency selective block fading channel, is presented. The construction of the presented multiuser STF is illustrated in Fig. 6.1. The STF code has been constructed from a threaded algebraic layering concept, which combines the space-frequency layering with algebraic component codes. The component code is estimated to be an algebraic number theoretic constellation. Each component code is assigned to a "thread" and interleaved over space time and frequency. Diophantine approximation theory is then used to make the threads transparent to each other. In addition, another approximation is used so that the users become transparent to each other. The presented STF code does not require the cooperation among the users in uplink process and also does not require zero-padding, which always ensures high symbol rate. The presented coding schemes are bandwidth efficient as the data streams of all the users are sent simultaneously through all the OFDM sub-channels. It is assumed that the source generates a block of $N_s = N A_t A_u$ information symbols $S^{(z)}$ for user z, where $z = 1, 2, \ldots, Z$ and $S^{(z)} \in \mathcal{T}^{N A_t A_u}$, which are QAM from the discrete alphabet τ and the system has N-OFDM tones.

Let, $Q = W_z W_L W_t$ where $W_L = 2^{\lceil \log_2 L \rceil}$, $W_t = 2^{\lceil \log_2 A_t \rceil}$, $W_Z = 2^{\lceil \log_2 Z \rceil}$. The block of $N A_t A_u$ information symbols $S^{(z)} = [S_1{}^{(z)} S_2{}^{(z)} \ldots S_{BQ}{}^{(z)}]^T$ are normalized into the unit power and are evenly split into $B = \frac{N}{Q}$ sub blocks,

$$S^{(z)} = \left[\left(S_1{}^{(z)} \right)^T \left(S_2{}^{(z)} \right)^T \ldots \left(S_B{}^{(z)} \right)^T \right]^T \tag{6.1}$$

B. Ahmed and M. Abdul Matin, *Coding for MIMO-OFDM in Future Wireless Systems*, SpringerBriefs in Electrical and Computer Engineering,
DOI 10.1007/978-3-319-19153-9_6

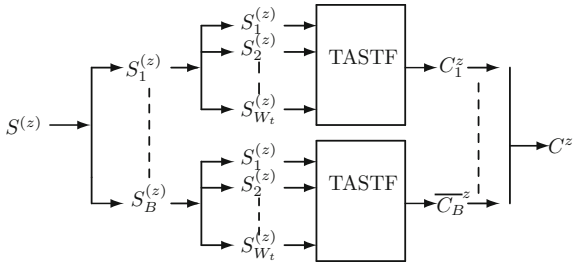

Fig. 6.1 STF coding structure in MIMO-OFDM system

Each sub block $S_b^{(z)} \in (\mathcal{T})^{\mathcal{W}_{\mathcal{Z}}\mathcal{A}_{\sqcup}\mathcal{W}_{\mathcal{L}}\mathcal{W}_{\sqcup}}$, where $b = 1, 2, \ldots, B$, is composed of the signal vectors $S_w(^z) \in \mathcal{T}^{\tilde{=}}$, $w = 1, 2, 3, \ldots$, and $\tilde{w} = W_Z W_L A_t$. and given by

$$S_b{}^{(z)} = \left[\left(S_1{}^{(z)}\right)^T \left(S_2{}^{(z)}\right)^T \ldots \left(S_{w_t}{}^{(z)}\right)^T\right]^T \tag{6.2}$$

Each one of the component vector S_w is than encoded independently using constituent encoder $\bar{X}_w^{(z)} : \mathcal{T}^{\tilde{W}} \to \chi^{\tilde{W}}$, where, χ is the output alphabet and given by

$$\bar{X}_w^{(z)} = \phi\Theta S_w{}^{(z)} \tag{6.3}$$

$$= \left[x_{w,1}^{-1\,(z)} \ldots x_{w,W_L}^{-1\quad(z)} \ldots x_{w,1}^{-A_u\,(z)} \ldots x_{w,W_L}^{A_u\quad(z)}\right]^T \tag{6.4}$$

where Θ, is an $\tilde{w} \times \tilde{w}$ unitary matrix (rotational matrix) and it is constructed by the first principal $\tilde{w} \times \tilde{w}$ matrix of the following $\tilde{y} \times \tilde{y}$ matrix:

$$\psi = F_{\tilde{y}}^H diag\left(1, \varphi, \ldots, \varphi^{\tilde{y}}\right) \tag{6.5}$$

where, $\tilde{y} = 2^{\lceil \log_2 \tilde{w} \rceil}$, $F_{\tilde{y}}$ is the $\tilde{y} \times \tilde{y}$ discrete Fourier transform (DFT) matrix and $\varphi = e^{\left(\frac{j2\pi}{4\tilde{y}}\right)}$. It is worth noting that, multiplying information symbol vector S_w by the rotational matrix Θ maximize the associated minimum product distance,

$$d_{\tilde{w}} \stackrel{\Delta}{=} \min_{\bar{X}^{(z)}=\Theta\left(S^{(z)}-S'^{(z)}\right), S^{(z)} \neq S'^{(z)}} \prod_{w=1}^{\tilde{w}} \left(\bar{X}_w^{(z)}\right) \tag{6.6}$$

where $\bar{X}^{(z)} = \left[\bar{X}_1^{(z)} \bar{X}_2^{(z)} \ldots \bar{X} w_t{}^{(z)}\right]^T$. As coding gains are proportional to the minimum product distances associated with the rotational matrix used, the maximization of the coding gain in the code design criteria is achieved.

Each one of the encoded component vector S_w is then multiplied by the Diophantine number $\phi_{1,w}$ that is chosen to ensure full diversity and maximize the coding gain for the joint code. Each $\phi_{1,w}$ is chosen from the wth diagonal layer of the $W_t \times A_t$ matrix,

$$\Phi_1 = \begin{pmatrix} 1 & {\phi_1}^{(w_t-1)} & \dots & {\phi_1}^{(w_t-A_t)+1} \\ \phi_1 & 1 \dots & & {\phi_1}^{(w_t-A_t)+2} \\ {\phi_1}^2 & \phi_1 \dots & & \vdots \\ \vdots & \vdots \ddots & & \vdots \\ {\phi_1}^{(w_t-1)} & {\phi_1}^{(w_t-2)} & \dots & \phi_1^{\left(1-\frac{A_t}{W_t}\right)W_t} \end{pmatrix}$$

Φ_1 will be defined latter. The term $(\bar{\chi}_{w,i}^{d})^{(z)}$ in (6.3) is given by,

$$(\bar{\chi}_{w,i}^{d})^{(z)} = \left[{X_w}^{(z)} \left(P_{i,d}^{l} + 1 \right) \dots {X_w}^{(z)} \left(P_{i,d}^{l} + A_t \right) \right] \tag{6.7}$$

For $i = 1, \dots W_L$, where the index, $P_{i,d^l} = (i-1)\, A_t + (l-1) W_z W_L A_t$ and $l = 1, 2, ..., W_Z$.

Next, a space-frequency formatter $f_W \left(\bar{X}_w^{(z)} \left(S_w^{(z)} \right) \right)$ assigns the wth code symbols $X_w^{(z)} \left(P_{i,d^l} + n \right), n = 1, 2, \dots, A_t$ of the row vector $\bar{x}_{w,i^d}^{(z)}$ on the wth layer of the $W_t \times A_t$ matrix,

$$\bar{X}_{i,l}^{(z)} = {\chi_{i,d}}^{(z)} \circ \Phi_1 \tag{6.8}$$

where $W_t \times A_t$ matrix $\chi_{i,d}^{(z)}$ is given by,

$$\chi_{i,d}^{(z)} = \begin{pmatrix} {X_1}^{(z)} \left(P_{i,d}^{l} + 1 \right) & {X_{W_t}}^{(z)} \left(P_{i,d}^{l} + 1 \right) & \dots\dots & {X_{(W_t-A_t)+2}}^{(z)} \left(P_{i,d}^{l} + 1 \right) \\ {X_2}^{(z)} \left(P_{i,d}^{l} + \left\lfloor \frac{\mathrm{A_t}}{\mathrm{w_t}} + 1 \right\rfloor \right) & {X_1}^{(z)} \left(P_{i,d}^{l} + 2 \right) & \dots\dots & {X_{(W_t-A_t)+3}}^{(z)} \left(P_{i,d}^{l} + 2 \right) \\ {X_3}^{(z)} \left(P_{i,d}^{l} + 2 \right) & {X_2}^{(z)} \left(P_{i,d}^{l} + \left\lfloor \frac{\mathrm{A_t}}{\mathrm{w_t}} + 2 \right\rfloor \right) & \ddots & {X_{(W_t-A_t)+4}}^{(z)} \left(P_{i,d}^{l} + 3 \right) \\ \vdots & \vdots & \vdots & \vdots \\ {X_{W_t}}^{(z)} \left(P_{i,d}^{l} + \mathrm{A_t} \right) & {X_{W_t-1}}^{(z)} \left(P_{i,d}^{l} + \mathrm{A_t} \right) & \dots\dots & {X_{\left(1-\frac{A_t}{W_t}\right)W_t+1}}^{(z)} \left(P_{i,d}^{l} + \mathrm{A_t} \right) \end{pmatrix}$$

The diagonal layer index of $(\bar{X}_{i,l}^{d})^{(z)}$ is shown in below, $A_t = 3$ and $W_t = 4$

$$\begin{pmatrix} 1 & 4 & 3 \\ 2 & 1 & 4 \\ 3 & 2 & 1 \\ 4 & 3 & 2 \end{pmatrix} \tag{6.9}$$

Thus, each sub-block, ${S_b}^{(z)}$ $b = 1, 2, 3, ., B$ is encoded into an SF code matrix C_b of size $Q \times A_t A_u$ matrix, where,

$$\begin{pmatrix} (\bar{X}^1_{1,1})^{(z)} & \cdots & (\bar{X}^{A_u}_{1,1})^{(z)} \\ \vdots & \ddots & \vdots \\ (\bar{X}^1_{1,W_Z})^{(z)} & \cdots & (\bar{X}^{A_u}_{1,W_Z})^{(z)} \\ \vdots & \ddots & \vdots \\ (\bar{X}^1_{W_L,1})^{(z)} & \cdots & (\bar{X}^{A_u}_{W_L,1})^{(z)} \\ \vdots & \ddots & \vdots \\ (\bar{X}^1_{W_L,W_Z})^{(z)} & \cdots & (\bar{X}^{A_u}_{W_L,W_Z})^{(z)} \end{pmatrix} \tag{6.10}$$

For multi-user MIMO-OFDM MAC, the encoded $\bar{C}_b^{(z)}$ is given by,

$$\bar{C}_b^{(z)} = \left(\Phi_{2,z} \otimes 1_{1\times A_t A_u}\right) \circ {C_b}^{(z)} \tag{6.11}$$

where, $\Phi_{2,z}$ is the zth column of the matrix $Q \times W_Z$, Φ_2

$$\Phi_2 = \begin{pmatrix} 1 & {\phi_2}^{(Q-1)} & \ldots & {\phi_2}^{(Q-W_z)+1} \\ \phi_2 & 1 & \ldots & {\phi_2}^{(Q-W_z)+2} \\ \vdots & \vdots & \ldots & \vdots \\ \vdots & \vdots & \ddots & \vdots \\ {\phi_2}^{(Q-1)} & {\phi_2}^{(Q-2)} & \ldots & {\phi_2}^{\left(1-\frac{W_z}{Q}\right)Q} \end{pmatrix} \tag{6.12}$$

The choice of ϕ_1 and ϕ_2 are as follows: $\phi_1 = \theta^{\frac{1}{w_t}}$, where θ is an algebraic clement with degree at least $W_t W_L$ over $\mathcal{A}$, where $\phi_2 = \phi^{\frac{1}{Q}}$ is an algebraic number with degree of at least $Q W_L$ over $\mathcal{A}$, where $\mathcal{A}$ is the field extention of $\mathbb{Q}$ which contains the signal alphabet $\mathcal{T} \subset \mathbb{Z}[j]$, Θ and $e^{\frac{-j2\pi\eta_l}{T_s}}$, $(l = 0, 1, \ldots, \mathrm{L}-1)$ and all the entries of Θ.

It is worth noting that, according to the *Theorems 1 and 2* given in [3], the coding gain expresses the simultaneous Diophantine approximation of the numbers $\{\phi_1^0, \phi_1^1 = \theta^{\frac{1}{w_t}}, \ldots, \phi_1^{w_t-1} = \theta^{\frac{w_t-1}{w_t}}\}$ and $\{\phi_2^0 = 1, \phi_2^1 = \phi^{\frac{1}{\rho}}, \ldots, \phi_2^{Q-1} = \phi^{\frac{Q-1}{\rho}}\}$ by other algebraic numbers, depending on the constellation used. This observation implies that optimizing the coding gain is equivalent to choosing these Diophantine numbers to be "badly approximated" by other algebraic number.

The STF coding applies the same coding strategy to every encoded sub block $\overline{C}_b^z$, $b = 1, 2, \ldots, B$. So, for convenience, here, the STF coding of one sub block $\overline{C}_b^z$ is illustrated in Fig. 6.2. Thus, the proposed STF codes codes $C^{(z)} \in \mathcal{T}^{N\times A_t A_u}$ for the zth user is of the form:

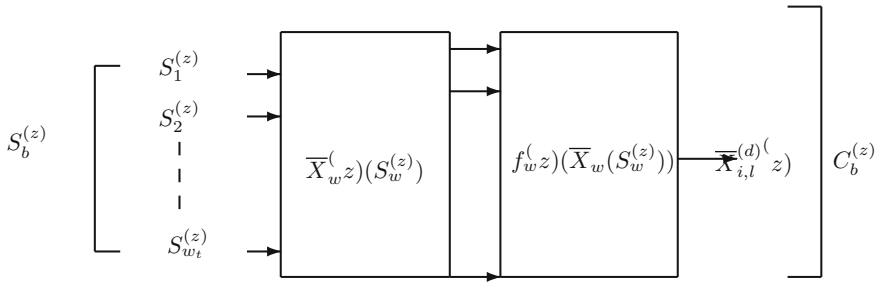

Fig. 6.2 Threaded algebraic STF code design

$$C^{(z)} = \left[\left(\bar{C}_1^{(z)} \right)^T \left(\bar{C}_2^{(z)} \right)^T \cdots \left(\bar{C}_B^{(z)} \right)^T \right]^T \tag{6.13}$$

Note that as no zero-padding matrix is required in the code structure, the rate-A_t can always be guaranteed. Also note that the difference of the STF codes between two users is made by the selection of different columns of $Q \times W_z$ matrix given in (6.12). As Φ_2 can be known in advance and each transmitter can know its fixed selected column $\Phi_{2,z}$ before the data transmission, the cooperation among the different users is not necessary in the uplink process.

6.1.1 Code Design Example

In this section, an example of the proposed STF code is presented. For convenience, we have just shown the sub-block $\bar{C}_1^{(z)}$, because the same coding strategies can be applied to every sub-block $\bar{C}_b^{(z)}$, $b = 1, \ldots, B$.

Example: Let, $A_u = 1$, $A_t = 2$, $L = 2$, $Z = 2$. So $W_L = W_t = W_z = 2$

Thus Φ_1, is 2×2 matrix and given by, $\Phi_1 = \begin{pmatrix} 1 & \phi_1 \\ \phi_1 & 1 \end{pmatrix}$ and Φ_2 is 8×2 matrix and given by,

$$\Phi_2 = \begin{pmatrix} 1 & \phi_2^7 \\ \phi_2^2 & \phi_2^6 \\ \phi_2^3 & \phi_2^5 \\ \phi_2^4 & \phi_2^4 \\ \phi_2^5 & \phi_2^3 \\ \phi_2^6 & \phi_2^2 \\ \phi_2^7 & 1 \end{pmatrix} \tag{6.14}$$

Now, for:
i = 1, l = 1, d = 1, $P^1_{1,1} = 0$;
i = 1, l = 2, d = 1, $P^2_{1,1} = 4$;
i = 2, l = 1, d = 1, $P^1_{1,1} = 2$;
i = 2, l = 2, d = 1, $P^2_{1,1} = 6$;

For z = 1, $(\bar{X}^1_{1,1})^{(1)} = \begin{pmatrix} X_1^{(1)}(1) & (\phi_1 X_2)^{(1)}(1) \\ (\phi_1 X_2)^{(1)}(2) & X_1^{(1)}(2) \end{pmatrix}$,

$(\bar{X}^1_{2,1})^{(1)} = \begin{pmatrix} X_1^{(1)}(3) & (\phi_1 X_2^{(1)}(3) \\ (\phi_1 X_2)^{(1)}(4) & X_1^{(1)}(4) \end{pmatrix}$,

$(\bar{X}^1_{1,2})^{(1)} = \begin{pmatrix} X_1^{(1)}(5) & (\phi_1 X_2)^{(1)}(5) \\ (\phi_1 X_2)^{(1)}(6) & X_1^{(1)}(6) \end{pmatrix}$,

$(\bar{X}^1_{2,2})^{(1)} = \begin{pmatrix} X_1^{(1)}(7) & (\phi_1 X_2)^{(1)}(7) \\ (\phi_1 X_2)^{(1)}(8) & X_1^{(1)}(8) \end{pmatrix}$

Now, $c_1{}^{(z)} = \begin{pmatrix} (\bar{X}^1_{1,1})^{(1)} \\ (\bar{X}^1_{2,1})^{(1)} \\ (\bar{X}^1_{1,2})^{(1)} \\ (\bar{X}^1_{2,2})^{(1)} \end{pmatrix} = \begin{pmatrix} X_1{}^{(1)}(1) & \phi_1 X_2{}^{(1)}(1) \\ \phi_1 X_2{}^{(1)}(2) & X_1{}^{(1)}(2) \\ X_1{}^{(1)}(3) & \phi_1 X_2{}^{(1)}(3) \\ \phi_1 X_2{}^{(1)}(4) & X_1{}^{(1)}(4) \\ X_1{}^{(1)}(5) & \phi_1 X_2{}^{(1)}(5) \\ \phi_1 X_2{}^{(1)}(6) & X_1{}^{(1)}(6) \\ X_1{}^{(1)}(7) & \phi_1 X_2{}^{(1)}(7) \\ \phi_1 X_2{}^{(1)}(8) & X_1{}^{(1)}(8) \end{pmatrix}$

Thus,

$$\bar{C}_1^{(1)} = \left(\Phi_{2,1} \otimes 1_{1\times 2}\right) \circ c_1{}^{(1)} = \begin{pmatrix} X_1{}^{(1)}(1) & \phi_1 X_2{}^{(1)}(1) \\ \phi_2\phi_1 X_2{}^{(1)}(2) & \phi_2 X_1{}^{(1)}(2) \\ \phi_2^2 X_1{}^{(1)}(5) & \phi_2^2\phi_1 X_2{}^{(1)}(5) \\ \phi_2^3\phi_1 X_2{}^{(1)}(6) & \phi_2^3 X_1{}^{(1)}(6) \\ \phi_2^4 X_1{}^{(1)}(3) & \phi_2^4\phi_1 X_2{}^{(1)}(3) \\ \phi_2^5\phi_1 X_2{}^{(1)}(4) & \phi_2^5 X_1{}^{(1)}(4) \\ \phi_2^6 X_1{}^{(1)}(7) & \phi_2^6\phi_1 X_2{}^{(1)}(7) \\ \phi_2^7\phi_1 X_2{}^{(1)}(8) & \phi_2^7 X_1{}^{(1)}(8) \end{pmatrix} \tag{6.15}$$

Similarly, for $z = 2$

$$\bar{C}_1^{(2)} = \left(\Phi_{2,1} \otimes 1_{1\times 2}\right) \circ {c_1}^{(1)} = \begin{pmatrix} \phi_2^7 {X_1}^{(2)}(1) & \phi_2^7\phi_1 {X_2}^{(2)}(1) \\ \phi_1 {X_2}^{(2)}(2) & {X_1}^{(2)}(2) \\ \phi_2 {X_1}^{(2)}(5) & \phi_2\phi_1 {X_2}^{(2)}(5) \\ \phi_2^2\phi_1 {X_2}^{(2)}(6) & \phi_2^2 {X_1}^{(2)}(6) \\ \phi_2^3 {X_1}^{(2)}(3) & \phi_2^3\phi_1 {X_2}^{(2)}(3) \\ \phi_2^4\phi_1 {X_2}^{(2)}(4) & \phi_2^4 {X_1}^{(2)}(4) \\ \phi_2^5 {X_1}^{(2)}(7) & \phi_2^5\phi_1 {X_2}^{(2)}(7) \\ \phi_2^6\phi_1 {X_2}^{(2)}(8) & \phi_2^6 {X_1}^{(2)}(8) \end{pmatrix} \tag{6.16}$$

Example: Let, $A_t = A_u = 2$, $L = 2$, $Z = 2$, For for user-1,

$$\bar{C}_1^{(1)} = \begin{pmatrix} {X_1}^{(1)}(1) & \phi_1 {X_2}^{(1)}(1) & {X_1}^{(1)}(9) & \phi_1 {X_2}^{(1)}(9) \\ \phi_2\phi_1 {X_2}^{(1)}(2) & \phi_2 {X_1}^{(1)}(2) & \phi_2\phi_1 {X_2}^{(1)}(10) & \phi_2 {X_1}^{(1)}(10) \\ \phi_2^2 {X_1}^{(1)}(5) & \phi_2^2\phi_1 {X_2}^{(1)}(5) & \phi_2^2 {X_1}^{(1)}(13) & \phi_2^2\phi_1 {X_2}^{(1)}(13) \\ \phi_2^3\phi_1 {X_2}^{(1)}(6) & \phi_2^3 {X_1}^{(1)}(6) & \phi_2^3\phi_1 {X_2}^{(1)}(14) & \phi_2^3 {X_1}^{(1)}(14) \\ \phi_2^4 {X_1}^{(1)}(3) & \phi_2^4\phi_1 {X_2}^{(1)}(3) & \phi_2^4 {X_1}^{(1)}(11) & \phi_2^4\phi_1 {X_2}^{(1)}(11) \\ \phi_2^5\phi_1 {X_2}^{(1)}(4) & \phi_2^5 {X_1}^{(1)}(4) & \phi_2^5\phi_1 {X_2}^{(1)}(12) & \phi_2^5 {X_1}^{(1)}(12) \\ \phi_2^6 {X_1}^{(1)}(7) & \phi_2^6\phi_1 {X_2}^{(1)}(7) & \phi_2^6 {X_1}^{(1)}(15) & \phi_2^6\phi_1 {X_2}^{(1)}(15) \\ \phi_2^7\phi_1 {X_2}^{(1)}(8) & \phi_2^7 {X_1}^{(1)}(8) & \phi_2^7\phi_1 {X_2}^{(1)}(16) & \phi_2^7 {X_1}^{(1)}(16) \end{pmatrix} \tag{6.17}$$

for user-2,

$$\bar{C}_1^{(2)} = \begin{pmatrix} \phi_2^7 {X_1}^{(2)}(1) & \phi_2^7\phi_1 {X_2}^{(2)}(1) & \phi_2^7 {X_1}^{(2)}(9) & \phi_2^7\phi_1 {X_2}^{(2)}(9) \\ \phi_1 {X_2}^{(2)}(2) & {X_1}^{(2)}(2) & \phi_1 {X_2}^{(2)}(10) & {X_1}^{(2)}(10) \\ \phi_2 {X_1}^{(2)}(5) & \phi_2\phi_1 {X_2}^{(2)}(5) & \phi_2 {X_1}^{(2)}(13) & \phi_2\phi_1 {X_2}^{(2)}(13) \\ \phi_2^2\phi_1 {X_2}^{(2)}(6) & \phi_2^2 {X_1}^{(2)}(6) & \phi_2^2\phi_1 {X_2}^{(2)}(14) & \phi_2^2 {X_1}^{(2)}(14) \\ \phi_2^3 {X_1}^{(2)}(3) & \phi_2^3\phi_1 {X_2}^{(2)}(3) & \phi_2^3 {X_1}^{(2)}(11) & \phi_2^3\phi_1 {X_2}^{(2)}(11) \\ \phi_2^4\phi_1 {X_2}^{(2)}(4) & \phi_2^4 {X_1}^{(2)}(4) & \phi_2^4\phi_1 {X_2}^{(2)}(12) & \phi_2^4 {X_1}^{(2)}(12) \\ \phi_2^5 {X_1}^{(2)}(7) & \phi_2^5\phi_1 {X_2}^{(2)}(7) & \phi_2^5 {X_1}^{(2)}(15) & \phi_2^5\phi_1 {X_2}^{(2)}(15) \\ \phi_2^6\phi_1 {X_2}^{(2)}(8) & \phi_2^6 {X_1}^{(2)}(8) & \phi_2^6\phi_1 {X_2}^{(2)}(16) & \phi_2^6 {X_1}^{(2)}(16) \end{pmatrix} \tag{6.18}$$

Example: Let, $A_u = 2$, $A_t = 2$, $L = 2$, $Z = 2$, For for user-1,

$$\tilde{C}_1^{(1)} = \begin{pmatrix} X_1{}^{(1)}(1) & \phi_1^3 X_4{}^{(1)}(1) & \phi_1^2 X_3{}^{(1)}(1) & X_1{}^{(1)}(13) & \phi_1^3 X_4{}^{(1)}(13) & \phi_1^2 X_3{}^{(1)}(13) \\ \phi_2\phi_1 X_2{}^{(1)}(1) & \phi_2 X_1{}^{(1)}(2) & \phi_2\phi_1{}^3 X_4{}^{(1)}(2) & \phi_2\phi_1 X_2{}^{(1)}(13) & \phi_2 X_1{}^{(1)}(14) & \phi_2\phi_1{}^3 X_4{}^{(1)}(14) \\ \phi_2{}^2\phi_1{}^2 X_3{}^{(1)}(2) & \phi_2{}^2\phi_1 X_2{}^{(1)}(2) & \phi_2{}^2 X_1{}^{(1)}(3) & \phi_2{}^2\phi_1{}^2 X_3{}^{(1)}(14) & \phi_2{}^2\phi_1 X_2{}^{(1)}(14) & \phi_2{}^2 X_1{}^{(1)}(15) \\ \phi_2{}^3\phi_1{}^3 X_4{}^{(1)}(3) & \phi_2{}^3\phi_1{}^2 X_3{}^{(1)}(3) & \phi_2{}^3\phi_1 X_2{}^{(1)}(3) & \phi_2{}^3\phi_1{}^3 X_4{}^{(1)}(14) & \phi_2{}^3\phi_1{}^2 X_3{}^{(1)}(14) & \phi_2{}^3\phi_1 X_2{}^{(1)}(15) \\ \phi_2{}^4 X_1{}^{(1)}(7) & \phi_2{}^4\phi_1{}^3 X_4{}^{(1)}(7) & \phi_2{}^4\phi_1{}^2 X_3{}^{(1)}(7) & \phi_2{}^4 X_1{}^{(1)}(19) & \phi_2{}^4\phi_1{}^3 X_4{}^{(1)}(19) & \phi_2{}^4\phi_1{}^2 X_3{}^{(1)}(19) \\ \phi_2{}^5\phi_1 X_2{}^{(1)}(7) & \phi_2{}^5 X_1{}^{(1)}(8) & \phi_2{}^5\phi_1{}^3 X_4{}^{(1)}(8) & \phi_2{}^5\phi_1 X_2{}^{(1)}(19) & \phi_2{}^5 X_1{}^{(1)}(20) & \phi_2{}^5\phi_1{}^3 X_4{}^{(1)}(20) \\ \phi_2{}^6\phi_1{}^2 X_3{}^{(1)}(8) & \phi_2{}^6\phi_1 X_2{}^{(1)}(8) & \phi_2{}^6 X_1{}^{(1)}(9) & \phi_2{}^6\phi_1{}^2 X_3{}^{(1)}(20) & \phi_2{}^6\phi_1 X_2{}^{(1)}(20) & \phi_2{}^6 X_1{}^{(1)}(21) \\ \phi_2{}^7\phi_1{}^3 X_4{}^{(1)}(9) & \phi_2{}^7\phi_1{}^2 X_3{}^{(1)}(9) & \phi_2{}^7\phi_1 X_2{}^{(1)}(9) & \phi_2{}^7\phi_1{}^3 X_4{}^{(1)}(21) & \phi_2{}^7\phi_1{}^2 X_3{}^{(1)}(21) & \phi_2{}^7\phi_1 X_2{}^{(1)}(21) \\ \phi_2{}^8 X_1{}^{(1)}(4) & \phi_2{}^8\phi_1{}^3 X_4{}^{(1)}(4) & \phi_2{}^8\phi_1{}^2 X_3{}^{(1)}(4) & \phi_2{}^8 X_1{}^{(1)}(16) & \phi_2{}^8\phi_1{}^3 X_4{}^{(1)}(16) & \phi_2{}^8\phi_1{}^2 X_3{}^{(1)}(16) \\ \phi_2{}^9\phi_1 X_2{}^{(1)}(4) & \phi_2{}^9 X_1{}^{(1)}(5) & \phi_2{}^9\phi_1{}^3 X_4{}^{(1)}(5) & \phi_2{}^9\phi_1 X_2{}^{(1)}(16) & \phi_2{}^9 X_1{}^{(1)}(17) & \phi_2{}^9\phi_1{}^3 X_4{}^{(1)}(17) \\ \phi_2{}^{10}\phi_1{}^2 X_3{}^{(1)}(5) & \phi_2{}^{10}\phi_1 X_2{}^{(1)}(5) & \phi_2{}^{10} X_1{}^{(1)}(6) & \phi_2{}^{10}\phi_1{}^2 X_3{}^{(1)}(17) & \phi_2{}^{10}\phi_1 X_2{}^{(1)}(17) & \phi_2{}^{10} X_1{}^{(1)}(18) \\ \phi_2{}^{11}\phi_1{}^3 X_4{}^{(1)}(6) & \phi_2{}^{11}\phi_1{}^2 X_3{}^{(1)}(6) & \phi_2{}^{11}\phi_1 X_2{}^{(1)}(6) & \phi_2{}^{11}\phi_1{}^3 X_4{}^{(1)}(18) & \phi_2{}^{11}\phi_1{}^2 X_3{}^{(1)}(18) & \phi_2{}^{11}\phi_1 X_2{}^{(1)}(18) \\ \phi_2{}^{12} X_1{}^{(1)}(10) & \phi_2{}^{12}\phi_1{}^3 X_4{}^{(1)}(10) & \phi_2{}^{12}\phi_1{}^2 X_3{}^{(1)}(10) & \phi_2{}^{12} X_1{}^{(1)}(22) & \phi_2{}^{12}\phi_1{}^3 X_4{}^{(1)}(22) & \phi_2{}^{12}\phi_1{}^2 X_3{}^{(1)}(22) \\ \phi_2{}^{13}\phi_1 X_2{}^{(1)}(10) & \phi_2{}^{13} X_1{}^{(1)}(11) & \phi_2{}^{13}\phi_1{}^3 X_4{}^{(1)}(11) & \phi_2{}^{13}\phi_1 X_2{}^{(1)}(22) & \phi_2{}^{13} X_1{}^{(1)}(23) & \phi_2{}^{13}\phi_1{}^3 X_4{}^{(1)}(23) \\ \phi_2{}^{14}\phi_1{}^2 X_3{}^{(1)}(11) & \phi_2{}^{14}\phi_1 X_2{}^{(1)}(11) & \phi_2{}^{14} X_1{}^{(1)}(12) & \phi_2{}^{14}\phi_1{}^2 X_3{}^{(1)}(23) & \phi_2{}^{14}\phi_1 X_2{}^{(1)}(23) & \phi_2{}^{14} X_1{}^{(1)}(24) \\ \phi_2{}^{15}\phi_1{}^3 X_4{}^{(1)}(12) & \phi_2{}^{15}\phi_1{}^2 X_3{}^{(1)}(12) & \phi_2{}^{15}\phi_1 X_1{}^{(1)}(12) & \phi_2{}^{15}\phi_1{}^3 X_4{}^{(1)}(24) & \phi_2{}^{15}\phi_1{}^2 X_3{}^{(1)}(24) & \phi_2{}^{15}\phi_1 X_1{}^{(1)}(24) \end{pmatrix} \tag{6.19}$$

for user-2,

$$\tilde{C}_1^{(2)} = \begin{pmatrix} \phi_2{}^{15} X_1{}^{(2)}(1) & \phi_2{}^{15}\phi_1{}^3 X_4{}^{(2)}(1) & \phi_2{}^{15}\phi_1{}^2 X_3{}^{(2)}(1) & \phi_2{}^{15} X_1{}^{(2)}(13) & \phi_2{}^{15}\phi_1{}^3 X_4{}^{(2)}(13) & \phi_2{}^{15}\phi_1{}^2 X_3{}^{(2)}(13) \\ \phi_1 X_2{}^{(2)}(1) & X_1{}^{(2)}(2) & \phi_1{}^3 X_4{}^{(2)}(2) & \phi_1 X_2{}^{(13)}(1) & X_1{}^{(2)}(14) & \phi_1{}^3 X_4{}^{(2)}(14) \\ \phi_2{}^1\phi_1{}^2 X_3{}^{(2)}(2) & \phi_2{}^1\phi_1 X_2{}^{(2)}(2) & \phi_2{}^1 X_1{}^{(2)}(3) & \phi_2{}^1\phi_1{}^2 X_3{}^{(2)}(14) & \phi_2{}^1\phi_1 X_2{}^{(2)}(14) & \phi_2{}^1 X_1{}^{(2)}(15) \\ \phi_2{}^2\phi_1{}^3 X_4{}^{(2)}(3) & \phi_2{}^2\phi_1{}^2 X_3{}^{(2)}(3) & \phi_2{}^2\phi_1 X_2{}^{(2)}(3) & \phi_2{}^2\phi_1{}^3 X_4{}^{(2)}(15) & \phi_2{}^2\phi_1{}^2 X_3{}^{(2)}(15) & \phi_2{}^2\phi_1 X_2{}^{(2)}(15) \\ \phi_2{}^3 X_1{}^{(2)}(7) & \phi_2{}^3\phi_1{}^3 X_4{}^{(2)}(7) & \phi_2{}^3\phi_1{}^2 X_3{}^{(2)}(7) & \phi_2{}^3 X_1{}^{(2)}(19) & \phi_2{}^3\phi_1{}^3 X_4{}^{(2)}(19) & \phi_2{}^3\phi_1{}^2 X_3{}^{(2)}(19) \\ \phi_2{}^4\phi_1 X_2{}^{(2)}(7) & \phi_2{}^4 X_1{}^{(2)}(8) & \phi_2{}^4\phi_1{}^3 X_4{}^{(2)}(8) & \phi_2{}^4\phi_1 X_2{}^{(2)}(19) & \phi_2{}^4 X_1{}^{(2)}(20) & \phi_2{}^4\phi_1{}^3 X_4{}^{(2)}(20) \\ \phi_2{}^5\phi_1{}^2 X_3{}^{(2)}(8) & \phi_2{}^5\phi_1 X_2{}^{(2)}(8) & \phi_2{}^5 X_1{}^{(2)}(9) & \phi_2{}^5\phi_1{}^2 X_3{}^{(2)}(20) & \phi_2{}^5\phi_1 X_2{}^{(2)}(20) & \phi_2{}^5 X_1{}^{(2)}(21) \\ \phi_2{}^6\phi_1{}^3 X_4{}^{(2)}(9) & \phi_2{}^6\phi_1{}^2 X_3{}^{(2)}(9) & \phi_2{}^6\phi_1 X_2{}^{(2)}(9) & \phi_2{}^6\phi_1{}^3 X_4{}^{(2)}(21) & \phi_2{}^6\phi_1{}^2 X_3{}^{(2)}(21) & \phi_2{}^6\phi_1 X_2{}^{(2)}(21) \\ \phi_2{}^7 X_1{}^{(2)}(4) & \phi_2{}^7\phi_1{}^3 X_4{}^{(2)}(4) & \phi_2{}^7\phi_1{}^2 X_3{}^{(2)}(4) & \phi_2{}^7 X_1{}^{(2)}(16) & \phi_2{}^7\phi_1{}^3 X_4{}^{(2)}(16) & \phi_2{}^7\phi_1{}^2 X_3{}^{(2)}(16) \\ \phi_2{}^8\phi_1 X_2{}^{(2)}(4) & \phi_2{}^8 X_1{}^{(2)}(5) & \phi_2{}^8\phi_1{}^3 X_4{}^{(2)}(5) & \phi_2{}^8\phi_1 X_2{}^{(2)}(16) & \phi_2{}^8 X_1{}^{(2)}(17) & \phi_2{}^8\phi_1{}^3 X_4{}^{(2)}(17) \\ \phi_2{}^9\phi_1{}^2 X_3{}^{(2)}(5) & \phi_2{}^9\phi_1 X_2{}^{(2)}(5) & \phi_2{}^9 X_1{}^{(2)}(6) & \phi_2{}^9\phi_1{}^2 X_3{}^{(2)}(17) & \phi_2{}^9\phi_1 X_2{}^{(2)}(17) & \phi_2{}^9 X_1{}^{(2)}(16) \\ \phi_2{}^{10}\phi_1{}^3 X_4{}^{(2)}(6) & \phi_2{}^{10}\phi_1{}^2 X_3{}^{(2)}(6) & \phi_2{}^{10}\phi_1 X_2{}^{(2)}(6) & \phi_2{}^{10}\phi_1{}^3 X_4{}^{(2)}(18) & \phi_2{}^{10}\phi_1{}^2 X_3{}^{(2)}(18) & \phi_2{}^{10}\phi_1 X_2{}^{(2)}(18) \\ \phi_2{}^{11} X_1{}^{(2)}(10) & \phi_2{}^{11}\phi_1{}^3 X_4{}^{(2)}(10) & \phi_2{}^{11}\phi_1{}^2 X_3{}^{(2)}(10) & \phi_2{}^{11} X_1{}^{(2)}(22) & \phi_2{}^{11}\phi_1{}^3 X_4{}^{(2)}(22) & \phi_2{}^{11}\phi_1{}^2 X_3{}^{(2)}(22) \\ \phi_2{}^{12}\phi_1 X_2{}^{(2)}(10) & \phi_2{}^{12} X_1{}^{(2)}(11) & \phi_2{}^{12}\phi_1{}^3 X_4{}^{(2)}(11) & \phi_2{}^{12}\phi_1 X_2{}^{(2)}(22) & \phi_2{}^{12} X_1{}^{(2)}(23) & \phi_2{}^{12}\phi_1{}^3 X_4{}^{(2)}(23) \\ \phi_2{}^{13}\phi_1{}^2 X_3{}^{(2)}(11) & \phi_2{}^{13}\phi_1 X_2{}^{(2)}(11) & \phi_2{}^{13} X_1{}^{(2)}(12) & \phi_2{}^{13}\phi_1{}^2 X_3{}^{(2)}(23) & \phi_2{}^{13}\phi_1 X_2{}^{(23)}(11) & \phi_2{}^{13} X_1{}^{(2)}(24) \\ \phi_2{}^{14}\phi_1{}^3 X_4{}^{(2)}(12) & \phi_2{}^{14}\phi_1{}^2 X_3{}^{(2)}(12) & \phi_2{}^{14}\phi_1 X_1{}^{(2)}(12) & \phi_2{}^{14}\phi_1{}^3 X_4{}^{(2)}(24) & \phi_2{}^{14}\phi_1{}^2 X_3{}^{(2)}(24) & \phi_2{}^{14}\phi_1 X_1{}^{(2)}(24) \end{pmatrix} \tag{6.20}$$

6.2 Performance Results

This section provides the simulation results to evaluate the performance of multiuser SF/STF codes. Two users scenario has been considered where each user is equipped with two transmit antennas and two receive antennas with equal power gain. A two

ray channel model has been simulated for each pair of transmit-receive antennas. The length of the cyclic prefix is chosen as 16 and $N = 64$ OFDM tones is used for each transmit antenna. The second path delay is assumed to be 0.5 s that is, 10 times the sampling interval. In the simulation, the channel coefficients are independent from one OFDM block to other block but are remain constant during one OFDM block. The simulation result shows the performance comparison between the baseband symbol, multiuser SF codes with 16-QAM, multiuser space-frequency code [2] with 16-QAM and the proposed multiuser space-time-frequency codes [5] with 16-QAM. From Fig. 6.3, it can be seen that in the low-to-middle SNR region, SF code in [2] shows the similar performance as [3]. But, in the high SNR region, multi-user SF codes in [2] have better performance than [3]. Therefore, a higher coding gain is achieved compared with multi-user SF code in [3] in the high SNR region. Again it can be seen from the simulation result that the presented multiuser STF codes [4] have larger slope curve, compared with the two SF codes (i.e. multiuser SF codes [3], proposed multiuser space-frequency) and with the baseband signal.

This implies that the STF codes [4] achieve a larger diversity gain than both SF codes. From the analysis in Sect. 6.1, we see that the full-diversity multiuser STF code [4] can achieve a diversity gain $A_t A_r A_u L = 16$, whereas the full-diversity multiuser SF [2] and the multiuser SF codes [3] codes achieves $A_t A_r L = 8$ only. Moreover, it is observed that the presented multiuser rate-2 STF code achieves the best SER performance among the simulated cases, and outperforms the rate-1 SF code [3] and proposed rate-2 multiuser SF codes over all the examined SNR values. This indicates that the rate-2 STF code from 16-QAM has a better coding and the

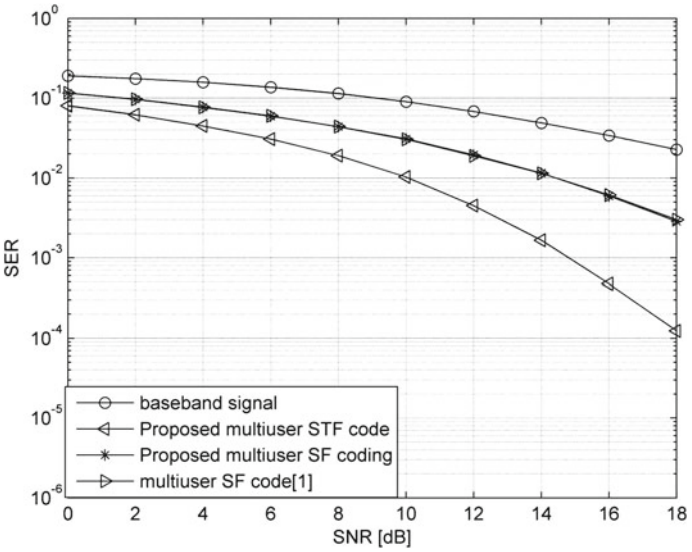

Fig. 6.3 SER performance comparison between the proposed multiuser SF, multiuser STF code, the multiuser SF code in [3] and the baseband symbol

diversity gain than the rate-1 SF code [3] and proposed rate-2 SF from 16QAM. The simulation result also has showed that our proposed high rate multiuser SF and STF codes achieve much better performance than the baseband symbols that justifies the presented schemes. Therefore, the presented multiuser SF and STF codes do not affect the code performance while the symbol rate is increased to A_t. On top of that, the presented multiuser STF/SF coding can guarantee the maximum diversity and high bandwidth efficiency as well as the minimum multiuser interference.

6.3 Conclusion

A systematic design of high-rate, full-diversity multi-user STF coding for MIMO frequency-selective fading MAC has been reported in this chapter. Moreover, the performance comparison between multiuser SF code (explained in Chap. 3) and multiuser STF code for MIMO-OFDM has also been reported in this chapter. In both cases, the high-rate (rate-A_t) and full-diversity $A_t A_r L$ (for multiuser SF codes) and $A_t A_r A_u L$ (for multiuser STF codes) for each user has been achieved without bandwidth expansion which validate the theoretical analysis. The presented multi-user SF and STF code are bandwidth efficient and always ensures rate-A_t as no zero padding is needed. Moreover, the proposed coding scheme does not require the co-operation of multiple transmitters in the uplink process. A few examples of code designs have been given. Simulation result showed that in the high SNR region, the SF [2] codes has a better coding gain in compare to [3], while, the STF codes [3] has a better coding and diversity gain in compare to [3] in both low and high SNR regions. However, the presented coding schemes do not affect the code performance while the symbol rate is increased to rate-A_t.

References

1. Shelim R, Matin MA, Alam AU (2011) High-rate full-diversity space-time-frequency code for multiuser MIMO-OFDM systems over frequency selective multiple access channels. J Converg Inf Technol 6
2. Shelim R, Matin MA, Alam AU (2013) A systematic design of high-rate full-diversity space-frequency codes for multiuser MIMO-OFDM system. WSEAS Trans Commun 12
3. Zhang W, Letaief KB (2010) A systematic design of full diversity multiuser space-frequency codes, IEEE Trans Signal Process 58:03
4. Shelim R, Matin MA, Alam AU (2014) Performance analysis of high-rate full-diversity space time frequency/space frequency codes for multiuser MIMO-OFDM. WSEAS Trans Commun 13(2):51–61, ISSN:1109–2742
5. Shelim R, Alam AU, Matin MA (2011) High-rate full-diversity space-time-frequency code for multiuser MIMO-OFDM systems over frequency selective multiple access channels. J Converg Inf Technol 6(8):8–22

Chapter 7
Generale Conclusion

Multiple-input multiple-output (MIMO) technology brings wireless revolution in providing higher throughput and improved performance over wireless channel by exploiting spatial multiplexing and diversity gain through multiple antennas. However, the multipath linear distortion of the environment causes frequency selective fading of MIMO channel. Orthogonal frequency division multiplexing (OFDM) technology turns the wideband frequency selective channel into a number of parallel narrowband sub-channels where various resources can be dynamically allocated. Due to the robustness against multipath fading of OFDM technique, MIMO technology is combined with OFDM in order to deliver high data rates and spectral efficiency, as well as enhanced link reliability, coverage, and/or energy efficiency.

Chapter 1 introduces the reader with MIMO-OFDM system. The combination of OFDM with spectral efficient multiple antenna techniques makes the OFDM a good candidate to overcome the frequency selective fading. PAPR reduction and frequency synchronization should take into consideration while working with OFDM.

Chapter 2 examines the MIMO wireless channel and determines its capacity under different conditions. This chapter illustrates different types of fading. In information theory, the notion of the channel takes on another meaning. In fact, this theory concerned with the amount of information carried by the issued message. Thus, the transmission channel is seen as a factor that degrades the amount of transmitted information.

MIMO-OFDM systems offer huge freedoms in space, time, and frequency. Therefore, ST, SF, and STF can be applied to exploit the maximum diversity from MIMO channels. In Chap. 3, code design criteria for MIMO-OFDM links with frequency-selective fading are investigated. A multiuser SF code design procedure is also demonstrated in this chapter.

Chapter 4 introduces the reader with Algebraic Space-Time Codes (ASTC). The construction of ASTC codes is based on the following approach-Choice of the base,

B. Ahmed and M. Abdul Matin, *Coding for MIMO-OFDM in Future Wireless Systems*, SpringerBriefs in Electrical and Computer Engineering,
DOI 10.1007/978-3-319-19153-9_7

Choice of the extension, Definition of the cyclic algebra, Definition of ST code. Moreover, theoretical and simulation results of the performance of the most performed ASTC, named Golden codes are presented in this chapter.

Chapter 5 analyzes the capacity of a MIMO-OFDM system using the ASTC codes in Rayleigh frequency selective channels. A new algebraic Carrier Frequency Offset (CFO) estimation technique for MIMO-OFDM system is also examined to overcome the sensitivity of ASTC to frequency synchronization.

Coding for multiuser MIMO-OFDM systems is mostly unexplored. Chapter 6 reports a systematic design of high rate full diversity STF coding for multiuser MIMO-OFDM and evaluates the performance of multiuser SF/STF code.

Appendix A
MIMO-OFDM Empirical BER

For a coherent channel $\boldsymbol{H}$, the pairwise error probability is performed as in [1, 2]:

$$P_e = Prob(\boldsymbol{x}_1 \rightarrow \boldsymbol{x}_2 \mid \boldsymbol{H}, \boldsymbol{x}_1 transmit) \tag{A.1}$$

$$= \boldsymbol{Q}\left(\frac{\|\boldsymbol{H}(\boldsymbol{x}_1 - \boldsymbol{x}_2)\|^2}{2\sigma_n^2}\right) \tag{A.2}$$

We derive first an upper Chernoff bounds for the conditional error probability [2–4]:

$$P_e \leq \exp\left(\boldsymbol{Q}\left(\frac{\|\boldsymbol{H}(\boldsymbol{x}_1 - \boldsymbol{x}_2)\|^2}{4\sigma_n^2}\right)\right) = \exp\left(\boldsymbol{Q}\left(\frac{\|\boldsymbol{y}\|^2}{4\sigma_n^2}\right)\right) \tag{A.3}$$

We define $\boldsymbol{y}$ as:

$$\boldsymbol{y} = \boldsymbol{H}\left(\frac{\boldsymbol{x}_1}{\sigma_{x_1}} - \frac{\boldsymbol{x}_2}{\sigma_{x_2}}\right) \tag{A.4}$$

Since $\boldsymbol{y}$ is a hermitian matrix and if we suppose that $\sigma_{x_1} = \sigma_{x_2} = \sigma_s$ then $\Longrightarrow$:

$$(A.3) \Rightarrow Pe \leq \exp\left(\frac{-\sigma_s^2}{4\sigma_n^2}\boldsymbol{y}^H \times \boldsymbol{y}\right) \tag{A.5}$$

By averaging over the all frequency selective Channel coefficients $\Rightarrow$ that means we are averaging mathematically over all $\boldsymbol{y}$ then:

$$Pe \leq \int_y \exp\left(\frac{-\sigma_s^2}{4\sigma_n^2}\boldsymbol{y}^H \times \boldsymbol{y}\right) P(\boldsymbol{y})d\boldsymbol{y} \tag{A.6}$$

B. Ahmed and M. Abdul Matin, *Coding for MIMO-OFDM in Future Wireless Systems*, SpringerBriefs in Electrical and Computer Engineering,
DOI 10.1007/978-3-319-19153-9

If we use (A.18) the inequality number (A.6) becomes:

$$Pe \leq \int_y \exp\left(\frac{-\sigma_s^2}{4\sigma_n^2}\boldsymbol{y}^H\boldsymbol{y}\right)\frac{1}{\det(\pi\boldsymbol{Q}_y)}\exp\left(-(\boldsymbol{y})^H\boldsymbol{Q}_y^{-1}(\boldsymbol{y})\right)d\boldsymbol{y} \tag{A.7}$$

$$Pe \leq \int_y \frac{1}{\det(\pi\boldsymbol{Q}_y)}\exp\left(\frac{-\sigma_s^2}{4\sigma_n^2}\boldsymbol{y}^H\boldsymbol{y} - (\boldsymbol{y})^H\boldsymbol{Q}_y^{-1}(\boldsymbol{y})\right)d\boldsymbol{y} \tag{A.8}$$

$$Pe \leq \int_y \frac{1}{\det(\pi\boldsymbol{Q}_y)}\exp\left(-\boldsymbol{y}^H\left(\frac{\sigma_s^2}{4\sigma_n^2}\boldsymbol{y} + \boldsymbol{Q}_y^{-1}(\boldsymbol{y})\right)\right)d\boldsymbol{y} \tag{A.9}$$

$$Pe \leq \int_y \frac{1}{\det(\pi\boldsymbol{Q}_y)}\exp\left(-\boldsymbol{y}^H\left(\frac{\sigma_s^2}{4\sigma_n^2}\boldsymbol{I}_{Nt} + \boldsymbol{Q}_Y^{-1}\right)\boldsymbol{y}\right)d\boldsymbol{y} \tag{A.10}$$

Now if we define $\boldsymbol{B} = \left(\frac{\sigma_s^2}{4\sigma_n^2}\boldsymbol{I}_{Nt} + \boldsymbol{Q}_Y^{-1}\right)^{-1}$

$$Pe \leq \int_y \frac{1}{\pi\det(\boldsymbol{Q}_y)}\exp\left(-\boldsymbol{y}^H(\boldsymbol{B}^{-1})\boldsymbol{y}\right)d\boldsymbol{y} \tag{A.11}$$

And if we multiply $\det(\boldsymbol{B})$ and we divide by $\det(\boldsymbol{B})$ we obtain:

$$Pe \leq \frac{\det(\boldsymbol{B})}{\det(\boldsymbol{Q}_y)}\int_Y \frac{1}{\pi\det(\boldsymbol{B})}\exp\left(-\boldsymbol{y}^H(\boldsymbol{B}^{-1})\boldsymbol{y}\right)d\boldsymbol{y} \tag{A.12}$$

$$Pe \leq \frac{\det(\boldsymbol{B})}{\det(\boldsymbol{Q}_y)}\int_y \boldsymbol{P}(\boldsymbol{y})d\boldsymbol{y} \tag{A.13}$$

and as

$$\int_y \boldsymbol{P}(\boldsymbol{y})d\boldsymbol{y} = 1 \tag{A.14}$$

$$Pe \leq \frac{\det(\boldsymbol{B})}{\det(\boldsymbol{Q}_y)} = \frac{\det\left(\frac{\sigma_s^2}{4\sigma_n^2}\boldsymbol{I}_{N_t} + \boldsymbol{Q}_y^{-1}\right)^{-1}}{\det(\boldsymbol{Q}_y)} \tag{A.15}$$

$$Pe \leq \det\left(\boldsymbol{I}_{N_t} + \frac{\sigma_s^2}{4\sigma_n^2}\boldsymbol{Q}_y\right)^{-1} \tag{A.16}$$

The following mathematic tools is used to complete the last derivation:
$\boldsymbol{A}$ is a hermitian matrix $\Rightarrow \boldsymbol{A} = \boldsymbol{A}^H$.
$\|\boldsymbol{A}\|_2^2 = \boldsymbol{A} \times \boldsymbol{A}$.

$$\det(\boldsymbol{I}_{Nt} + \alpha \boldsymbol{A}) = 1 + \alpha \sum_{n=1}^{N} a_{xx} + \alpha^2 \sum_{n=1}^{N-1} \sum_{y=x+1}^{N} \det \begin{pmatrix} a_{xx} & a_{xy} \\ a_{yx} & a_{yy} \end{pmatrix} + \ldots \quad \text{(A.17)}$$

$Q_{\boldsymbol{y}} = E(\boldsymbol{y}\boldsymbol{y}^H) =$ the Covariance matrix of $\boldsymbol{y}$
For a hermitian matrix $\boldsymbol{Z}$ of covariance $\boldsymbol{Q}_z$ with $E(\boldsymbol{Z}) = \mu_z$ mean, the probability density of $\boldsymbol{Z}$ is performed as:

$$P(\boldsymbol{Z}) = det(\pi \boldsymbol{Q}_z)^{-1} exp(-(\boldsymbol{Z} - \mu_z)^H \boldsymbol{Q}_z^{-1}(\boldsymbol{Z} - \mu_z)) \quad \text{(A.18)}$$

The development given let us to conclude:

$$Pe \leq \left(1 + \frac{\sigma_s^2}{4\sigma_n^2} N_t + \sum_{i=1}^{N_i} \lambda_i + \left(\frac{\sigma_s^2}{4\sigma_n^2} \right)^{N_i N_t} \left(\prod_{i=1}^{N_i} \lambda_i \right)^{N_t} \right)^{-1} \quad \text{(A.19)}$$

where λ_i is the ith eigenvalues of $\boldsymbol{Q}_Y$ matrix.

References

1. Oggier F (2005) Algebraic methods for chanel coding. Ph.D. dissertation, EPFL
2. Tarokh V, Seshadri N, Calderbank AR (1998) Space-time codes for high data rate wireless communication: performance criterion and code construction. IEEE Trans Inf Theory 44:744–765
3. Bolcskei H, Paulraj AJ (2000) Space-frequency coded broadband OFDM systems. IEEE Wirel Commun Netw Conf 1:1–6
4. Proakis J (2000) Digital communications. McGraw-Hill Series in electrical and computer engineering, 4th edn., ISBN: 9780072321111,0072321113

Index

B. Ahmed and M. Abdul Matin, *Coding for MIMO-OFDM in Future Wireless Systems*, SpringerBriefs in Electrical and Computer Engineering,
DOI 10.1007/978-3-319-19153-9